Wave Theory based Extensions to Standard Room-acoustic Particle Models

vorgelegt von

Mahesh Bansal

aus Ajmer, Indien

Von der Fakultät V – Verkehrs und Maschinensysteme

(Institut für Strömungsmechanik und Technische Akustik)
der Technischen Universität Berlin

zur Erlangung des akademischen Grades

Dr. –Ing.

genehmigte Dissertation

Promotionsausschuss:

Vorsitzender: Prof. Dr.-Ing. P.-U. Thamsen

Gutachter: Prof. Dr.-Ing. M. Möser

Gutachter: Prof. Dr.-Ing. habil. W. Ahnert

Tag der wissenschaftlichen Aussprache: 10 July 2008

Berlin 2009

D 83

Dedicated to

MY FAMILY

And

ALL MY WELL-WISHERS

Acknowledgements

First of all, I would like to thank my advisor Professor Möser for giving me the opportunity of conducting this reseach. His helpful suggestions were always beneficial for the accomplishment of this work.

I am really thankful to Stefan Feistel from SDA for guiding me all through this research. I have learned a lot from him. From technical part to philosophical part, he was always there to guide me. He always tried to find time for me from his busy schedule.This whole work has been completed only because of his deep involvement, constant encouragement, and above all, his faith in me.

I am deeply thankful to Dr. Wolfgang Ahnert from ADA for advising me in every aspect of life. Without him it would have been difficult to keep myself motivated all through this work. All the colleagues at ADA and SDA were also very helpful. I thank all ADA and SDA members for providing an excellent working environment.

I am ever indebted to all my family members for their faith in me. Without their support it would not have been possible for me to take the challenging task of pursuing a PhD.

Living in Germany for four years was truly an enriching experience. From learning german language at volkshochschule to watching world cup football matches at "fanmeile" in Berlin, I enjoyed everything here. I enjoyed the company of several friends especially Jatin, Anand, Umesh, Vinay and Manohar who made my stay in berlin a wonderful experience.

Lastly, I thank ADA Foundation gGmbH for supporting this work financially.

Abstract

This thesis addresses the need of incorporating the wave based model in room acoustics to extend the existing sound particle models like ray tracing and image source methods. Chapter 1 starts with the introduction of approaches being used for auralization purpose in room acoustics. Detailed methodology behind particle approaches are discussed. However, such particle or ray based approaches are not sufficient in small and complex shaped rooms to take proper account of the wave nature of the sound field. These methods fail to obtain room acoustic characteristics of higher quality in the low frequency bands. In order to effectively simulate the sound field at low frequencies, where the dimensions of the walls are comparable to the wavelength, one needs to clearly know the reflection and diffraction properties of walls. This thesis presents the use of numerical techniques like finite element method (FEM) and boundary element method (BEM) to solve the Helmholtz wave equation in order to obtain a better or more realistic impulse response.

Solving differential equations using numerical methods like FEM and BEM require discretization or "mesh" of continuous geometrical domain. Several algorithms have been developed to automate the process of mesh generation, but most of them do not provide a guarantee about the quality of the resulting mesh. Generally, hexahedrals are preferred over tetrahedrals as they avoid flat and sharp angles hence better mesh quality can be obtained. But no approach so far guarantees the automatic hexahedral mesh generation of the whole domain. This thesis in Chapter 2, introduces a new approach "cutting plane algorithm" to generate an all-hexahedral mesh. The cutting plane algorithm is based upon cutting the polyhedron as proposed by Chazelle [24] into simpler shaped elements and the main emphasis in this work is to investigate it's practical applicability in architectural designs. It is shown that after applying a sequence of cuts on the given arbitrary polyhedron, one can obtain convex and trivalent polyhedrons. These polyhedrons can then be converted into a hexahedral mesh using Mid-Point subdivision scheme. Special cutting schemes are suggested using examples for typical architectural designs. Special considerations are given to mesh quality in acoustical models where balconies, domes (for mosques), stairs, pillers etc. are very common. Furthermore, for curved surfaces a new projection algorithm is introduced. It is shown that with proper combination of cutting plane and projection algorithms, a good quality mesh can be obtained.

Chapter 3 discusses the detailed acoustical analysis using the FEM. An overview of using the FEM for performing modal analysis and frequency domain simulation in closed environments is presented. Moreover, the diffraction effect which is not possible to observe below Schroeder frequency by means of particle models is viewed using FEM. For this purpose the solution of the general quadratic eigenvalue problem arising from the finite element analysis in enclosures with complex shapes and general impedance boundary condition is considered. This work is mainly concerned with the attempt of showing the practical feasibility of FEM in room acoustics and to combine it with particle models in order to obtain the broad band response of the room. Also, fundamental points regarding the finite element method, iterative methods and required mesh quality are discussed.

In Chapter 4, the thesis tries to investigate the scattering behavior of incident plane waves at arbitrarily shaped wall surfaces using BEM. For comparison purposes, a simple point-source

based model to calculate scattered wave fronts is also introduced. The incident plane waves are considered at various angles and scattering coefficients computed in both models are then compared with the measured data. It is found that while the point-source model can give reasonable asymptotic results, the advanced numerical model matches with the measurement data significantly better in quantity and quality.

Chapter 5 concludes the thesis by summarizing the work and provides some guidelines for future work.

Table of Contents

List of Symbols

ρ : Mass density of air (taken as 1.205 kg/m³)
ω: Angular frequency
Z: Impedance
K: Stiffness matrix
C : Damping matrix
M: Mass matrix
c : velocity of sound
Ω: 3D enclosure, problem domain
Γ: Boundary of any domain/enclosure
p: Sound Pressure
k: wavenumber

1. CHAPTER

Approaches in Room Acoustics

1.1. INTRODUCTION

The acoustics of enclosures like concert halls, theatres, worship spaces etc for auralization [1] purpose has been investigated for many years. One needs to predict the acoustic behavior of such spaces at the design stage so as to avoid the problems after they are built. The sound field created in such rooms depends upon many parameters like volume, absorbing materials, geometry type and the frequency at which the sound is considered. The modeling of enclosures with all these parameters is not simple and so far different approaches have been proposed. We can classify these methods/approaches depending upon the methodology (arranged left to right in chronological order) they follow as mentioned below (fig. 1.1):
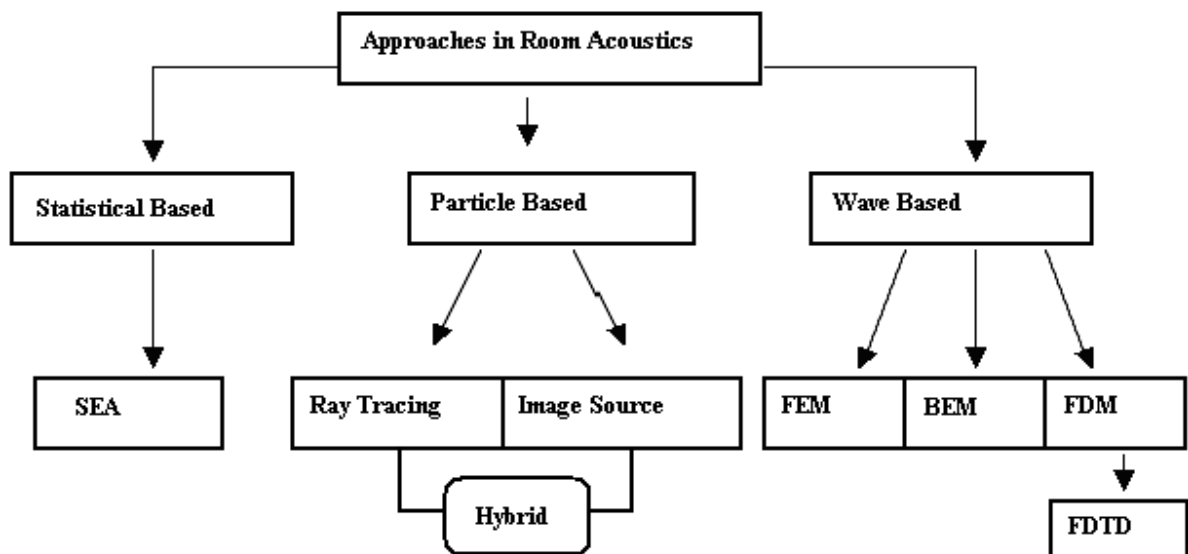
Fig 1.1: Approaches in Room Acoustics

As mentioned in fig. 1.1, one can classify the modeling algorithms in three categories. The first and the initial approach to model the sound field was based on statistical [2] assumptions. An example of one such approach is SEA [3, 4]. Generally SEA is used for prediction of noise levels where sound is propagated mainly by structures. Second is particle based approaches [5, 6, 7] where sound is considered to behave like a particle. Image source method and ray tracing method are two examples of particle based approach. Some hybrid approaches [8, 9] are also proposed where image source is used for early reflections and ray tracing method for late reflections. However, the particle based assumption of sound is valid only when the wavelength considered

is small compared to the area of wall surfaces. Therefore, the wave effects like diffraction and interference are not taken into account. Hence, one needs to solve the wave equation to model the actual sound field at low frequencies. As the analytic solution for complicated surfaces with different boundary conditions is almost impossible, a third model based on numerical methods like finite element method (FEM) [10, 11, 12], boundary element method (BEM) [13, 14] and finite difference methods (FDM) like finite difference time domain method (FDTD) [15, 16] is proposed. These methods can be applied quite effectively but the associated computational cost increases as the frequency increases. However, with the fast improving computational facilities, efforts are being made to make use of these approaches more and more to simulate the sound field. BEM requires discretization or "mesh" of the boundary surface of the given geometry whereas in FEM the whole domain needs to be discretized. Both approaches have some advantages and disadvantages over the other. In the next section, we explain all the approaches shortly.

1.2. PARTICLE APPROACHES

1.2.1. Ray Tracing Method

Ray tracing method is a well known geometrical based approach. Rays are emitted by a sound source and the sound field is modelled by following the path taken by these rays as they interact with surfaces. Therefore the sound is behaved to be like a particle where certain particles are emanating from the speaker and then they are bouncing back on forth following the specular reflection rule i.e. angle of incidence equals angle of reflection.
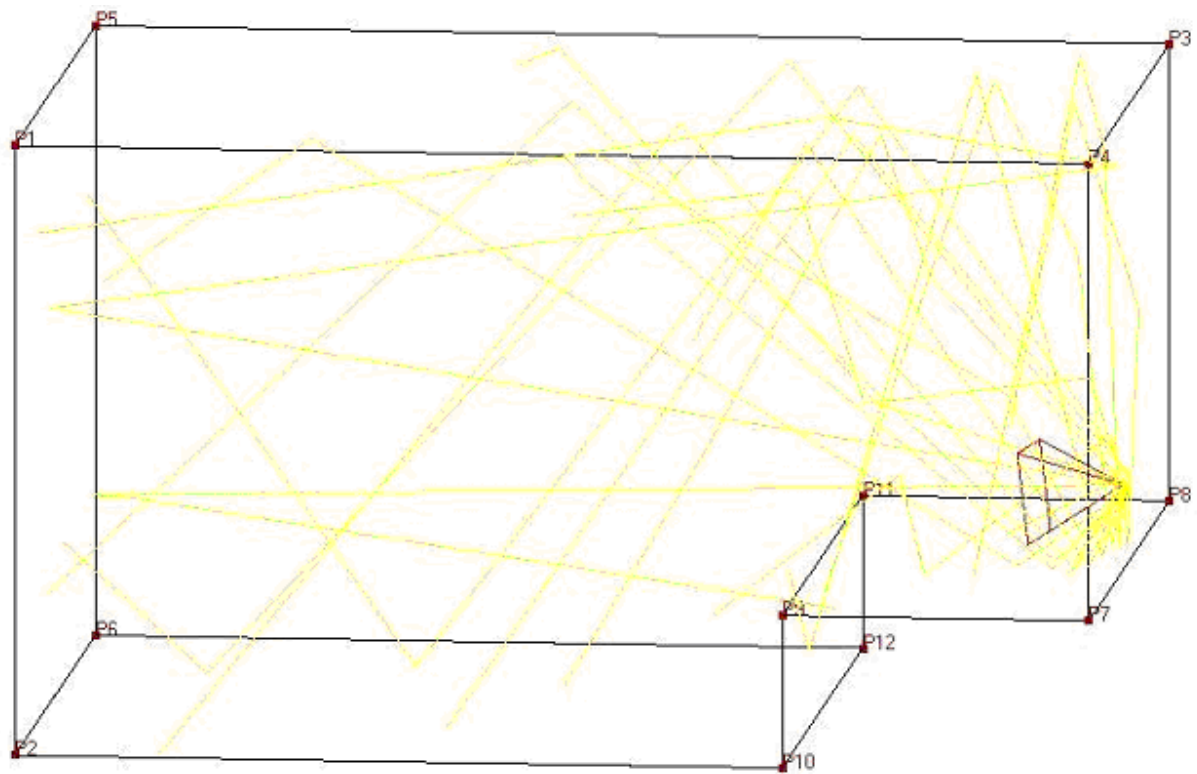

Fig 1.2: Ray Tracing Method

13

One needs to keep track of all the audible rays at the desired listener locations. The figure (1.2) illustrates the priniciple of ray tracing for a simple room with one source. It shows the sound rays coming out from the speaker and getting reflected due to walls. The objective is to discover all possible reflection paths. Monte-Carlo [17, 18] ray tracing simulation is quite effective to handle the complex geometric models.

Nowadays many efforts are being made to incorporate the scattering coefficient as well into the ray tracing model. However, the literature for scattering coefficient [19] data is very limited and it's quite impractical to measure for all the real life geometrical shapes. Particulary when they are fixed on wall structures. Hence, in this work, a computation tool using Boundary element method (BEM) to calculate the scattering coefficient for any given arbritrary surface has been developed. Then the simulated data were compared with the measured data [20] and they were quite in agreement with each other. We shall discuss about it in detail in the chapter 3 of this thesis.

The assumption of considering sound to behave like a particle is valid only when the room dimensions are large enough compared to the wavelength. At low frequencies, as room size decreases the wavelength becomes comparable to room dimensions and the wave nature of sound cannot be ignored.

1.2.2. Image Source Method

The image-source method is a procedure to simulate a room by replacing all surface reflections at receiver locations with image sources. The assumptions made here are same as that for ray tracing method. In this approach also no scattering is taken into account. Basic principle is shown below for one source.
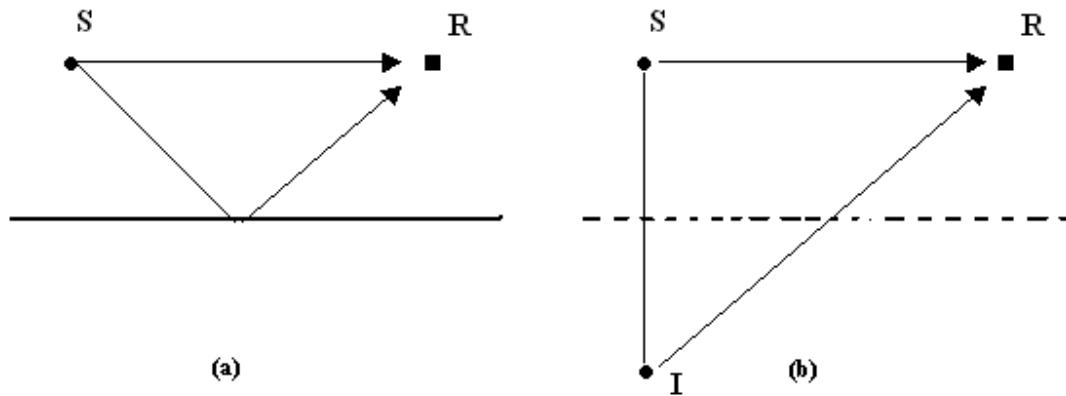
Fig. 1.3a; 1.3b

So, in the example above it is shown that the contribution of sound energy by the reflected ray at receiver location is being replaced by the direct sound from the image source. Similarly, when there are more surfaces there will be more mirror image sources. Generally speaking, a sound ray is reflected by multiple surfaces before arriving to a listener.

Example figure (1.4) shows how one can visualize direct sound, first order and second order reflections using image source method. I_{floor} is the image of the source due to the first order floor reflection and similarly $I_{ceiling}$ is due to the ceiling wall. $I_{floor\_ceiling}$ denotes the image created by second order reflection of floor's image with that of ceiling. The graphical ray diagram shows how to calculate the contribution of various "visible" sound sources at receiver location. For instance, the contribution from $I_{ceiling\_floor}$ will not be counted at receiver location in this case as it in not visible due to an obstacle. Therefor after every image calculations, visibility check must be performed.

Fig. 1.4: Mirror Image Method

1.2.3. Comparison between Ray Tracing and Image Source Methods

The ray tracing method is simple and easy to be applied but the image source method can provide more exact results as early reflections are more accurately calculated in image source

method. However, with the increase in number of reflections, the images increases exponentially [8, 9]. Hence hybrid approaches are also preferred where image source is used for early reflections and ray tracing for later reflections.

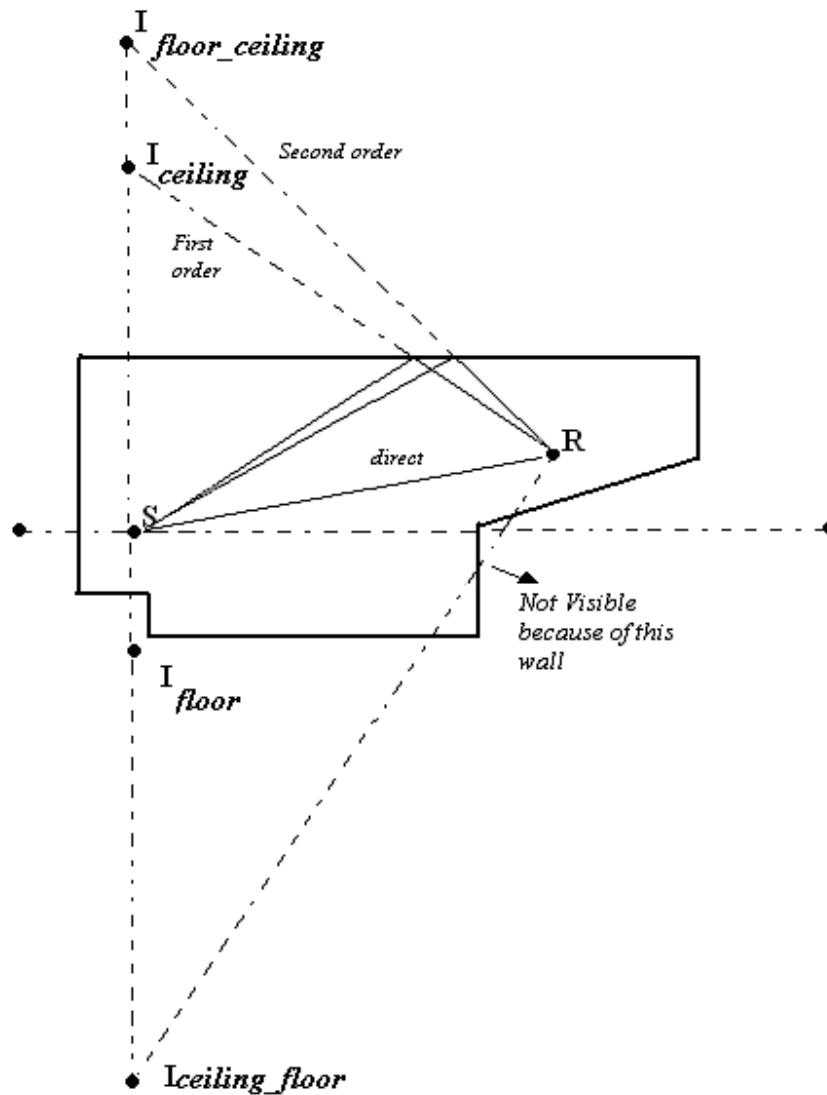However, still both approaches fail when the room dimensions are comparable to the wavelength, and there exists some energy distribution due to the wave nature of sound. Roughly speaking below Schroeder frequency, such wave related features like diffraction and interference cannot be ignored. Schroeder frequency is an approximate transition frequency and below this the modal density in small rooms is low. Therefore, the uniform distribution of sound energy cannot be assumed as used in statistical approaches. Hence, for low frequency bands it is essential to consider an approach of solving the wave equation for sound in order to obtain the room acoustic characteristics of higher quality. More detailed modal analysis and comparison is provided in chapter 3.

1.3. WAVE BASED APPROACHES

These approaches try to solve the wave equation directly. As the analytical solution is not possible for all arbitrary shapes and boundary conditions, one needs to rely upon numerical methods. In this chapter only the wave based methods have been introduced and in the later chapters, detailed analysis will be provided.

The general methodology followed in wave approaches is mentioned in the chart below. For any given physical system i.e. any closed space in our case, the mathematical system is derived based on certain assumptions and phenomenon which expresses the state of the system mathematically. In our case, the mathematical system is the Helmholtz equation. Afterwards, the equation described over continuous geometry is approximated by a discrete model. This step of subdividing the domain into smaller elements is called as mesh generation. The contribution from each discretised element is then added to the global matrix and finally the global matrix is then solved to obtain the solution at each nodal points. Each of the modeling step is explained in detail in the coming sections.
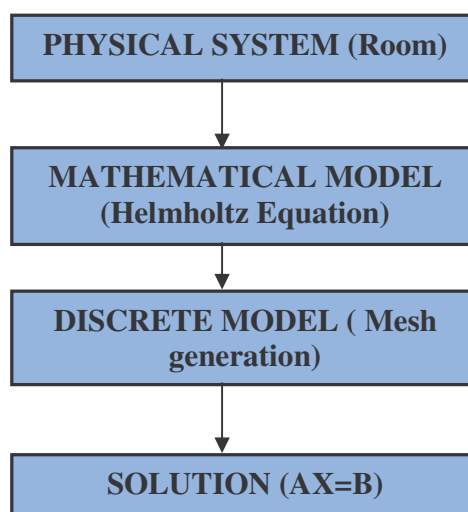
PHYSICAL SYSTEM (Room)

↓

MATHEMATICAL MODEL
(Helmholtz Equation)

↓

DISCRETE MODEL (Mesh generation)

↓

SOLUTION (AX=B)

Fig 1.5

16

One can further classify between wave based models as element or difference based approaches.

In element based approaches, the continuous domain is discretized into elements and basis /trial functions are then defined over nodes of element. The solution is then approximated as a linear combination of such basis functions. Examples of such type of approaches include BEM and FEM.

However, in difference based approaches (FDM), the derivatives are directly approximated by an algebraic expression. Finite difference time domain (FDTD) is an example of one such approach.

Difference based approaches utilizes uniformly spaced grid whereas element based approaches utilizes either uniform or non-uniformly spaced grids. Therefore, element based approaches offers more powerful method to model engineering problems involving complex three dimensional domain. In this work, we have chosen FEM and BEM approaches to simulate the sound field in room acoustics.

FEM is quite popular technique to solve the partial differential equations. Adaptiveness and the ease of incorporating the impedance boundary conditions makes it even more preferred over other approaches. However, here the whole volume needs to be discretized while in BEM only the boundary surface needs to be meshed. Therefore the final system matrix in FEM is very large but sparse and symmetric. In BEM, the size of the final matrix is small because of less number of discretized elements but the system matrix is very dense and highly asymmetric.

Before explaining the theory behind FEM and BEM, first as an introduction we explain basic mathematical concepts behind element based [21, 22, 23] methodology.

1.3.1. Discretization and Basis Functions

Consider a one dimensional field where we seek to find a mathematical expression to evaluate $U(x)$. For acoustics purpose, $U(x)$ could be the sound pressure distribution over the one dimensional field.

If we discretize the field into four elements, the five nodes numbered (N1, N2, N3, N4, N5) will look as follows.
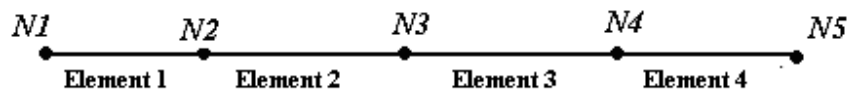
Fig.1.6a

If we define the linear variation between two nodal values, then U can be interpolated as follows:

$$U(\xi) = u_1 * \xi + u_2 * (1- \xi)$$

where $0< \xi <1$ and for the first element, $u_1 = N1$, $u_2 = N2$. For second element, $u_1 = N2$, $u_2 = N3$. Similarly for the third element, $u_1 = N3$, $u_2 = N4$ and so on.

17

It is shown in the figure (1.6b), that each of the elements in the physical space (x) is mapped onto the mathematical space (ξ).
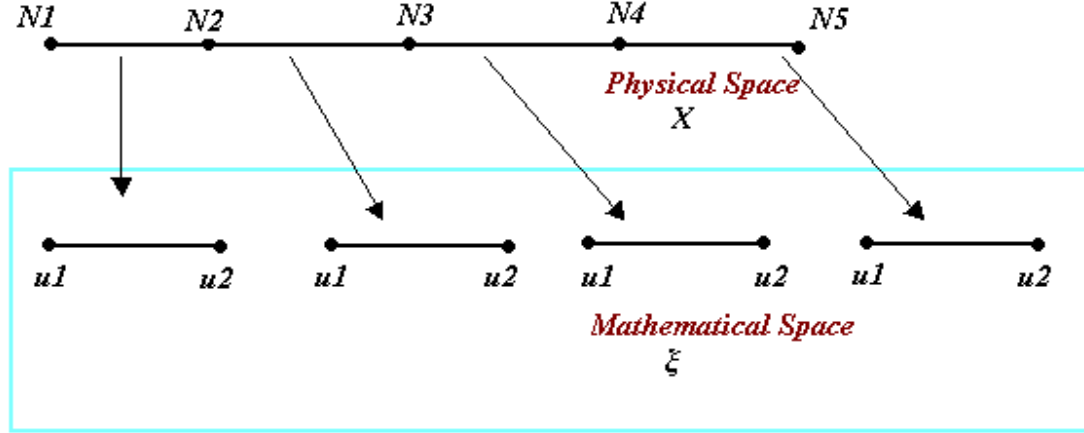
Fig.1.6b: Mapping onto Mathematical Space

Further we define:

$\Phi_1(\xi) = 1-\xi$

$\Phi_2(\xi) = \xi$

Such that the following holds:

$$U(\xi) = \Phi_1(\xi)*u_1 + \Phi_2(\xi)*u_2$$

These $\Phi_1(\xi)$ and $\Phi_2(\xi)$ are then called as linear basis functions for the nodes u_1 and u_2. Therefore we have a piecewise continuous representation of sound field $U(\xi)$. However, to calculate $U(X)$, one needs to define the mapping between x and ξ for each element. A simpler way to do that is to define X as an interpolation of the nodal values of x:

$$X(\xi) = \Phi_1(\xi)*x_1 + \Phi_2(\xi)*x_2$$

where $x_1 < x < x_2$ and $0 < \xi < 1$ for each element. Here, x_1 and x_2 are the nodal values of the element in physical space.

Now, we come to some properties of basis functions. They can be regarded as a weighting function on the nodal parameters. Basis function for an associated node takes the value *one* when evaluated at that point and is *zero* at all other element nodes. Keeping this in mind, one can define basis functions for two and three dimensional elements as well. For example, for two dimensional four noded element (fig. 1.7a), one can define:

18

$$U(\xi_1, \xi_2) = \Phi_1(\xi_1, \xi_2)u_1 + \Phi_2(\xi_1, \xi_2)u_2 + \Phi_3(\xi_1, \xi_2)u_3 + \Phi_4(\xi_1, \xi_2)u_4$$
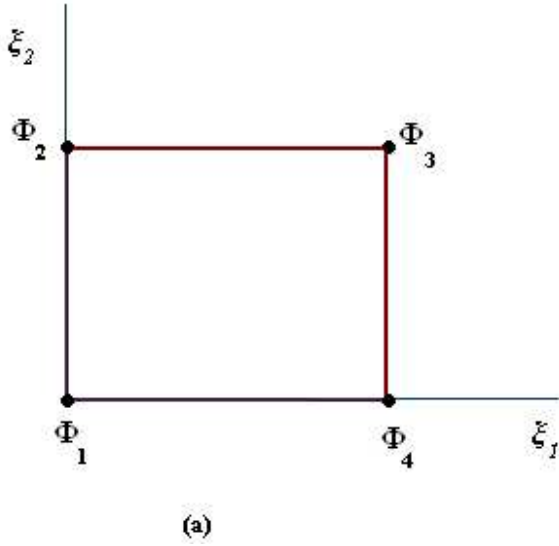
Fig 1.7a: 4-noded element   Fig. 1.7b: 8-noded element
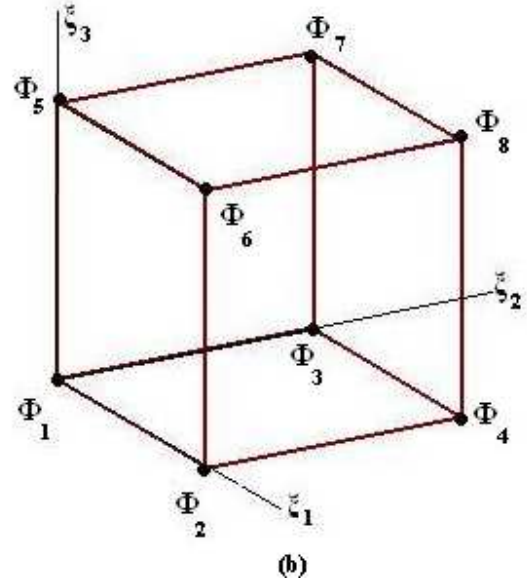
where,

$\Phi_1(\xi_1, \xi_2) = (1 - \xi_1)(1 - \xi_2)$, $\Phi_2(\xi_1, \xi_2) = (1 - \xi_1)\xi_2$, $\Phi_3(\xi_1, \xi_2) = \xi_1(1 - \xi_2)$ and $\Phi_4(\xi_1, \xi_2) = \xi_1\xi_2$.

Similarly for 8 noded hexahedral element (fig. 1.7b) in 3D, one can calculate the corresponding linear basis functions. One thing to note here is one can mesh the domain into triangles or tetrahedrals as well. Some more mesh elements are shown in figure 1.7c.
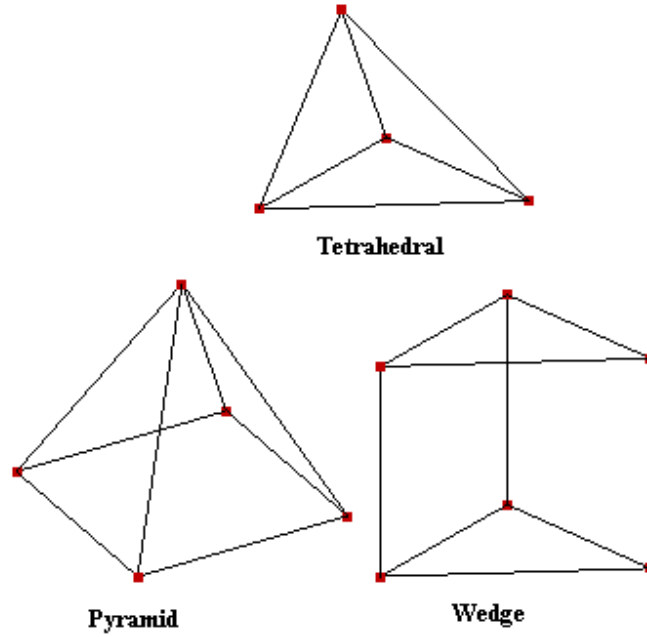
Fig 1.7c: 3D Mesh Elements

1.3.2. Finite Element Method

1.3.2.1. Theoretical Background

1.3.2.1.1.   Helmholtz Equation and FEM Formulation

The behavior of sound inside an enclosure (Ω) we are trying to analyze can be expressed mathematically using Helmholtz equation as follows:

$$\nabla^2 p(x) + k^2 p(x) = 0 \quad , \qquad x \in \Omega \tag{1.1}$$

where p is the acoustic pressure and k is the wavenumber, x is a coordinate belonging to Ω.. First we define an approximate solution p over each mesh/finite element as the linear combination of basis functions (φ) as defined earlier:

$$\tilde{p} = \sum_i \varphi_i p_i \approx p \tag{1.2}$$

On substituting 1.2 into 1.1, leaves a residual R:

$$R = \nabla^2 p + k^2 p \neq 0 \tag{1.3}$$

If p were an exact solution, the residual would be zero everywhere over the whole domain. But it's not the case in numerical problems. Next, instead of solving equation 1.1 directly, we form the weighted residual as follows:

$$\int_{\Omega} wR.d\Omega = 0 \qquad (1.4)$$

where w is the weighting function. Equation 1.4 is also called as the weak form of the original equation and FEM uses this integral form to find the approximate solution. Basically it tries to distribute the residual or error evenly over the domain.

Substituting R from eq. 1.3 into eq. 1.4, we have:

$$\int_{\Omega} w(\nabla^2 p + k^2 p)d\Omega = 0 \qquad (1.5)$$

Integrating the weak form (eq. 1.5) by parts, one has :

$$-\int_{\Omega} (\nabla w \nabla p)d\Omega + \int_{\Omega} (wk^2 p)d\Omega + \int_{\Gamma} (w\frac{\partial p}{\partial n})d\Gamma = 0 \qquad (1.6)$$

where $\frac{\partial p}{\partial n}$ denotes the normal derivative of pressure p.

In the Galerkin formulation [21], the weighting function is chosen to be the basis function itself. Moreover, in the third term of equation (1.6), one can incorporate the impedance Robin boundary conditions defined as:

$$\frac{\partial p}{\partial n} = -\frac{i\omega p \rho}{Z}, \qquad (1.7)$$

to obtain the final FEM formulation matrices:

$$[K]\{p\} + i\omega[C]\{p\} - \omega^2[M]\{p\} = -\rho\omega^2 u\{W\} \qquad (1.8)$$

where u: Displacement, and $\{W\}$: Nodal distribution vector respectively. K: Global stiffness matrix, C : Global damping matrix, M: Global mass matrix are defined as follows:

$$[K] = \int_{\Omega} (\nabla \lfloor \Phi \rfloor \nabla \{\Phi\})d\Omega,$$

$$[C] = \int_{\Gamma} \frac{\rho}{Z}(\lfloor \Phi \rfloor \{\Phi\})d\Gamma,$$

$$[M] = \frac{1}{c^2} \int_{\Omega} (\lfloor \Phi \rfloor \{\Phi\})d\Omega$$

Numerical evaluation of these matrices for each mesh element will be explained using an example in the section 1.3.2.2.

1.3.2.1.2. Modal Analysis

For modal analysis, we need to consider the steady state solution. Hence, the equation (1.8) reduces to the following quadratic eigenvalue problem:

$$[K]\{p\} + i\omega[C]\{p\} - \omega^2[M]\{p\} = 0 \tag{1.9}$$

The quadratic eigenvalue problem can be linearized to,

$$\begin{bmatrix} K & 0 \\ 0 & M \end{bmatrix}\begin{bmatrix} p \\ \omega p \end{bmatrix} = \omega\begin{bmatrix} -iC & M \\ M & 0 \end{bmatrix}\begin{bmatrix} p \\ \omega p \end{bmatrix} \tag{1.10}$$

With this approach, the dimension of the problem is doubled but on the other hand the advantage is that we can use the currently existing linear eigenvalue solvers that solve problems of the type:

$$AX = BX\,\lambda \tag{1.11}$$

1.3.2.1.3. Transfer Function

A transfer function determines the relation between input and output of a system. It is the measure of any system's response at the output to a signal of varying frequency at its input.
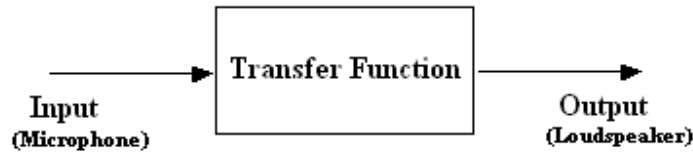
Fig. 1.8

For transfer function calculations using FEM, one can enter the input in the right hand side of equation (1.8) and can solve the system of equations for every value of ω. So the problem reduces to solving the linear matrix equation, for values of ω in the desired range

$$[A]\{p\} = [b] \tag{1.12}$$

where $A = K + i\omega C - \omega^2 M$. Equation (1.12) then can be solved by effective iterative methods [43, 44]. These equations are solved for each frequency of interest and the sound pressure level can be determined at any observation point. In the next example, we illustrate the how to solve the Helmholtz equation for a given geometry using FEM.

1.3.2.2. Example: Rectangular Model (2D)

Consider the rectangular model (2x1 m^2) shown in figure (1.9).
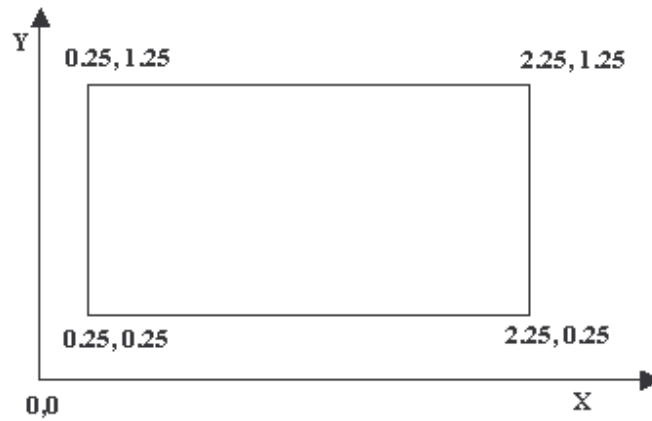
Fig. 1.9: 2D Rectangular Shaped Geometry

1.3.2.2.1.   Discretization and Basis Functions

Now if one meshes the rectangular model into 8 equal pieces (0.5x0.5 m^2), then the mapping would look like as follows (fig 1.10):
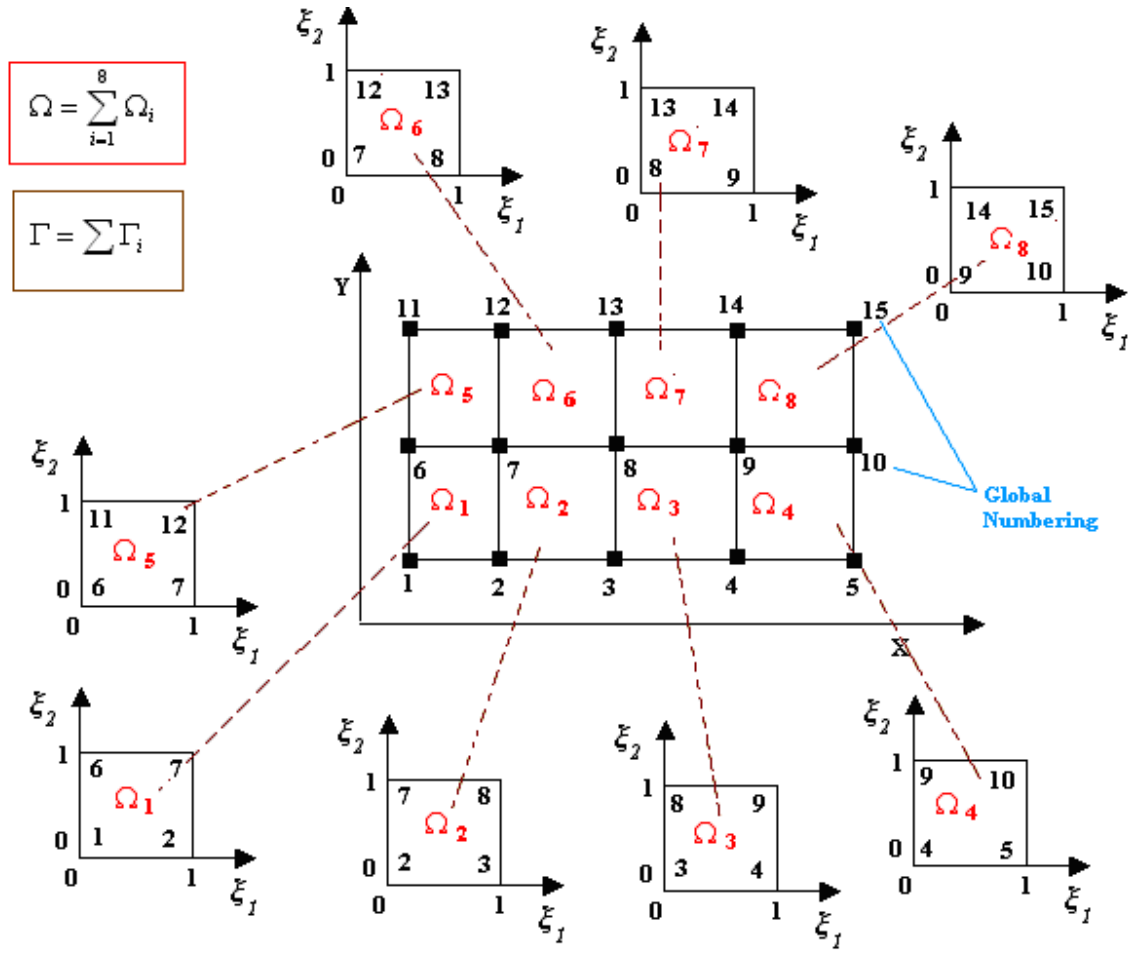
Fig. 1.10: Mapping of each element

Every element is numbered and mapped onto the mathematical space. Next if we take the linear 2D FEM element (fig 1.11) for Ω_i as also defined earlier, we have:

24
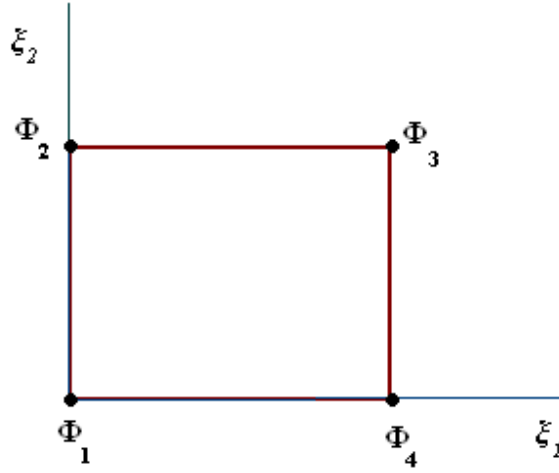
Fig. 1.11: 4-noded 2d element

where,

$$\Phi_1(\xi_1, \xi_2) = (1- \xi_1)\,(1- \xi_2), \qquad \frac{\partial \Phi_1}{\partial \xi_1} = -(1-\xi_2)\ ;\ \ \frac{\partial \Phi_1}{\partial \xi_2} = -(1-\xi_1)$$

$$\Phi_2(\xi_1, \xi_2) = (1- \xi_1)\,\xi_2, \qquad \frac{\partial \Phi_2}{\partial \xi_1} = -\xi_2\ ;\qquad \frac{\partial \Phi_2}{\partial \xi_2} = (1-\xi_1)$$

$$\Phi_3(\xi_1, \xi_2) = \xi_1\,(1- \xi_2) \qquad \frac{\partial \Phi_3}{\partial \xi_1} = (1-\xi_2)\ ;\quad \frac{\partial \Phi_3}{\partial \xi_2} = -\xi_1$$

$$\Phi_4(\xi_1, \xi_2) = \xi_1\xi_2. \qquad \frac{\partial \Phi_4}{\partial \xi_1} = \xi_2\ ;\qquad \frac{\partial \Phi_4}{\partial \xi_2} = \xi_1$$

1.3.2.2.2. Element Integrals

Now, going back to our integral (equation 1.5) which we want to solve:

$$-\int_\Omega (\nabla w.\nabla p)d\Omega + \int_\Omega (wk^2 p)d\Omega + \int_\Gamma (w\frac{\partial p}{\partial n})d\Gamma = 0$$

Now for a Galerkin formulation, we have:

$$w = \Phi_m$$

and for each Ω_j the pressure p can be expressed as $p = \sum \Phi_n p_n$

Moreover, if we take impedance boundary conditions (equation 1.7):

$$\frac{\partial p}{\partial n} = -\frac{i\rho\omega p}{Z}$$

the equation (1.5) becomes:

$$-\sum_i p_n \int_\Omega \left(\frac{\partial \Phi_m}{\partial x} \frac{\partial \Phi_n}{\partial x} + \frac{\partial \Phi_m}{\partial y} \frac{\partial \Phi_n}{\partial y} \right) d\Omega - i\omega \sum_i p_n \int_\Gamma \frac{\rho}{Z}(\Phi_m \Phi_n d\Gamma) + \omega^2 \sum_i p_n \int_\Omega (\Phi_m . \Phi_n) d\Omega = 0$$

$$\ldots\ldots \quad (1.13)$$

For 2 dimensional rectangle with 8 elements, the above domain integrals can be replaced by the sum of integrals taken over 8 elements:

$$\int_{0.25}^{1.25} \int_{0.25}^{2.25} (f) dxdy \;=\; \int_{0.25}^{0.75} \int_{0.25}^{0.75} (f) dxdy \;+\; \int_{0.25}^{0.75} \int_{0.75}^{1.25} (f) dxdy + \ldots\ldots\ldots \;+\; \int_{0.75}^{1.25} \int_{1.75}^{2.25} (f) dxdy$$

Now in the integrand, Φ_m and Φ_n are functions of ξ_1 and ξ_2, one needs to convert the derivatives with .respect to x and y to derivatives with respect to ξ_1 and ξ_2. This will basically map the integral onto ξ space.

So every integral can be mapped as follows:

$$\int_{y1}^{y2} \int_{x1}^{x2} (f) dxdy \;=\; \int_0^1 \int_0^1 (f) J d\xi_1 d\xi_2 \qquad (1.14)$$

where **J** is the Jacobian for the required transformation and the derivatives can be calculated using the chain rule:

$$\frac{\partial \Phi_m}{\partial x} = \frac{\partial \Phi_m}{\partial \xi_1} \frac{\partial \xi_1}{\partial x} + \frac{\partial \Phi_m}{\partial \xi_2} \frac{\partial \xi_2}{\partial x}$$

then equation 1.13 takes the form:

$$K_{mn}\, p_n + i\omega C_{mn} - \omega^2\, M_{mn}\, p_n = 0$$

Where, K_{mn} (stiffness matrix), C_{mn} (damping matrix) and M_{mn} (mass matrix) are:

$$K_{mn} = \int_{\Omega}\left(\frac{\partial\Phi_m}{\partial x}\frac{\partial\Phi_n}{\partial x} + \frac{\partial\Phi_m}{\partial y}\frac{\partial\Phi_n}{\partial y}\right)d\Omega, \quad C_{mn} = \int_{\Gamma}\frac{\rho}{Z}(\Phi_m\Phi_n)d\Gamma, \quad M_{mn} = \frac{1}{c^2}\int_{\Omega}(\Phi_m.\Phi_n)d\Omega$$

and m = 1, 2, 3, 4 and n =1, 2, 3, 4 for Ω_i.

Now we illustrate how to calculate these integrals using above mentioned rules.

For first element i.e. Ω_1,

$$K_{11} = \int_{\Omega_1}\left(\frac{\partial\Phi_1}{\partial x}\frac{\partial\Phi_1}{\partial x} + \frac{\partial\Phi_1}{\partial y}\frac{\partial\Phi_1}{\partial y}\right)d\Omega_1 = \iint\left(\left(\frac{\partial\Phi_1}{\partial\xi_1}\frac{\partial\xi_1}{\partial x}\right)^2 + \left(\frac{\partial\Phi_1}{\partial\xi_2}\frac{\partial\xi_2}{\partial y}\right)^2\right)|J|d\xi_1 d\xi_2$$

Substituting the earlier calculated linear 2d basis functions, we obtain:

$$K_{11} = \iint\left(4(1-\xi_2)^2 + 4(1-\xi_1)^2\right)\frac{1}{4}d\xi_1 d\xi_2 = \frac{2}{3},$$

similarly for $K_{12,}$ we obtain:

$$K_{12} = -\frac{1}{6}$$

And finally after calculating all the K_{mn}, we obtain the following 4 x 4 matrix :

$$K = \begin{bmatrix} \frac{2}{3} & -\frac{1}{6} & -\frac{1}{6} & -\frac{1}{3} \\ -\frac{1}{6} & \frac{2}{3} & -\frac{1}{3} & -\frac{1}{6} \\ -\frac{1}{6} & -\frac{1}{3} & \frac{2}{3} & -\frac{1}{6} \\ -\frac{1}{3} & -\frac{1}{6} & -\frac{1}{6} & \frac{2}{3} \end{bmatrix}$$

In the same manner, one can also calculate the element mass matrix for Ω_1. However, for the damping matrix, one needs to evaluate integral only at the boundary. Afterwards, the contributions of each of the element matrix is needed to be assembled into global stiffness matrix **K**, global damping matrix **C** and global mass matrix **M**.

Next, we start adding the contribution from Ω_1. It has global numbers 1, 2, 6, 7 and local number as 1, 2, 3, 4. So the contribution of Ω_1 into global **K** and **M** can be viewed as follows.
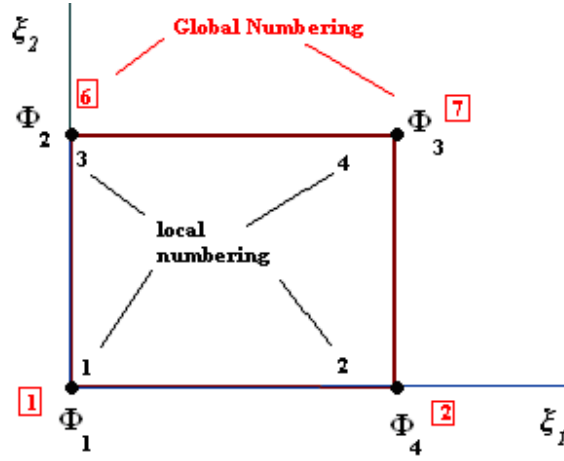
Fig. 1.12: Showing local and global numbering for Ω_1

K_{12} corresponds to global $\mathbf{K_{12}}$ whereas K_{13} corresponds to global $\mathbf{K_{16}}$. Similarly, K_{33} to $\mathbf{K_{66}}$ and so on. The matrix below further shows the addition of local stiffness matrix into global one.

$$[K]=\begin{bmatrix}
\left(0+\frac{2}{3}\right) & \left(0-\frac{1}{6}\right) & 0 & 0 & 0 & \left(0-\frac{1}{6}\right) & \left(0-\frac{1}{3}\right) & 0 & 0 & 0 & 0 & 0 & 0 & 0 & 0 \\
\left(0-\frac{1}{6}\right) & \left(0+\frac{2}{3}\right) & 0 & 0 & 0 & \left(0-\frac{1}{3}\right) & \left(0-\frac{1}{6}\right) & 0 & 0 & 0 & 0 & 0 & 0 & 0 & 0 \\
0 & 0 & 0 & 0 & 0 & 0 & 0 & 0 & 0 & 0 & 0 & 0 & 0 & 0 & 0 \\
0 & 0 & 0 & 0 & 0 & 0 & 0 & 0 & 0 & 0 & 0 & 0 & 0 & 0 & 0 \\
0 & 0 & 0 & 0 & 0 & 0 & 0 & 0 & 0 & 0 & 0 & 0 & 0 & 0 & 0 \\
\left(0-\frac{1}{6}\right) & \left(0-\frac{1}{3}\right) & 0 & 0 & 0 & \left(0+\frac{2}{3}\right) & \left(0-\frac{1}{6}\right) & 0 & 0 & 0 & 0 & 0 & 0 & 0 & 0 \\
\left(0-\frac{1}{3}\right) & \left(0-\frac{1}{6}\right) & 0 & 0 & 0 & \left(0-\frac{1}{6}\right) & \left(0+\frac{2}{3}\right) & 0 & 0 & 0 & 0 & 0 & 0 & 0 & 0 \\
0 & 0 & 0 & 0 & 0 & 0 & 0 & 0 & 0 & 0 & 0 & 0 & 0 & 0 & 0 \\
0 & 0 & 0 & 0 & 0 & 0 & 0 & 0 & 0 & 0 & 0 & 0 & 0 & 0 & 0 \\
0 & 0 & 0 & 0 & 0 & 0 & 0 & 0 & 0 & 0 & 0 & 0 & 0 & 0 & 0 \\
0 & 0 & 0 & 0 & 0 & 0 & 0 & 0 & 0 & 0 & 0 & 0 & 0 & 0 & 0 \\
0 & 0 & 0 & 0 & 0 & 0 & 0 & 0 & 0 & 0 & 0 & 0 & 0 & 0 & 0 \\
0 & 0 & 0 & 0 & 0 & 0 & 0 & 0 & 0 & 0 & 0 & 0 & 0 & 0 & 0 \\
0 & 0 & 0 & 0 & 0 & 0 & 0 & 0 & 0 & 0 & 0 & 0 & 0 & 0 & 0 \\
0 & 0 & 0 & 0 & 0 & 0 & 0 & 0 & 0 & 0 & 0 & 0 & 0 & 0 & 0
\end{bmatrix}$$

15x15 Matrix

28

So one can see in the above matrix (15x15) for 15 mesh nodes, initially all the elements were zero. Afterwards the values are added for Ω_1 at the respective global nodes i.e. 1, 2, 6, 7. For each Ω_i, one can calculate integrals and keep adding the contributions to the global matrices **K** and **M**. Similarly, one can calculate damping matrix for each Γ_i along with its impedance value and keep adding it to the global **C**. Finally these global matrices can then be solved for eigenmodes or transfer function using effective iterative methods. Physically, it means that every element is connected with other elements and there is flow of sound energy between nodes. The contribution of energy from each of the individual elements is calculated and assembled in the final system matrix at their associated location nodes. This system matrix contains the interaction information between these nodes. This matrix can then be solved to calculate the sound pressure level at these nodes.

1.3.2.2.3.   Assembly and Gaussian Quadrature

Due to a large number of elements, it is practically impossible to evaluate and assemble manually all local stiffness and mass matrices into global matrices, one can make use of data processing array (DPA). DPA keeps tracks of global number associated with each of the local node and would help in assembling the matrices. Furthermore, it is also practically impossible to evaluate the integrals K_{mn} and M_{mn} manually for large number of elements. In most real world problems the mesh could contain thousands of elements. Hence, a numerical integration scheme has to be used. Gaussian quadrature [45] is one such reliable scheme. One can approximate the integral for a given function $f(x)$, using Gaussian points as follows:

$$\int_{-1}^{1} f(x)dx \cong \sum_{i=1}^{N} W_i f(x_i)$$

where, W_i are the weights associated with points x_i and N denotes the number of Gaussian points chosen. For the list of gauss- legendre weights and associated sample gauss points one can see the table [Appendix A].

The pseudo code (fig. 1.13) further summarizes the above mentioned methodology. As written in the pseudo code, first a suitable Gaussian scheme is defined using *GaussQuadrature* function. The function returns the number of *GaussPoints* , weights and corresponding sample points array. Afterwards, one element at a time is read from already generated mesh using *fscanf* function. All the coordinates for element are arranged according to their local numbering as 1, 2, 3,..N. *CoordinateArray* variable stores the x, y, z coordinates of each node in the element and *DPA* is a data processing array storing the corresponding global number of each node.

Now for the element under consideration, the local stiffness and mass matrix is calculated using the earlier defined Gaussian scheme. Jacobian, basis functions and their derivatives are evaluated at each gauss sample point and are accordingly assigned as they are defined for stiffness and mass matrices.

Finally after obtaining the element stiffness/mass matrix, each of its entry values are added to global stiffness/mass matrices at locations calculated using DPA.

```
GaussPoints= GaussQuadrature(GaussPoint, Weight);

For each element in the mesh, do
{
   For each node i in the mesh element, do
   {
      fscanf(MeshData, "%lf %lf %lf %d\n", &CoordinateArray[i][0], &CoordinateArray[i][1],&CoordinateArray[i][2]
      &Dpa[i]);
   }
         // Evaluating integrals:

   For each Gauss Point, do
   {

        DefineBasisFunctions( BasisFn, DerBasisFn, GaussPoint );

        CalculateJacobian(CoordinateArray, DerBasisFn, Jacobian);

        CalculateIntegrandStiff( DerBasisFn, localStiff, Weight, Jacobian );

        CalculateIntegrandMass(BasisFn, localMass, Jacobian, Weight );

   }
      //Assembly starts here :

   For each local number (row), do                    //Local Node Numbers
   {
         For each local number (column), do           //Local Node Numbers
         {
            GlobalStiffnessMatrix[ Dpa[local1] ][ Dpa[local2] ] += localStiff[local1][local2];
            GlobalMassMatrix[ Dpa[local1] ][ Dpa[local2] ] += localMass[local1][local2];

         }
   }
}
```

Fig. 1.13: Pseudo Code

Similarly for each boundary mesh elements, one can follow the same procedure as mentioned above to calculate the global damping matrix. One thing to observe is that the matrix size could be large and most of the elements in the matrix are zero. Therefore, to store large sparse matrices effectively, compressed storage formats (CSR) are used. For instance, one can store only the non-zero entries in one matrix and the associated row-column indices in another matrix.

1.3.3. Boundary Element Method

1.3.3.1. Mathematical Formulation

The first step in the mathematical formulation of the BEM is to convert the differential equation governing the problem into a boundary integral equation/value problem [54]. We again start with the Helmholtz equation in frequency domain:

$$\nabla^2 p(r) + k^2 p(r) = 0, \qquad r \in \Omega \qquad (1.15)$$

where k is the wavenumber and p denotes the pressure at position r belonging to Ω.

Before trying to solve any problem using BEM, one needs to have the fundamental solution G (also called the freespace Green's function) of the problem. Next, similar to FEM, we form an integral from the Helmholtz equation by using a weighted residual method as follows:

$$\int_\Omega G(r; r_0)(\nabla^2 p(r) + k^2 p(r)) \ d\Omega = 0 \qquad (1.16)$$

The fundamental solution of a particular equation is the weighting function that is used in the boundary element formulation of that equation. It is therefore important to be able to find the fundamental solution for a particular equation. The Greens function for Helmholtz equation is given by [54]:

$$G(r_i, r_j) = \frac{i}{4} H_0^{(1)}(kr) \quad (2D)$$

$$G(r_i, r_j) = \frac{e^{-kr}}{4\pi r} \qquad (3D)$$

where $H_0^{(1)}$ is the Hankel function of first kind of order zero and r is the distance between points r_i and r_j.

Applying the Green-Gauss divergence theorem, equation (1.16) becomes:

$$c(r_0)p(r_0) + \int_\Gamma \frac{\partial G(r; r_0)}{\partial n} p(r)d\Gamma(r) - \int_\Gamma G(r; r_0)\frac{\partial p(r)}{\partial n}d\Gamma(r) + p_{in}(r_0) = 0 \qquad (1.17)$$

where

$$c(r_0) = \begin{cases} 1, r_0 \in \Omega \\ 0.5, r_0 \in \Gamma \end{cases}$$

One can notice that equation 1.17 contains only boundary integrals and no domain integrals as in FEM, hence called as boundary integral equation. Thus we solve for the boundary first and volume data can be obtained as a next separate step.

Next we divide the boundary into boundary elements, where each element has a center node representing a field quantity (here pressure) of the element. The surface Γ can then be expressed as follows:

$$\Gamma = \bigcup_{j=1}^{N} \Gamma_j$$

So the equation (1.17) is transformed into algebraic system of equations with relation to the center node quantity $p(r)$ and $\partial p(r)/\partial n$.

$$c(r_i)p(r_i) + p_{in}(r_i) + \sum \left\{ \int_{\Gamma_j} \frac{\partial G(r;r_i)}{\partial n} d\Gamma(r) \right\} p(r_j) = \sum \left\{ \int_{\Gamma_j} G(r;r_i) d\Gamma(r) \right\} \frac{\partial p(r_j)}{\partial n} \quad (1.18)$$

where, p_{in} represents the pressure of the incident wave.

1.3.3.2. Element Integrals

The integrals in equation 1.14 can be evaluated numerically. Gaussian quadrature is one such very widely used and reliable numerical integration scheme.
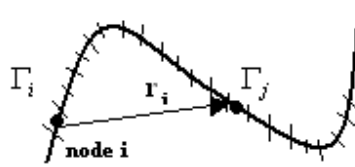
Fig. 1.14: Meshed 2D Surface

One can observe that, if the node point i is well removed from Γ_j standard Gaussian quadrature can be used. However if it lies within Γ_j, then as r_i approaches zero, the fundamental solution G tends to ∞. Therefore the integrand can become singular. Therefore, adaptive quadrature schemes [45, 61, 62] should be used to evaluate the integrals as the integral values are largest in magnitude in such cases and have the most influence in the results.

1.3.4. Comparison between FEM and BEM approaches

In this section, we briefly compare FEM and BEM approaches. First from the discretization point of view, FEM needs whole volume to be dicretized whereas in BEM the equations are

defined over boundary, hence only the boundary needs to be discretized. Therefore, the complexity associated with generating mesh for arbitrary enclosures is more for FEM. However, BEM mostly assumes the domain to be homogenous due to difficulties associated with finding a fundamental solution (Green's function). So the variations in the interior of domain if any can be modeled by FEM more effectively. Moreover, after discretization the evaluation of some element integrals for BEM require special attention as the integrand can become singular. For FEM, for every element, any quadrature scheme with sufficient number of gauss points can be employed. The final matrices are sparse, symmetric and large in FEM but small, asymmetric and highly dense in BEM. Storage requirement is lesser for BEM but again effective solvers are needed to solve the BEM matrix. After solving, the solution is obtained everywhere in FEM whereas in BEM the solution is obtained at the boundary first, and as a second step the solution can be obtained on the whole domain.

A brief overview of FEM and BEM is once again provided in the table (1.1). It is worth to note that while BEM is quite effective for exterior problems involving infinite homogenous domain, FEM is more adaptive and reliable for interior problems involving fluid structure interactions. As it is difficult to model exterior infinite sized domain using FEM, for scattering behavior calculations in chapter 4, we have chosen BEM.

	FEM	**BEM**
Discretization / Mesh	Whole volume needs to be meshed.	Only the boundary needs to be meshed. Hence avoiding the complexity involved with meshing complex 3d geometries.
Evaluation of Element Integrals	Easy to evaluate.	Special quadrature schemes required.
Storage (Matrix Size)	Matrix is large but sparse and symmetric. Therefore, easier to solve.	Final Matrix is small but dense and highly asymmetric.
Solution	Solution on entire domain is obtained.	Solution on the boundary is obtained first.
Approximations	Differential equation is approximated.	Boundary conditions are approximated.
Applicability	Can be applied to non-linear problems as well.	Cannot even solve all linear problems due to difficulties associated with finding a fundamental solution.

Table 1.1 Comparison between FEM and BEM approaches

In the next section, as meshing is integral part of both FEM and BEM, we shortly describe the state of existing meshing algorithms for FEM and BEM applications.

1.3.5. Meshing Algorithms: State of the Art

An important and difficult step in numerical computation using FEM and BEM is to find a proper discretization of a continuous domain. The process of dividing the domain into small and simpler elements like triangles and quadrilaterals in 2D and tetrahedrals [25, 26], and hexahedrals [27, 28, 29] in 3D is called mesh generation. As described in the previous sections, once we have a discretization or "mesh", differential equation for sound wave is then approximated by finite element or boundary element formulations. Discretization errors depend on the geometric shape and size of the elements while the computational complexity for finding the numerical solution depends on the number of elements in the mesh and often the overall geometric quality of the mesh as well. Generally speaking, for good quality mesh elements should not have edges creating flat (~180°) or sharp angles (~ 0°) internally (fig. 1.15a, 1.15b). For a mesh to be useful in approximating partial differential equations, it is necessary that the basis/shape functions generated from the mesh are capable of approximating the solutions required. After every meshing algorithm, some post-processing steps like smoothing and clean up etc. are required to improve the overall quality of the mesh [30, 31, 32]. In the end, sometimes mesh refinement is needed to achieve the desired resolution [33].
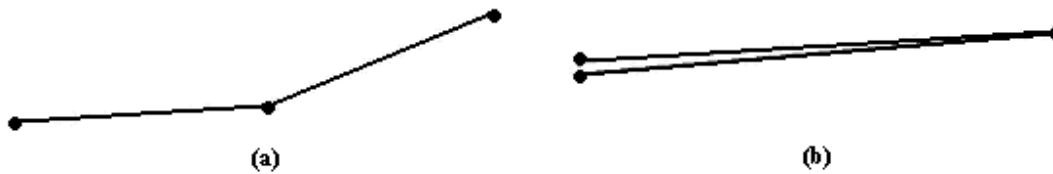

Fig.1.15a: Edges creating Flat Angle ; 1.15b: Edges creating Sharp Angle

The most general and versatile mesh is an unstructured triangular mesh in 2d and tetrahedralization in 3d. Such a mesh is simply a triangulation of the input domain (e.g., a polygon), along with some undesired extra vertices, called Steiner points [34]. Octree decomposition, Delaunay approach, advancing front methods are some of the algorithms available for triangulations and tetrahedrons [25, 35, 36, 37]. The Octree technique was primarily developed in the 1980s. With octree method, cubes containing the geometric model are recursively subdivided until the desired resolution is reached. The most popular of the triangle and tetrahedral meshing techniques are those utilizing the Delaunay criterion. The Delaunay criterion states that any node must not be contained within the circumsphere of any tetrahedra within the mesh. A circumsphere can be defined as the sphere passing through all four vertices of a tetrahedron. In advancing front method, the tetrahedra are built progressively inward from the triangulated surface. An active front is maintained where new tetrahedra are formed. However, hexahedrals are preferred over tetrahedrons as they avoid flat and sharp angles hence better mesh quality can be obtained. Obtaining an automated hexahedral mesh generator is a major bottleneck in the field of computational geometry. Dividing the domain automatically into hexahedrals is not an easy task. Many approaches have been suggested like Plastering [38],

advancing front method [26], octree decomposition [35], shrinking mapping method [29], medial surface subdivision [27, 28] etc. But no approach so far guarantees the automatic hexahedral mesh generation of the whole domain. In other words, no mathematically sound procedure for obtaining the 'best' mesh generation is currently available. The criteria are usually based on commonsense rule.

In this work, we introduce a new meshing approach called "cutting plane algorithm" to obtain automated hexahedral meshes for room acoustics models. This new meshing approach is inspired by Chazelle [24]. Chapter 2 provides a detailed explanation of cutting plane algorithm and its practical feasibilty in architectural designs is investigated.

1.4.   SCOPE OF THE THESIS

In this thesis, we have investigated both BEM and FEM approaches to extend the sound particle model at low frequencies. As the mesh generation is an integral part of both the approaches and it is very difficult to obtain a good quality mesh, in this work a new meshing algorithm called "cutting plane algorithm" to obtain hexahedral mesh elements has been developed.

This thesis is organized as follows. After having introduced the theory behind meshing elements, chapter 2 gives the introduction and description of new meshing algorithm to discretize the geometry into hexahedral elements. We will explain using real life indoor room models how one can obtain a quality mesh especially suited for architectural surfaces using our newly developed cutting plane algorithm. Chapter 3 provides a detailed FEM analysis of how to obtain eigenmodes and transfer function in rooms. Needless to say that for FEM meshing purposes, we have applied our own mesh generation algorithm discussed in chapter 2. Chapter 4 gives an overview of how one can investigate the scattering behavior of incident plane waves using BEM. Chapter 5 concludes the thesis along with future directions.

2. CHAPTER

A New Meshing Approach: Cutting Plane Algorithm for Architectural Designs

2.1. INTRODUCTION

In this chapter we introduce a new scheme called "cutting plane algorithm" (based on cutting the polyhedron) in order to obtain an all hexahedral mesh. Though our approach can be applied to other fields as well, we have given more considerations to room acoustics indoor models. We demonstrate how one can obtain good quality mesh especially suited to architectural designs using our approach. A good quality mesh element (in physical space) is one which is close to its FEM element (in mathematical space). For instance, a hexahedral mesh element is best if all the angles are close to 90°. In room acoustic models with plane walls, most of the edges lie in all three perpendicular directions therefore quite useful and desired for hexahedral mesh generation. A mesh generation software is written using the cutting plane algorithm and the results are presented in this work.

The cutting plane algorithm is inspired by the idea proposed by Chazelle [24]. It has been shown by Chazelle that the worst case time for obtaining $O(N^2)$ convex polyhedrons from a polyhedron without holes is $O(nN^2(N+\log n))$, where n and N designate respectively the size of the input and the number of reflex angles or notches into the polyhedron. Reflex edges/Notches are the edges whose adjacent faces make an interior dihedral angle greater than 180 degree with each other. Furthermore, it is also mentioned by Chazelle that repeating the cutting process on each remaining non-convex parts will eventually produce a convex decomposition in a finite number of cuts.

In this approach, apart from cutting notches, we are removing multivalent vertices (valence greater than three) as well. The *valence* of a vertex is defined as the number of edges connected to it. This would further increase the worst case time calculations. We do not perform its worst case calculations but as a first step, our main emphasis is to investigate its practical applicability in architectural designs. Here we include more degenerate cases which are not explained in [24]. As mentioned by B. Joe [25], it is more important to obtain better shaped convex polyhedrons, hence much consideration has been given to it in this work.

First we describe the general methodology of the meshing procedure using the cutting plane algorithm and then we illustrate our algorithm using indoor room examples. We explain in detail how one can cut the polyhedron into two polyhedrons along a defined cutting plane. Afterwards, we show that with the proper choice of the cutting plane one can reduce the number of cuts and good mesh quality can be obtained as well. Finally, for rooms with too many curved surfaces and dome-like structures requiring too many cuts to generate simple polyhedrons, a new scheme called projection technique is proposed. It is shown that after obtaining convex polyhedrons, the

projection algorithm can also be applied directly on some polyhedrons to further subdivide the polyhedron.

2.2.   CUTTING PLANE ALGORITHM

The cutting plane algorithm is based upon applying a series of cuts on a complex shaped geometry along certain defined directions and notches until one obtains only simple shaped trivalent and convex bodies. After this cutting procedure, we use the mid-point subdivision scheme to obtain an all-hexahedral mesh. We are applying a series of cuts because the mid-point subdivision scheme can result into all hexahedrons only if the body is convex and all the vertices are trivalent. So the first series of cuts is to obtain all convex shaped geometries [25]. The second series of cuts is to ensure all vertices are trivalent. After that, it is also cut based upon the aspect ratio of the elements as elements should not be very thin or elongated. First, we describe the general methodology used in the cutting plane algorithm and then we shall explain each step in detail.

Any architectural closed space can be treated as a polyhedron of arbitrary shape. As it is very difficult to obtain an automated mesh for complicated shapes, the cutting plane algorithm aims at reducing the complexity of the original polyhedron by applying a series of cuts unless one obtains only simple shaped polyhedrons. Two of such complexities which the cutting plane algorithm tries to remove are:

1. Notches / Reflex Edges : Edges whose adjacent faces make an interior dihedral angle greater than 180 degree with each other are called notches or reflex edges. In the illustration (figure 2.1a), one can see there is one such notch edge (marked with thick/bold line). The algorithm to detect a notch in a given polyhedra is mentioned in Appendix B.
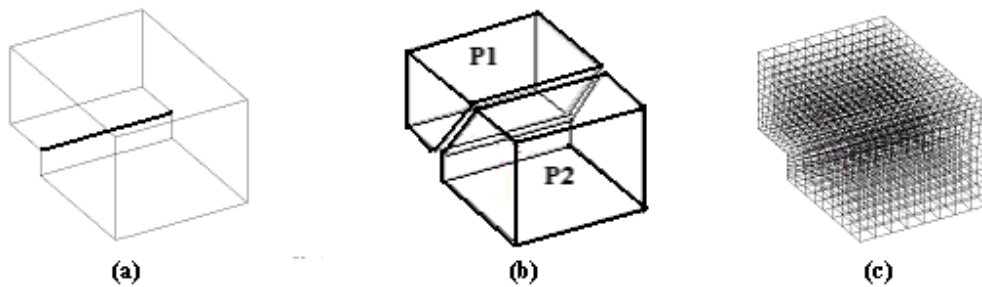

Fig. 2.1a: L-Shaped room; 2.1b: Notch Cut ; 2.1c: MPS

A cut is defined to be the procedure of cutting the polyhedron along such notches so as to remove the concavity in the geometry. For example, figure 2.1b shows two polyhedrons (**P1** and **P2**) obtained after cutting along the notch.

2. Multivalent Vertices: Next, one should observe that even after cutting notches, we might not be able to obtain all trivalent polyhedrons. For example, see figure 2.2a. Here the topmost vertex is four-valent. Hence we need to find some routine to decrease the valence of such vertices. For

such multivalent vertices, valence can be decreased by cutting along two adjacent edges such that at least two other adjacent edges are on the opposite side of the cutting plane. See figures 2.2b and 2.3a.
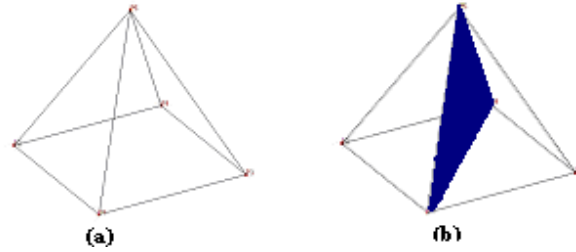

Fig 2.2a ; 2.2b

Now the topmost vertex is 3-valent in both polyhedrons.

Fig 2.3a ; 2.3b
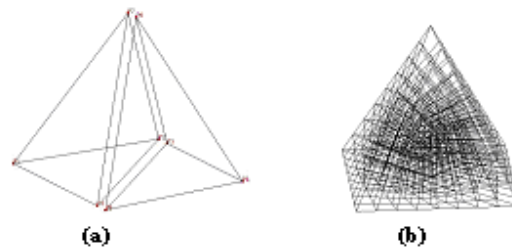
Now, after having removed these two complexities in the original geometry, one would obtain convex and trivalent polyhedrons. In the next step we further subdivide them using the midpoint subdivision approach [39] as shown in figures (2.1c, 2.3b). For example consider the shoebox model as shown in figure 4a.
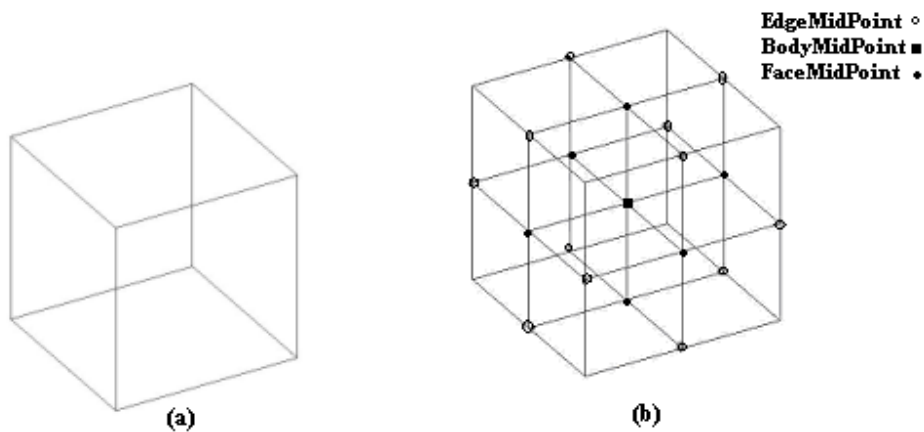

Fig. 2.4a: Shoebox Model ; 2.4b: Illustration of Mid-Point Subdivision scheme.

First, one needs to calculate the body-mid point of the geometry. Then for each face and edge, the face mid-point and edge mid-point are required. Afterwards for each vertex *v*, one has to find its three adjacent faces (trivalent) and join the corresponding face midpoints with the body midpoint and edge mid points. In the example (fig.2.4b), it is shown that 8-vertices shoebox model results into 8 hexahedrons of half side length. Similarly one can perform midpoint subdivision for any convex and trivalent polyhedron. For any such polyhedron with *n* vertices, one obtains the same number of hexahedrons.

After obtaining hexahedrons, one can keep applying the same scheme on each of the obtained polyhedron until the desired resolution has reached. One important thing to note here is that, shapes propagate in this scheme. If we start performing on perfect hexahedral, we will be obtaining all perfect hexahedrons and the same way if the initial polyhedron is not well shaped, one can expect to obtain the bad shaped hexahedral elements accordingly.
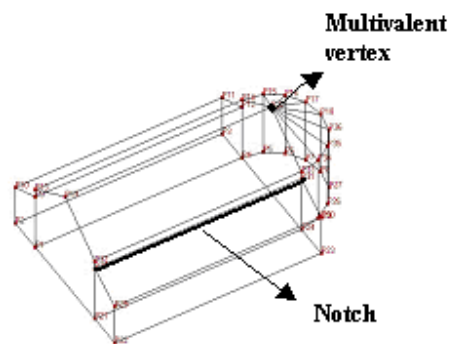

Fig. 2.5: Combination of Notches and multivalent vertices

Generally speaking, in any complex shaped rooms there are many notches or multivalent vertices or combinations of both (fig. 2.5). As mentioned before, shapes propagate in midpoint division scheme. Therefore in order to ensure that one obtains well-shaped elements, it is essential to define proper cutting schemes and algorithms involving decision-making as in which notch is better to cut first, which cutting plane to be chosen and so on. In the later parts [section 4] of this chapter, we will show using examples how the predetermined choices of cutting schemes can provide better shaped elements with a minimum number of cuts. For instance, it will be shown that balconies or stairs which are very typical in a room are actually nothing but continuous and consecutive notches and these can be removed by a single cut. Hence the number of cuts can also be reduced with the proper choice.

The chart (fig. 2.6) further explains the basic methodology adopted for mesh generation using the cutting plane algorithm. The cutting plane algorithm starts with examining the geometry type of the given room. Firstly, on the basis of geometry, it suggests some initial cutting directions. For instance, removing consecutive notches all at once or resolving some specific room structures like domes, stairs, holes, pillars etc. If initially one does not treat them in a proper manner, a random cutting scheme could destroy their identity and create badly-shaped polyhedrons. Furthermore, one can also make use of the symmetric nature of the geometry. This part we shall explain more in detail with examples later.

So first we cut the polyhedron along those predetermined specific cuts. Secondly, we check the notches one by one and remove them. Then in the third step, we remove multivalent vertices one by one. Fourth step is mainly to check and cut to improve aspect ratio of elements (needed only if the elements are stretched or elongated) and then finally in the fifth step, the simple shaped polyhedrons are meshed using midpoint division scheme to obtain a hexahedral mesh.

```
                    ┌─────────────────────────┐
                    │   Polyhedra / Enclosure │
                    └─────────────────────────┘
                                 │
                                 ▼
                 ┌───────────────────────────────┐
                 │ 1. Examine, Suggest Scheme, Cut│
                 └───────────────────────────────┘
                           │        ┌─────┐
                           ▼ ◄──────│ CUT │◄──────┐
                                    └─────┘        │
                       ╱─────────────────────╲     │
                      ╱                        ╲ YES│
                     ╱   2. Check for Concavity  ╲──┘
                      ╲                        ╱
                       ╲─────────────────────╱
                           │
                        NO │        ┌─────┐
                           ▼ ◄──────│ CUT │◄──────┐
                                    └─────┘        │
                       ╱─────────────────────╲     │
                      ╱                        ╲ YES│
                     ╱  3. Check For Multi-Valence╲─┘
                      ╲                        ╱
                       ╲─────────────────────╱
                           │
                        NO │
                           ▼
                 ┌───────────────────────────────┐
                 │     4. Aspect Ratio Cuts       │
                 └───────────────────────────────┘
                                 │
                                 ▼
                 ┌───────────────────────────────┐
                 │    5. Mid-Point Subdivision    │
                 └───────────────────────────────┘
                                 │
                                 ▼
                 ┌───────────────────────────────┐
                 │        Hexahedral Mesh         │
                 └───────────────────────────────┘
```
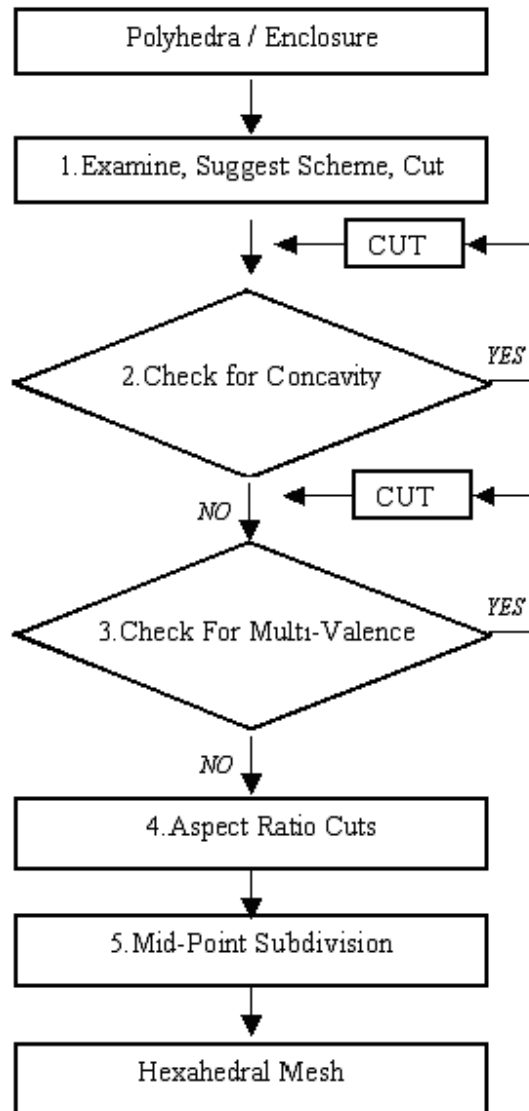
Fig. 2.6: Chart

Here, one can observe that the main algorithm is the cut procedure. No matter whether it is cutting specific notches, normal notches or multivalent vertices, the basic cut procedure is the same for all of them only the definition of cutting plane changes. Hence, in the next section we

will describe mathematically, how one can cut the polyhedron P into two parts namely **P1** and **P2** and how the cut procedure works.

2.2.1. Cutting Procedure

In this section we shall explain the basic mathematical background and algorithms used in the cutting plane algorithm. One can classify the cutting procedure in three phases or cutting sequences priority wise as follows:
1. Examining and Suggesting Predetermined Cuts.
2. Cutting Notches.
3. Cutting Multivalent vertices.

The pseudo code for the first series of cuts is shown below (fig.2.7):

```
Total_No_Polys =1

for i = 1 to Total_No_Polys, do
{
   Check=Examine_Suggest (PolyList, CuttingPlane, i) ;
   If Check equals 1, do
   {
       Cut_Poly( PolyList, P1, P2, CuttingPlane, i );

       AssignToPolyList (P1, P2, PolyList, i,
       Total_No_polys);

       UpdateAdjacentPolys(PolyList, i,Total_No_Polys);

       Total_No_Polys = Total_No_polys +1;
   }

}
```

Fig. 2.7

The first objective is to examine the geometry and suggesting some specific cuts which would ease the overall cutting procedure. This basically means identifying typical room elements like balconies, domes etc. and defining cutting scheme especially suited and reducing the number of cuts for such structures. Therefore, the algorithm tries to identify such elements and suggests specific edges to be cut initially.

In the pseudo code above, first the given polyhedron is assigned to an array of PolyList at zero index. Then the PolyList is examined using the Examine_Suggest function one by one. If the function returns the value one, it means that specific cuts are required and the Cut_Poly routine is called to cut the polyhedron into two pieces (**P1** and **P2**) along the defined cutting plane. Then **P1** and **P2** are assigned to the PolyList. After that, the adjacent polyhedrons affected (if any) due to the cut are updated at common intersection boundaries with edges or nodes so as to maintain the same number of nodes at common faces. This will be explained clearly using an illustration in next sections. Then the same algorithm continues for all of the polyhedrons in the PolyList unless one requires no specific predetermined cuts for any of the polyhedrons.

Afterwards, the similar cutting procedure for removing remaining notches is performed (fig 2.8).

```
for i = 1 to Total_No_Polys, do
{
 Check=Notch_Detect(PolyList, CuttingPlane, i);
   If Check equals 1, do
   {
       Cut_Poly( PolyList, P1, P2, CuttingPlane, i );

       AssignToPolyList (P1, P2, PolyList, i,
       Total_No_polys);

       UpdateAdjacentPolys (PolyList, i,Total_No_Polys);

       Total_No_Polys = Total_No_polys +1;
   }

}
```

Fig. 2.8

As one can see the basic pseudo code is the same for the notch-cutting procedure. All the polyhedrons in the PolyList are now checked for remaining notches. Notches are detected using the Notch_Detect function and a cutting plane is defined. The polyhedron is cut along the plane and the two obtained polyhedrons are assigned to the PolyList. After updating the adjacent polyhedrons again the procedure keeps on cutting unless only all convex polyhedrons remain.

Similarly then, for the multivalent cuts, using the Multivalent_Detect function, multivalent vertices are identified and then the cut procedure is followed in a similar manner unless one obtains all trivalent polyhedrons.

In the above written pseudo codes (fig 2.7, 2.8), the Cut_Poly function is the most difficult part to compute because it requires several other algorithms to calculate vertices and the face-to-edge list of newly obtained polyhedrons (**P1** and **P2**) after every cut. Hence, it is the major part of the algorithm. Once we clearly define this function incorporating all the degenerate cases, one can keep applying this function on any polyhedron with the desired cutting plane along any edge. Next, we provide an overview of the algorithm to explain how one can obtain two polyhedrons using the Cut_Poly function.

2.2.1.1. Description of Cut_Poly function

We have implemented and added new algorithms to solve more degenerate cases in order to obtain **P1** and **P2**. Regarding notations, we have tried to follow the same terminology for and definitions as introduced in [24]. We will explain them shortly here.

Every polyhedron can be represented using these three data structures:

1. Face to edge list: Sequence of vertices for each face in a consistent proper order (clockwise / anticlockwise)
2. Edge to face list: List of two adjacent faces for each edge.
3. Adjacency list: List showing connectivity of each vertex with others.

42

Our aim in this section is to compute face to edge lists of polyhedrons (**P1** and **P2**) obtained due to cuts. Afterwards, remaining two lists (Edge to face list and Adjacency list) can be obtained from it easily. Next, we list some more definitions which we need in order to understand our cutting procedure.

1. Cutting Plane **T**: plane defined along the notch to be cut.

2. Cut : procedure of cutting the polyhedron.

3. Cut Face **S** : is the unique face obtained for each cut and is common to **P1** and **P2.**

4. Maximum: maximum is the closed loop/boundary which is not contained inside any other loop/boundary.

5. Adj(q): the list storing the vertices adjacent to q.

Let us assume that we are trying to cut the notch **g**, whose adjacent faces are f_1 and f_2. The unique face containing **g** and shared by **P1** and **P2** is called the cut face **S**. One can divide the Cut_Poly function into several steps. We shall explain them shortly one by one.

a) For each Face finding those edges which are cut.

The very first objective is to calculate the list of edges being cut by the cutting plane **T**. This can be calculated easily using plane and line segment intersection algorithms.

For each face of the polyhedron, those edges are added in the list which are cut by the plane. Then we arrange the intersection points pair-wise along the plane in a pair-wise sequence. Consider the face F_j with two holes (fig. 2.9a),
The cut pair set becomes :

$$A_j = \{(a1, a2), (a3, a4), (a5, a6)\}$$

Next, we define:

$$U = \{A_1, A_2, ... A_n\}$$

where, A_i is cut pairs list for i^{th} face number and n is the number of faces.

Basically the set U contains the list of all the cut pairs for each face which is cut by the cutting plane. In a more general sense, this pairing explains which vertex is connected to which one and that there is no air/hole between these two vertices. For example in fig. 2.9a, a1 is connected to a2 but a2 is not connected to a3 as there is a hole/air between them.
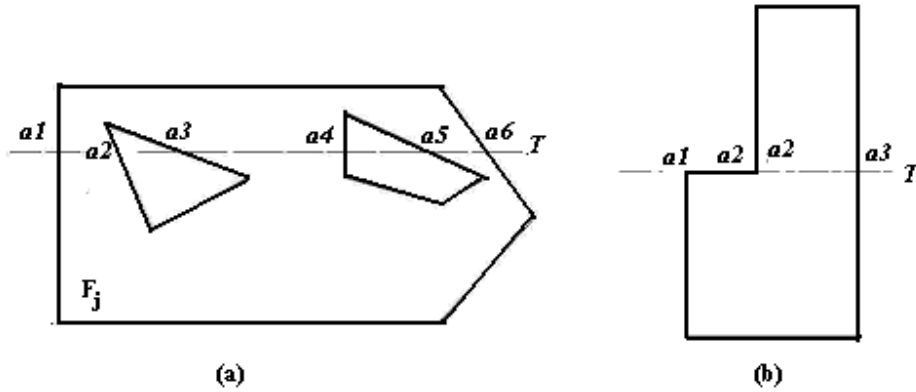
43

Fig. 2.9a ; 2.9b

When the plane passes through the edge, we may end up having an odd number of points in the face.

Consider for example, the face (fig 2.9b): here there are only 3 points through which the cutting plane is passing. To handle this, we introduce the concept of duplicating vertices. Here we duplicate the middle vertex and the cut pair set for the face becomes:

$$A_j = \{(a1, a2), (a2, a3)\}$$

This duplicate vertex will help in determining the Cut Face **S**. The idea behind duplicating is to ensure the connectivity of a2 with a1 and a3 both. One thing to note is that not all vertices lying on the cutting plane have to be duplicated.
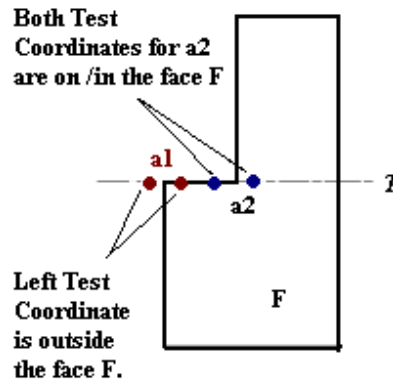
Fig. 2.10

We duplicate only those vertices lying on the cutting plane, for which if we take two test coordinates at small epsilon distance ($\varepsilon > 0$) from the vertex on both sides (left and right) along the plane **T**: either it should lie in or on the Face. Figure 2.10 shows that only two vertices a1 and a2 are lying on **T**. Out of these two, only a2 can be duplicated as a1's left coordinate is outside the face. Any test coordinate should not be outside the face. Consider the case in face (fig. 2.11).

44

Here only p2 and p5 need to be duplicated. P1 and P4 cannot be duplicated as if one takes a test coordinate in left side it will be outside the face. Therefore, the cut pair sequence becomes:

$$A_j = \{(a1, a2), (a2, a3), (a4, a5), (a5, a6)\}$$

Note that we actually do not duplicate the vertex, rather we just added it twice to the A_j list to maintain the connectivity between vertices.
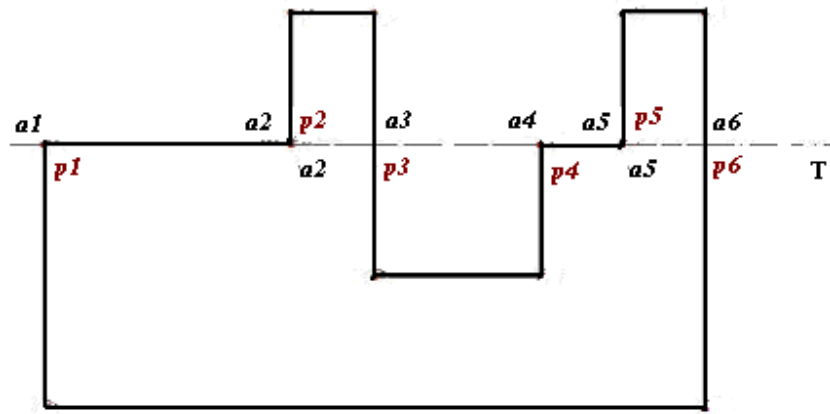
Fig. 2.11

b) *Finding the Cut Face S, the face generated due to cut and common to P1 and P2.*

The cut face **S** is the unique face obtained for each **cut** (Fig. 2.12) and is common to **P1** and **P2**.
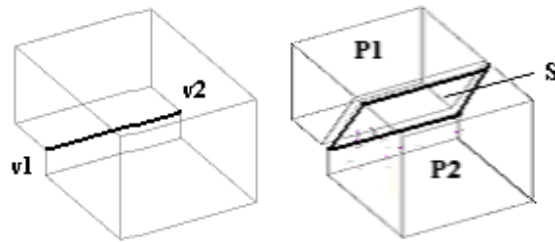
Fig. 2.12

The cut face **S** is comprised of outer and inner boundaries. Inner boundaries are obtained when the polyhedron has a hole and the cut is passing through it. Next we explain the algorithm used to calculate this cut face **S** for any notch cut.

To start with, we take the notch edge which is being cut. It has two end vertices say v1 and v2. Now, the initial vertex in **S** is v1, and we look for another pair from the U list which has one vertex as v1 and the other is not v2 . Say this *next vertex* is v3. Now, we again search for the pair having v3 and not v2. This way we keep on following all the pairs unless we end up having v2 as our last vertex. Every boundary forms a closed loop so the search ends at the starting notch edge.

45

Therefore the boundary S* becomes:

$$S^* = (v1 - v3 - v4 - v5...........vn - v2)$$

And this forms the outer boundary **S*** of the cut face **S**.

Now we come to the calculation part of inner boundaries of **S**. First of all we determine all the inner closed loops/boundaries present in **S** and then we discard those which are not maxima. A maximum is the closed loop/boundary which is not contained inside any other loop/boundary. We follow the same procedure as used for **S***. First we check if all the new vertices created are all exhausted. If not, we take any edge pair which is not in **S***. Then we perform the same calculation with this pair as v1 and v2 to obtain a closed loop. After this, we again check if all the new vertices are exhausted. At last we have all the closed loops. Then, if any loop is inside any other closed loop, we discard it as it cannot be a maximum. In the end we have only maxima and **S*** which comprises our **S**.

See the figure (2.13a, 2.13b). It is a polyhedron with a hole and a block is coming out it. If one cuts along the notch (p7-p18) marked by a bold thick line as shown in figure 14a, the Cut Face **S** will look like in fig.14c. Here one can see that there are initially two inner boundaries obtained due to cut inside **S*** (fig. 2.14b), but only the maximum was taken for **S** (fig. 2.14c).
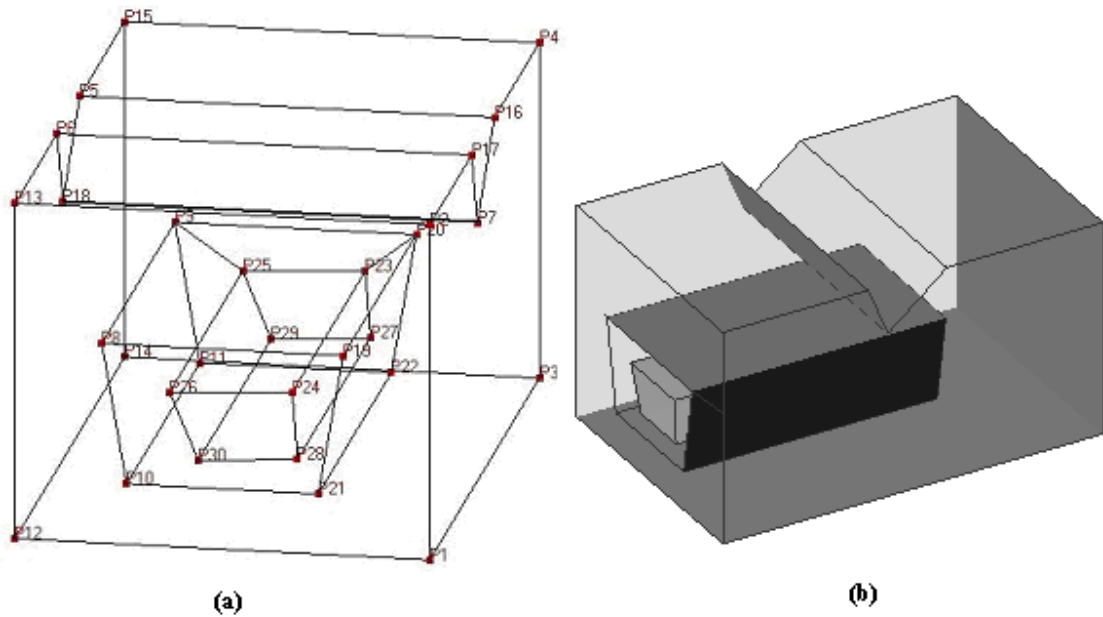
Fig. 2.13a: Model containing a hole; 2.13b: 3D Shaded Model
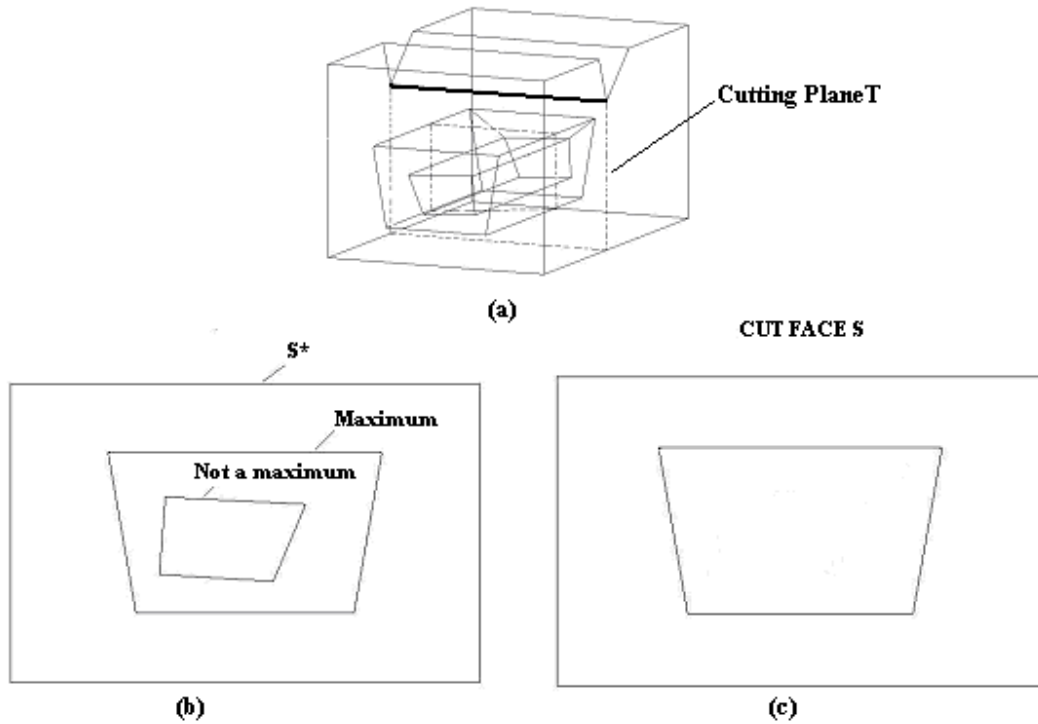
Fig. 2.14a:Dotted Surface T; 2.14b: All the boundaries formed by the cut; 2.14c: Actual Cut Face **S**

c)   *Creating Adjacency List of* **P1**

After calculating the Cut Face **S**, we can calculate the actual edges which are being cut by the polyhedron. This we do by checking if our initial edge list has an intersection point belonging to **S**. The cut face **S** also helps in calculating the adjacency list for **P1**. First we define Adj(q) to be the list storing the vertices adjacent to q.

Next, we choose any start vertex **W** on one side of the cutting plane and we call it as belonging to **P1**. Afterwards, for each edge pq which is cut by T but not lying on T, let v be the intersection and the unique vertex of **S** lying on pq. We can always assume that p lies on the same side of T as **W**, that is, is a vertex of polyhedron being cut whereas q is a vertex of **P2**. If v is distinct from p, we replace q by v in the list Adj (p) and delete the list Adj (q). If v is equal to p, we simply delete q from Adj (p) as well as the list Adj (q). Repeating these operations for all of the cut edges which do not lie on T has the effect of disconnecting **P1** from **P2**. Finally, since we have a description of the boundaries of **S**, we can set up the adjacency lists of the new vertices, that is, the vertices of **P1** lying on **S**.

 d) *Finding vertices of* **P1** *and* **P2** *using depth first search.*

First we calculate the vertices of **P1** (containing **W**) and then the remaining ones belong to **P2** automatically. We perform depth first search starting with **W** on the adjacency list of **P1** in order to obtain vertices belonging to **P1.** For the polyhedron without holes, all the vertices of **P1** are connected and the remaining ones including common intersection vertices belong to **P2**. In some

47

cases, for polyhedrons with holes, it is quite possible that performing depth first search on **W** may not return all vertices of **P1**. This can happen when the adjacency list is not interconnected with faces attached to internal holes and outer faces.

For that, one can verify that all the edges which are being cut by the plane should have one end vertex belonging to **P1**. So we check for all the edges if they have at least one vertex belonging to **P1** or not. If not, we make that vertex (on **P1** side) as new second start vertex W_2 and again start performing depth first search.

e) Finding face to edge list for **P1**

Now the last step of the cut procedure is to find the face-to-edge list of **P1** and **P2**. This we do by traversing each face F_i of **P** one by one and making use of A_i's list. We will explain this for **P1** and **P2** follows automatically.

First of all, we discard those faces all of whose vertices do not belong to **P1**. Then, since all the faces of **P** intersecting **S** have been previously calculated, it is easy to compute a description of the parts of those faces which lie in **P1**. Let F_i be such a face, with a1,.a2, .., ak from corresponding A_i's list being the vertices of **S** lying on F. Note that these ai's are in pairs and sorted along the face from one end to the other. The basic idea is to traverse along the face F_i taking each pairs of A_i's one by one. We discard those vertices which don't belong to **P1**.

For example consider the face shown in figure 2.9a. Suppose the upper part of the face belongs to **P1**. The face for **P1** would be as shown in figure 2.15.
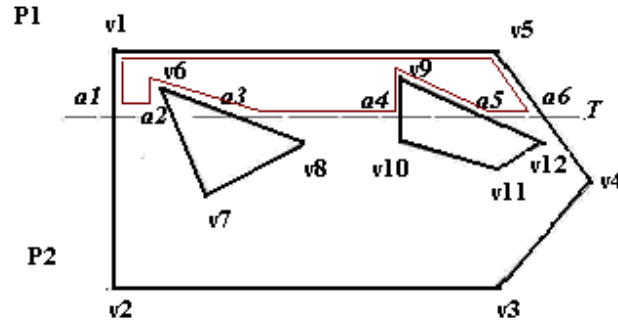

Fig. 2.15

From the edges being cut by **T**, first the starting vertex (here v1) on **P1** is chosen such that a1 is the intersection point. Then for a2, next vertex is chosen on **P1** (here v6) and it is traversed along the face unless the intersection with the next pair (a3, a4) is found. Then again the vertex for a4 is chosen on **P1** and again it is traversed along the face unless the intersection with next pair (a5, a6) is found. We keep on performing the similar procedure unless all the pairs are exhausted and we reach the end vertex as our starting vertex. So the resulting face for **P1** in this case would be consisting of vertices as follows.

$$F_{p1} = (v1, a1, a2, v6, a3, a4, v9, a5, a6, v5)$$

Similarly, for **P2** (below part) the face would be as follows.

$$F_{p2} = (v2, a1, a2, v7, v8, a3, a4, v10, v11, v12, a5, a6, v4, v3)$$

The computation part of **P1** and **P2** is now complete.

2.2.1.2. Updating Adjacent Polyhedrons and Cutting Procedure

After every cut, the adjacent polyhedrons need to be updated or modified as the faces and nodes should match at the common boundary faces of all polyhedrons. In this section, we shall explain clearly what we mean by updating adjacent polyhedrons and how to perform it after every cut.

We illustrate a cutting scheme using a simple example, and show how one can update the adjacent polyhedrons after every cut. Consider a polyhedron (fig. 2.16a) with two notches marked with bold lines. Now after having identified the notches, we illustrate graphically how to obtain convex polyhedrons. Fig. 2.16b shows two polyhedrons (**P1** and **P2**) obtained after cutting along one of the notches.
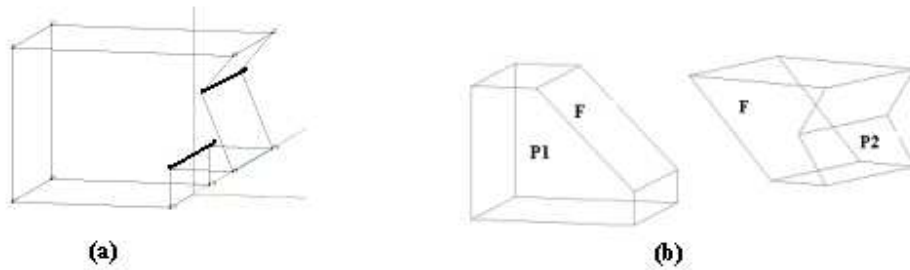
Fig. 2.16a; 2.16b

After the first cut, no update for adjacent polyhedrons is needed as there are only two polyhedrons and both have the same faces and nodes at the common intersection face. **P1** is now convex but there is still one notch in **P2**. Therefore one still needs one more cut.

Fig. 2.17b shows two polyhedron obtained due to second cut.
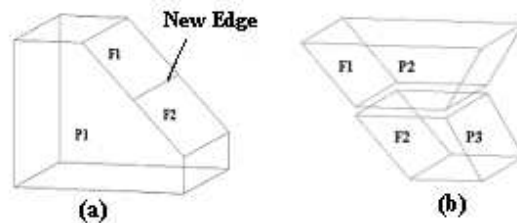
Fig. 2.17a; 2.17b

In order to maintain the same location of nodes, faces and edges at the common intersection faces of adjacent polyhedrons, here **P1** was updated by introducing the edge after the second cut (fig. 2.17a). One can see that the edge had to be introduced in **P1** because earlier face F was

common between **P1** and **P2** but after the second cut, face F gets divided into two faces F1 and F2. And now **P1** shares F1 with **P2** and F2 with **P3**. This procedure of introducing edges and faces to the adjacent polyhedrons, is performed by the routine called *UpdateAdjacentPolys* in the pseudo code (fig. 2.7, 2.8).
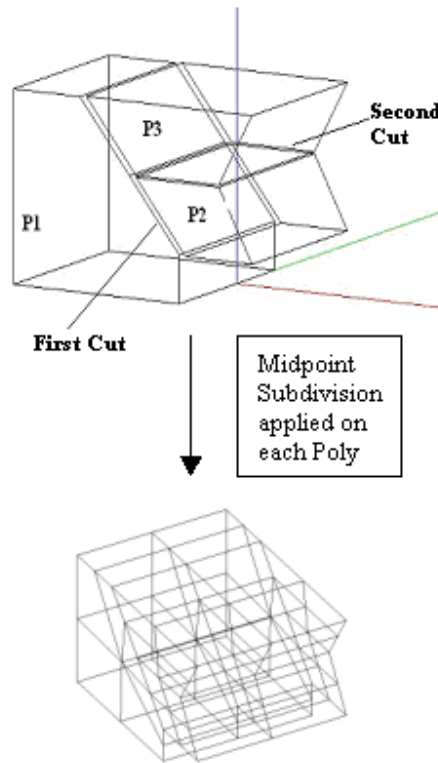

Fig. 2.18

One can see that for given example, convex decompositions can be obtained with two cuts(fig. 2.18) only. Below in the same figure 2.18 also illustrates the application of midpoint subdivision on each polyhedron. However if one looks closely at the side view (fig. 2.19a) of polyhedral **P1**, one can observe that it is not giving the desired mesh quality because of that extra edge introduced while updating **P1** after second cut. This extra edge has an internal angle of adjacent faces creating dihedral angle close to 180°. Hence if we perform mid-point subdivision on **P1**, it would look like the one in side view as shown in figure 2.19b.
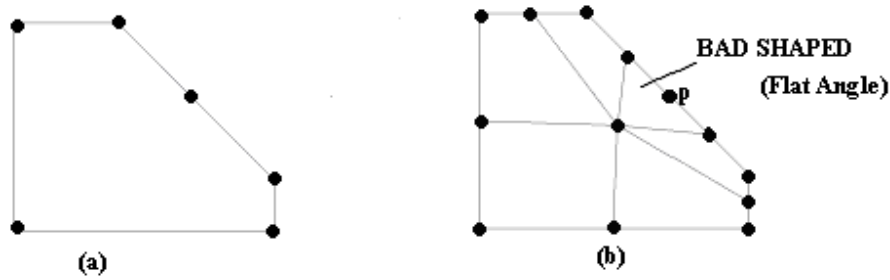
Fig. 2.19a: Side view of P1 showing vertices; 2.19b: Meshed Using Midpoint Subdivision

As shown in the figure 2.19b, the bad shaped element has one vertex *p* whose edges establish an internal angle of 180 degree. For better mesh quality, the internal angles of each hexahedral element should be close to 90° so that it approximates the FEM hexahedral element as close as possible.

However, one thing to note is that if we further cut **P1** along that extra introduced edge using **the same** cutting plane which was used for second cut. The cut sequence looks like:
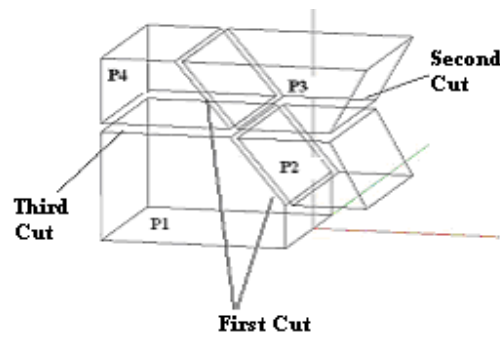
Fig. 2.20

Now in the second cut sequence we have cut the original polyhedron into four pieces (fig.2.20). And **P1** is further divided into two Polyhedrons namely **P1** and **P4**. The mesh quality of the overall polyhedrons is improved and displayed in fig. 2.21.
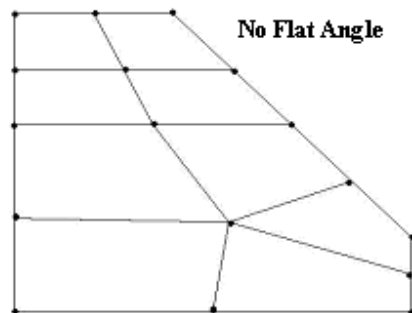
Fig. 2.21: Side view: mesh part belonged to **P1**

51

Looking at side view of meshes (fig. 2.19b, 2.21) one can compare between the two obtained meshes. In the latter case there are less flat and sharp angled edges. Moreover, side views (fig. 2.22a, 2.22b) show again the comparison after two levels of midpoint subdivision for both cases.
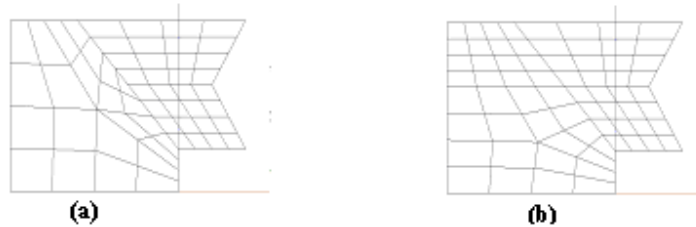

Fig. 2.22a: Cutting only 2 notches; 2.22b: Cutting all through

Hence, if the first level is better, the subsequent iterations of midpoint scheme will provide better results. This clearly shows that bad and good shapes propagate in this algorithm.

Hence, though the third cut was not needed (as all the three polyhedrons were already convex and trivalent), we still performed it in order to ensure better shaped elements i.e. avoiding edges having internal dihedral angle close to 180 degree. So this way we have always extended our cut all through the polyhedrons. Actually one can imagine the second and the third cut as only one cut sequence along one starting direction. Although for bigger and more complicated shaped polyhedrons, this approach of cutting all through can create many polyhedrons, still their number would be finite as the polyhedron is of finite size.

Once again, we would like to emphasize that the reason behind cutting all through the polyhedron is that we perform mid-point subdivision later to obtain a hexahedral mesh. For that, it is better to have well-shaped polyhedrons not having sharp or large angles. Hence, if one plans not to use a mid-point subdivision scheme later and is only interested in having convex polyhedrons, it is better not to cut all through.

To summarize, so far we have seen how one can cut or divide a polyhedron into two parts and that after applying such cuts several times, many intermediate polyhedrons will be obtained. These intermediate polyhedrons have many common faces with each other. As the nodes and edges should match at these common faces, for each cut of a polyhedron, one has to update and perform the corresponding changes at common boundaries of all of the other adjacent polyhedrons. Moreover, we further extend the cut along adjacent polyhedrons. The main routine called cut-procedure has already been explained in the previous section. In cuts of multivalent vertices only the cutting plane passes through the multivalent vertex instead of notches, the rest of the procedure is similar to that of cutting notches. Here, again after every cut we update the adjacent polyhedrons and cut the polyhedrons all through.

2.3. INTERMEDIATE ALGORITHMS

In addition to the above mentioned schemes, some other intermediate schemes have also been developed in general. Specifically we try to remove vertices located very close to each other, polyhedrons of near-zero volume and other degenerate conditions.

For instance, sometimes the cutting plane **T** passes very near to some vertices of a polyhedron but not exactly touching them. After the cutting procedure, this would lead to one polyhedron having some very nearby or close vertices. To avoid this, while cutting, we move the vertex slightly so that it exactly fits the cutting plane. For room acoustics purposes, such small variations in geometry are allowed as it does not make much of the difference especially when solving the equation of sound at low frequencies. Below 340 Hz where the wavelength is above 1 m, moving the vertex for 1-5 cm is quite admissible. In the example (fig 2.23a), p1 and p2 are very near to the cutting plane T, hence they are moved upwards (fig. 2.23b) so that they fit the cutting plane exactly.
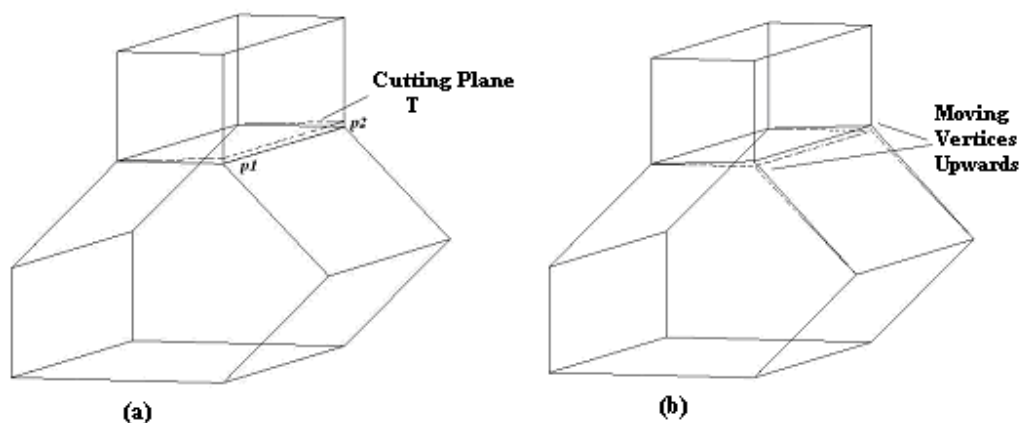
Fig. 2.23a; 2.23b

Furthermore, before every cut, we check if two vertices are very near to each other or very sharp angles in the polyhedron have been created due to previous cuts. If so, we join the two vertices or remove the two edges creating sharp angles and join them to a single edge (fig 2.24a, 2.24b). Subsequently, in order to maintain the conformity, the corresponding changes are performed in all the nearby polyhedrons sharing those two vertices or edges.
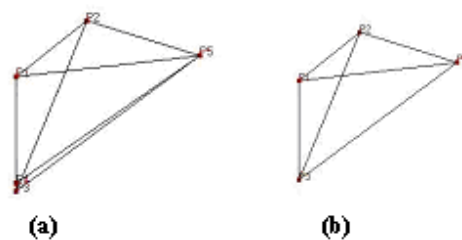

Fig. 2.24a; 2.24b

Figure 2.24b shows how one can remove undesired close vertices and sharp angles. Although the procedure looks simple it needs to be implemented with proper care as while joining the vertices, all the neighboring elements have to be updated and moreover with one less vertex, the renumbering of vertices has to be performed as well. So the disadvantage of joining such close vertices is the added complexity of verifying that the neighboring elements have been updated

properly especially if already many cuts have been performed and one is working in the middle of the complex shaped geometry.

2.4. CHOICE OF CUTTING PLANE

So far we have seen how, one can obtain simple shaped polyhedrons after applying a series of cuts. This sections now belongs to the part of our algorithm where we "examine, suggest, cut". For complicated rooms where there are many notches like balconies or stairs of room, it is better to define cutting schemes priority-wise. Otherwise, cutting one notch can multiply other notches and thus create more notches. Sometimes notches associated with symmetrical structures are to be cut first or else the symmetry could be lost because of other cuts. So the idea is to identify such notches which should be cut first and what cutting plane direction to be chosen and so on. This is mainly important to ease the overall cutting procedure and to also minimize the number of cuts as well as enhance the mesh quality.

In this section, we shall examine one by one for various architectural spaces, how one can identify the basic features of room like balconies, domes, stairs etc and choose the direction of the cutting plane accordingly in order to obtain good quality elements while minimizing the total number of cuts as well.

2.4.1. Cutting Consecutive Notches in one Cut

Balconies in a room is a very common feature in acoustic indoor models. One thing to observe is that they create continuously attached notches and can be identified using pre-checking algorithms. If we choose the direction of the cutting plane such that it cuts multiple or consecutive notches at the same time, we can reduce the number of cuts. See for example (Theatre, fig 2.25a) there are total 6 notches (marked by bold edges) all of which lie in two sequences of three notches each. So if we choose our cutting plane passing through three notches at a time, only two cuts (fig. 2.25b) are needed.

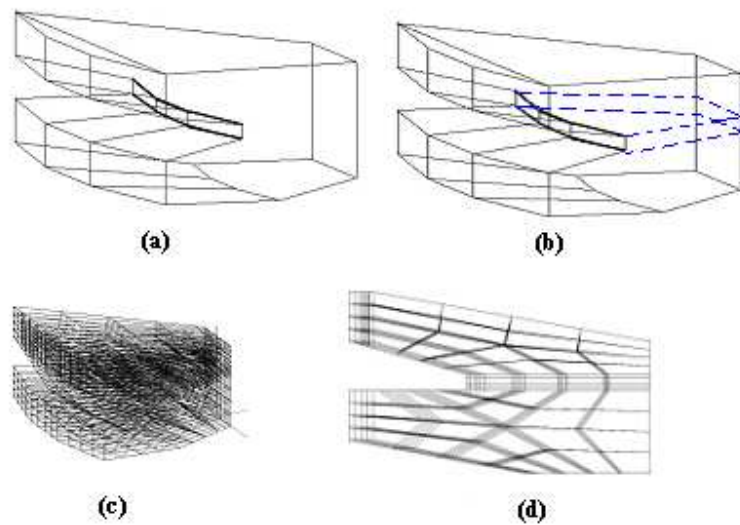
(a)   (b)

(c)   (d)

Fig. 2.25a: Theatre (6 Notches); 2.25b: Two cuts; 2.25c: Mesh; 2.25d: Side –View of Mesh

Corresponding to the approach mentioned (fig. 2.6), identifying these consecutive notches belongs to the part of the cut procedure concerned with "examining and suggesting". Therefore, only two specific, predetermined cuts have resulted into a set of convex polyhedrons. In the second part of the algorithm we check for normal notches, but for the above example there is none. Hence it goes directly to the third part of the procedure where it checks and transforms multivalent to trivalent vertices. And finally two levels of mid-point subdivision are performed (fig. 2.25c).

One can observe in the side-view (fig. 2.25d) of the meshed theatre that with the proper choice of the cutting plane **T**, the calculation time of the algorithm has been improved by minimizing the cuts and good mesh quality has been obtained as well. A good quality mesh element (in physical space) is one which is close to its FEM element (in mathematical space). For instance, a hexahedral mesh element is best if all the angles are close to 90°.

2.4.2. Cutting Consecutive Multivalent Vertices

Similar to consecutive notches, there are many typical examples of rooms where continuously attached or consecutive multivalent vertices exist. Consider the sporting hall as shown in figure 2.26a. Here the top four vertices are seven-valent and further connected with other multivalent (>3) vertices. If we do not decide properly, the random normal cutting procedure could result in very bad shaped elements and the symmetry of the room could be lost. However, such consecutive multivalent vertices can be handled if we define the cutting plane wisely. Here also, we look for that cutting plane first, which removes the maximum number of continuous multivalent vertices in a single cut (fig 2.26b). The resultant mesh obtained is shown in the figures (2.26c, 2.26d).
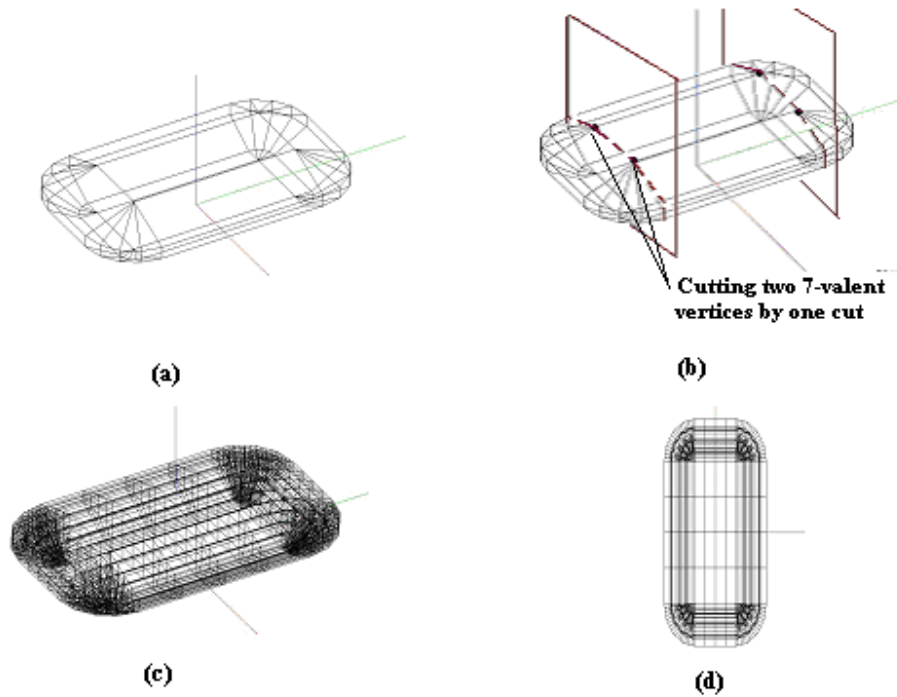
Fig. 2.26a; 2.26b; 2.26c; 2.26d

In the middle part of the hall (top view), the majority of the elements is almost well- shaped hexahedral although the aspect ratio is not very good. Aspect ratios can be treated later but our main concern is to avoid flat or sharp angles in elements. Hence, it can be observed that better choice of cutting sequence helps greatly in obtaining a good quality mesh.

2.4.3. Meshing Dome Like Structures

The presented cutting algorithm may not be able to cut geometrical shapes with too many curved surfaces. Surfaces like domes (figure 2.27) contain many four-valent vertices and it would require too many cuts in close neighborhood to obtain three-valent vertices. It is quite difficult or even impossible to keep cutting so closely and it is not easy to update the common intersection boundaries as many degenerate cases may arise. Moreover, even if one manages to perform all the cuts, the shapes of obtained polyhedrons would not be good.

Fig. 2.27

56
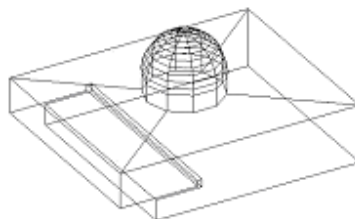
Therefore, in order to treat such curved surfaces where decreasing valence to three is quite difficult for all vertices, we introduce one more algorithm called projection technique. One still needs to perform the cutting plane algorithm to obtain the convex polyhedrons as the projection algorithm can be applied only on convex polyhedrons. First we describe the methodology behind the projection algorithm and then we show how to apply it to real-world examples.

The algorithm is based upon projecting the outer faces inwards towards a medial surface at a certain distance. The idea is based on the fact that when one projects or extrudes the face it gives rise to a three dimensional polyhedron. Similarly, here the projected and original faces creates convex and trivalent polyhedrons. Then we apply midpoint subdivision on each of these polyhedrons. The basic principle is demonstrated in the figure shown below (fig. 2.28a) for the shoebox model.

(a)   (b)   (c)
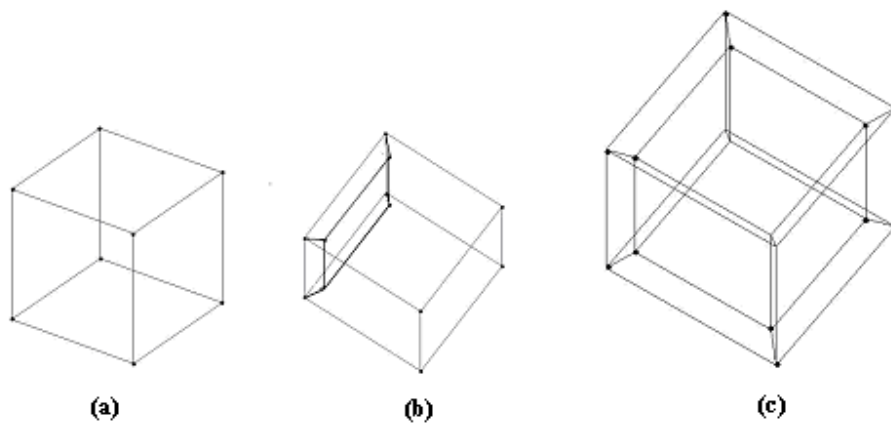
Fig. 2.28a; 2.28b; 2.28c

First, the average angle bisector for each vertex is calculated. Afterwards, every edge is taken and it is projected inwards along the angle bisectors. In the figure above, the first figure (2.28a) shows a shoebox model. The idea is to project every face by projecting its edges inward. The second figure (2.28b) displays how one can obtain a projected face for a given outer face. Similarly the third figure 2.28c shows the result after projecting every face. Now, if a face in two dimension is extruded, it yields a three dimensional polyhedron. Similarly, one can observe in the second figure, that the projection has created a polyhedron consisting of the projected face, the original outer face and the faces created due to connecting edges. In the next step, we perform midpoint subdivision on this newly created polyhedron (fig. 2.29a). Similarly one can perform these steps for all of the faces and their polyhedrons (fig. 2.29b).
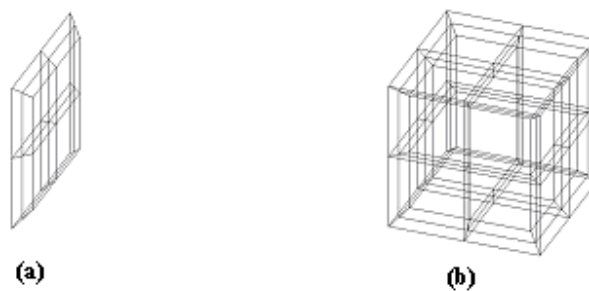

(a)   (b)

Now this set of projected faces can be further projected inside as long as the resolution permits. The figure below (2.30a, 2.30b) shows the second level of projection. Convergence criterion is that if the shortest distance of the body midpoint (defined as the average centre/ centroid of polyhedron) to any projected face is less than the desired projected distance, we do not project them further but rather we just join the midpoint with all the innermost projected faces. Hence, one can understand that if the model is radially symmetric, all the faces would converge to a single point. Every face projection results in a polyhedron and then mid-point subdivision is performed on it.
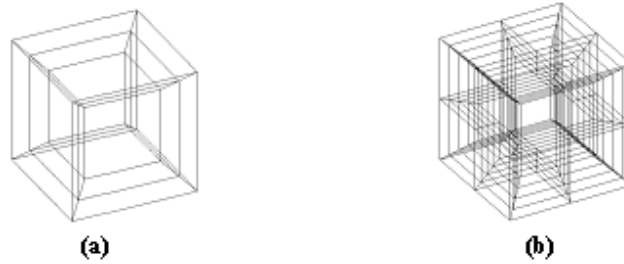
Fig. 2.30a: Two projections; 2.30b: MPS

The next set of figures (2.31a, 2.31b) shows the convergence criterion of the projection algorithm and demonstrates how it fills the void in the interior. Figure 31a shows all the possible projections. Then in the second figure 31b, all of the innermost projected faces are joined with the body midpoint. Such faces then create pyramids inside. These pyramids are further meshed using midpoint subdivision as applied to other polyhedrons. The advantage of using midpoint subdivision is that the nodes match at adjacent polyhedrons, so one does not have to worry about the location of nodes at common boundaries.
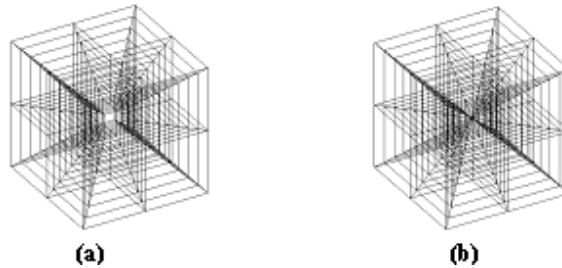

Fig. 2.31a: All projections; 2.31b: Filling Void

Now we would like to explain why we are projecting the faces edge-wise. For complicated projects, it is highly possible that while projecting inwards, the edges intersect each other (fig. 2.32b) and the projection is not possible for the given resolution **Ro**.

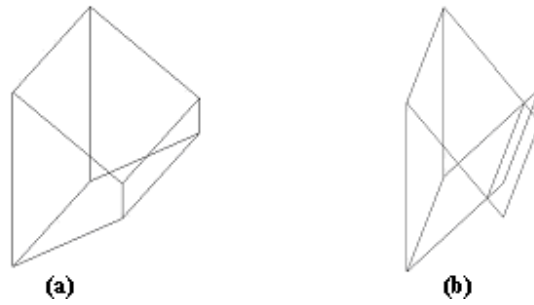Now there could be two cases as shown in figures 2.32a and 2.32b:

Fig. 2.32a: Successful projection; 2.32b: Intersection

So after every projection one needs to check if any of the edges of every face projected is intersecting. If so, one can find the intersection points (fig. 2.33) and based on that the allowed maximum projection distance (**Rn**) is calculated. Then all of the other faces are projected for this new projection distance.
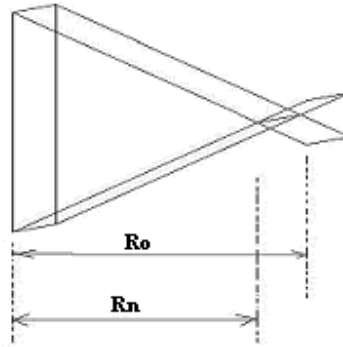

Fig. 2.33

So the objective is to keep projecting each edge inwards unless it is collapsed or converged or no more projection is possible or needed. Then in the end, the innermost projected faces are joined with the body midpoint to fill the remaining void.

Now we show some results for more complicated architectural spaces. We start with the same mosque (fig. 2.27) and try to solve it using the projection approach. First, we apply a series of cuts to obtain convex polyhedrons. Then, the projection algorithm can be applied on each of the polyhedrons. The upper dome can be removed in a single cut (fig.2.34a). The second figure (fig. 2.34b) shows a small dome inside the dome. It is obtained due to the projection of each of the outer faces. The distance for the projection was assigned as the average of all of the edge lengths. The third figure 2.34c illustrates again how to obtain polyhedrons by joining the outer and projected face. Finally the result is shown for all faces (fig. 2.34d) with one level of projection and mid-point subdivision each.
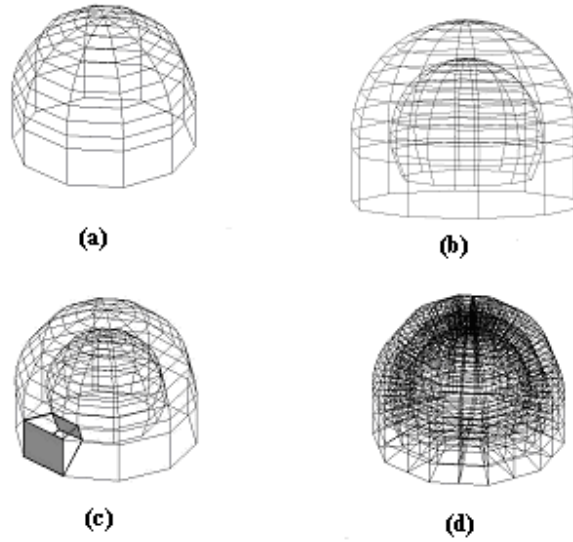
Fig. 2.34a; 2.34b; 2.34c; 2.34d

Similarly if one keeps on performing the projection, one obtains the results as shown in the next set of figures (fig 2.35a, 2.35b).
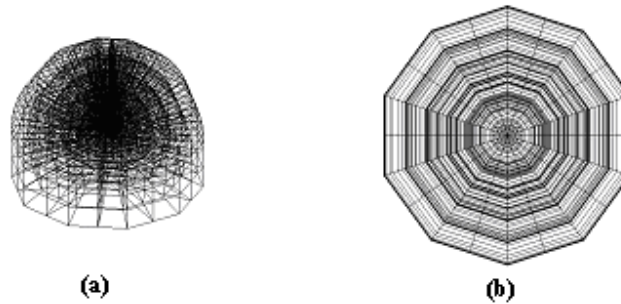

Fig. 2.35a; 2.35b

One can clearly notice the projected faces as domes inside the domes. The mesh seems to be of reasonable good quality. Hence, after obtaining convex decomposition using the cutting plane algorithm, when the number of multivalent vertices is large, one can directly apply the projection technique to some polyhedrons to further subdivide the domain. Afterwards, all the parts can be assembled together to realize the mesh for the whole room. Though this algorithm is best suitable for radially symmetrical geometries, one can still apply it to other bodies at least to have a starting mesh. Hence, one can see how to obtain a mesh for projects having complicated or curved geometries.

2.5.   REAL WORLD APPLICATIONS

In order to demonstrate the applicability and advantages of our algorithm, we show how one can apply it to more complicated and real-life typical rooms where much acoustical considerations are needed. Consider, the Church example (fig. 2.36a) . This room is a combination of

60

consecutive reflex edges and multivalent vertices. Figure 36b shows the mesh after applying the proper sequence of cutting planes. This mesh can be used by any FEM solver in order to simulate the sound field inside the church.
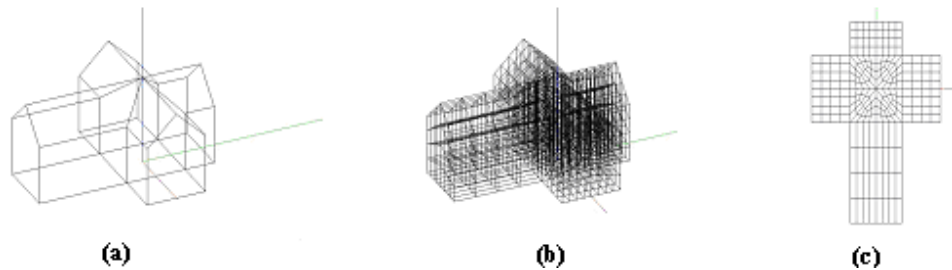

(a)   (b)   (c)

Fig. 2.36a; 2.36b; 2.36c

Next, we consider a more complicated shaped room. See the Gothic Dome example (figure 2.37a). It is again a combination of continuous notches in addition to a half dome like structure in the right side. First the dome was removed and then the consecutive notches were cut sequentially in order to obtain the mesh shown in figure 2.37b.

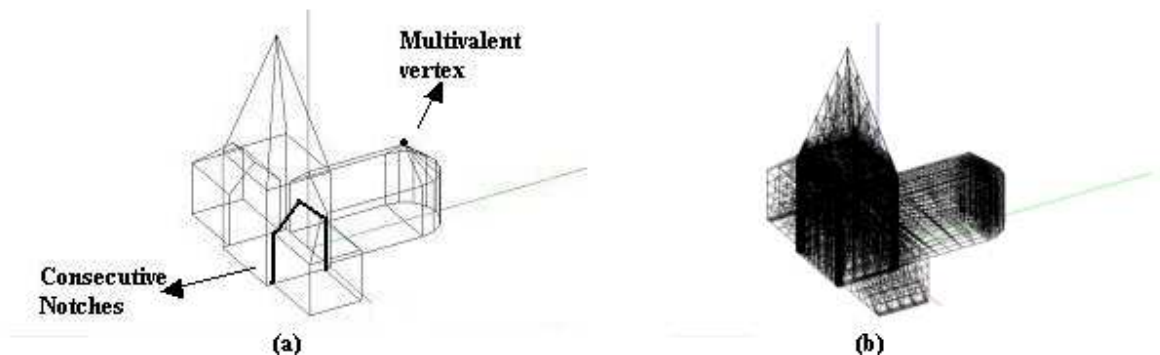Multivalent vertex

Consecutive Notches

(a)   (b)

Fig. 2.37a; 2.37b

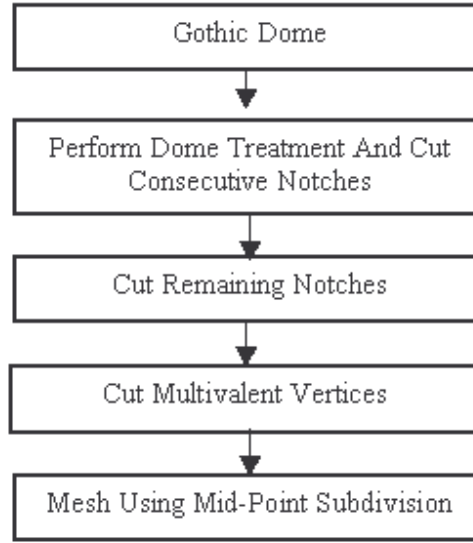The rough cutting scheme can be realized as follows:

Fig. 2.38

From the above illustrated examples, it is quite clear that using our approach many such complicated real-life geometry examples can be meshed. Afterwards, these meshes can be used to simulate the sound field in such spaces using finite element method [40].

2.6. FURTHER DISCUSSION

In this section we briefly discuss about advantages and disadvantages of using the cutting plane algorithm. First, as it looks, the approach of obtaining convex polyhedrons is easy to understand though complex to implement. In this work we have used the midpoint subdivision scheme to further subdivide the polyhedrons, however one can use any other desired or better scheme for the subdivision of convex polyhedrons.

As we have seen, for rooms with symmetrical structure and plane surfaces, cutting plane algorithm can provide a very good quality automated hexahedral mesh and for curved surfaces projection technique can be applied. It automatically minimizes the number of cuts by identifying the consecutive notches, consecutive multivalent vertices etc and defining the cut sequence accordingly. All other available meshing schemes require human intervention at some level or a prior knowledge of mesh generation softwares. This work is aimed at obtaining an automated hexahedral mesh just by the click of a button. In that respect, for geometries with not many notches, we have been able to discretize them successfully using our cutting plane approach.

However, roughly speaking for geometries containing more than 40-50 notches, automated cutting plane approach could be difficult to perform. For instance, geometries involving diffusers or stairs could contain large number of closed notches and it would be then impossible to predefine cutting schemes for such designs. See the figure 2.39.
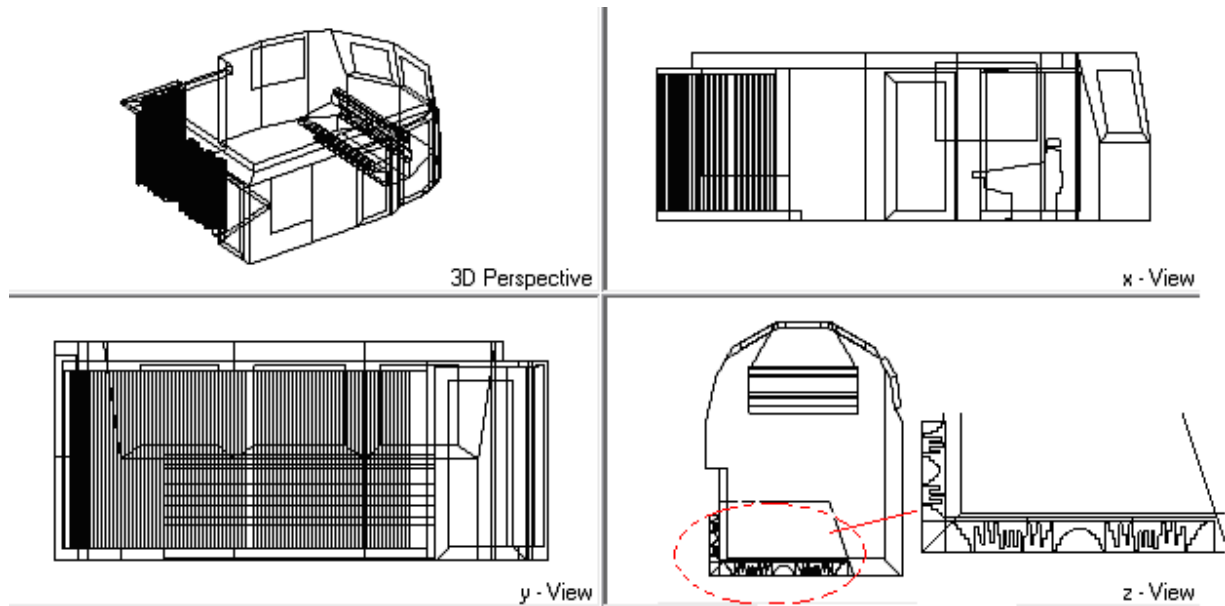
Fig. 2.39

It is a recording studio with diffusers at the rear side. If one looks on the top view (z-view), the diffuser (encircled and zoomed in) is creating too many closed reflex edges and its difficult to identify and define cutting schemes automatically for such shapes. Moreover, cutting only one notch at a time could create polyhedrons with bad aspect ratios. As a future work, for such projects a better cutting approach is required.

2.7.   CONCLUSIONS

A new scheme called cutting plane algorithm has been suggested to obtain an automatic hexahedral mesh. It has been shown that with the proper choice of the cutting scheme, a quality hexahedral mesh for many surfaces can be obtained in an automated manner. Special schemes have been suggested and the general idea of a cutting procedure especially suited for architectural spaces has been given. The cutting procedure is not very specific or fixed, it can be modified according to the desired outcome. For instance, if only convex polyhedrons are needed, one does not have to cut the polyhedron all through and no more multivalent vertex cuts are required. Furthermore, to model curved geometries, a new projection technique has been introduced. It has been shown that for curved polyhedrons it is quite effective. A robust and automatic mesh generator is very hard to realize. This chapter has given an approach which is quite effective to generate meshes especially suited to architectural spaces.

3. CHAPTER

Extension of Sound Particle Model using FEM

3.1. INTRODUCTION

Various methods based on geometrical and statistical approaches have been suggested and are being used for simulation in room acoustics, but it is always a problem when detailed acoustic investigation is needed in the low frequency region for small rooms with complex shapes. The ray tracing method as explained in chapter 1 is simple and easy to be applied but the image source method can provide more exact results in closed cavities. However, it is also not sufficient to consider the diffraction effect below Schroeder frequency.

As introduced in chapter 1, several wave models based on numerical methods and involving large computational requirements have been suggested like FEM, BEM and finite difference method. In all the above mentioned methods, the most difficult part is to define the boundary conditions. Generally complex impedance data is required but it is rarely measured or published.

The finite element method is being used extensively nowadays because of its adaptiveness and the simplicity in handling the complex absorbing boundary conditions as well as complex shapes. Basic modeling in FEM includes discretization, evaluation of element integrals, assembling into global matrices and then solving the large sparse system of equations using direct or indirect methods [43, 44].

In this chapter the finite element method has been used to obtain the eigenmodes and the transfer function of complex rooms with general boundary conditions and its practical feasibility in room acoustics has been investigated.

3.2. MODAL ANALYSIS

3.2.1. Shoebox Model

After explaining the main steps behind FEM approach in chapter 1, now we move on directly to calculations in three dimensional rooms. First, we carried out the modal analysis for a shoebox model (fig.3.1a) in order to verify it first with the existing analytic solution for rigid case and then we moved to general complex shaped rooms.
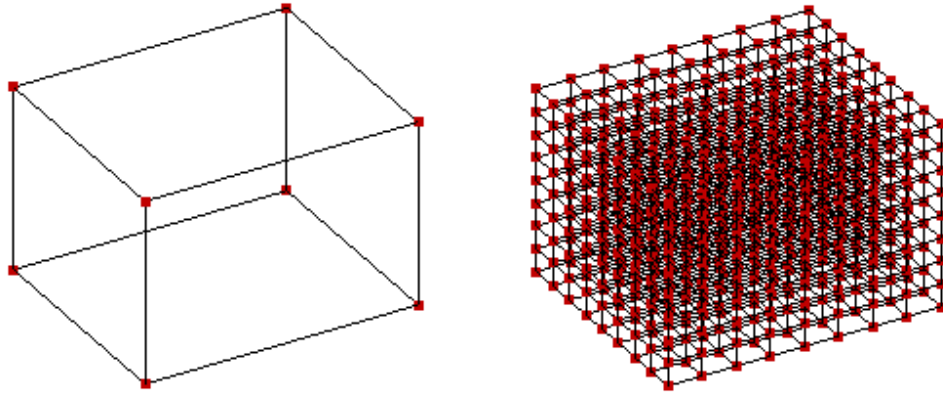
Fig. 3.1a: Shoebox Model created in EASE; 3.1b: Mesh.

Using the linearized approach as mentioned earlier (for the 2D rectangular case), for a shoebox model (fig.3.1) of size (3 x 2.5 x 2) m³, we calculated the eigenmodes first for rigid walls and then with the absorbing surfaces having different impedance values. Regarding mesh generation, the room was discretized by performing three levels of Mid-point subdivisions. Here no cuts are required as the polyhedron is already convex and trivalent. We used an 8-noded linear (Lin8) finite element. As a general rule of thumb 6 nodes per wavelength for linear and 3 nodes per wavelength for a quadratic element are needed. With this mesh, we can perform the FEM analysis roughly up to 250 Hz. The Gaussian integration [45] scheme was used for evaluating element integrals.

Treating the shoebox case analytically, eigenmodes were calculated using the well known relation:

$$f = \frac{c}{2} \sqrt{\left(\frac{p}{length}\right)^2 + \left(\frac{q}{width}\right)^2 + \left(\frac{r}{height}\right)^2}$$

where c is the velocity of sound and p, q, r are numbers taking values : 0, 1, 2, 3…

The values of p, q, r determine if the mode is axial, tangential or oblique. If only one of them is positive the mode is axial and if two of them are positive the mode is tangential and if all of them are positive then the mode is oblique.

The first six eigenfrequencies obtained in each case are shown in Table 3.1.

Mode (p,q,r)	Analytic, f(Hz)	FEM (Rigid) f(Hz)	FEM (Z/ρc=2) f(Hz)
(1,0,0)	57.16	57.62	53.84
(0,1,0)	68.60	69.15	66.70
(0,0,1)	85.75	86.43	85.66
(1,1,0)	89.29	90.02	88.14

65

(1,0,1)	103.05	103.89	103.21
(0,1,1)	109.81	110.71	110.42

Table 3.1 Comparing the modes of the analytic and of the FEM modal analysis.
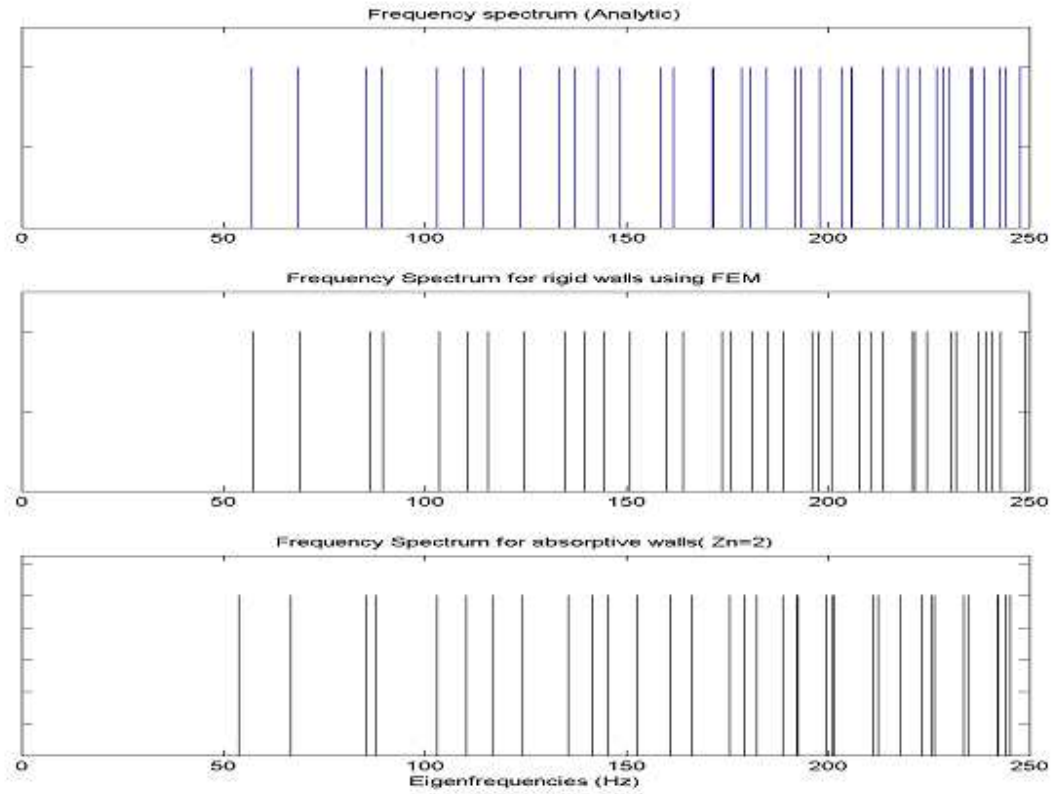

Fig. 3.2a: Analytic, 3.2b: FEM rigid, 3.2c: FEM with normalized acoustic impedance $Z_n = 2$ at each walls.

From the Table 3.1, one can see that the frequencies in the rigid case match fairly with the analytic solution. For a larger view, we are showing the frequencies up to 250 Hz for all the three cases in the figure 3.2.

In the fourth column of Table 3.1, only the real part of the complex eigenfrequencies have been shown. These are also called the natural frequencies of the system.

The expected shift in the natural frequencies of the eigenmodes towards smaller values due to resistance can be seen when we move from rigid walls to absorbing surfaces. Hence it is essential to take proper account of absorption at the walls.

3.2.2. L-Shaped Room

Next as a second example where the analytic approach is not easily applicable, we analyzed the eigenmodes for a L-shaped room shown (fig. 3.3a).
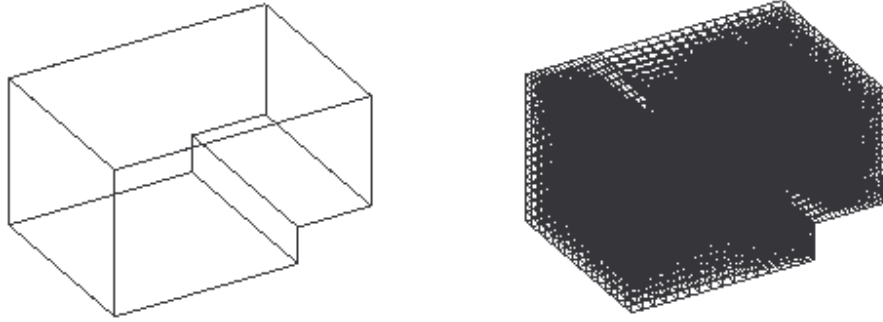
66

Fig. 3.3a: L-shaped Room; 3.3b: Mesh.

Room coordinates are as follows:

Vertex	X(m)	Y(m)	Z(m)
P1	-2.50	-1.50	2.00
P2	-2.50	-1.50	0.00
P3	1.00	1.00	2.00
P4	1.00	-1.50	2.00
P5	- 2.50	1.00	2.00
P6	- 2.50	1.00	0.00
P7	1.00	-1.50	0.50
P8	1.00	1.00	0.50
P9	0.00	-1.50	0.50
P10	0.00	-1.50	0.00
P11	0.00	1.00	0.50
P12	0.00	1.00	0.00

Table 3.2 L-Shaped Room Coordinates.

The impedance boundary condition (equation 1.7) is used: :

$$\frac{\partial p}{\partial n} = -\frac{i\rho\omega p}{Z}$$

We can write the surface impedance Z as follows:

$$Z = R + i\, I$$

Here the real part R represents the resistance which contributes to the damping and shifting of the modes and the imaginary part I is the reactance which causes phase changes in the system.

As an approximation, the impedance is assumed to be real and for FEM calculations, its value was estimated from the statistical absorption coefficient by use of an equivalent angle of

incidence around 60° [46]. The relation between absorption coefficient and impedance values obtained can be viewed as follows (fig. 3.4a):
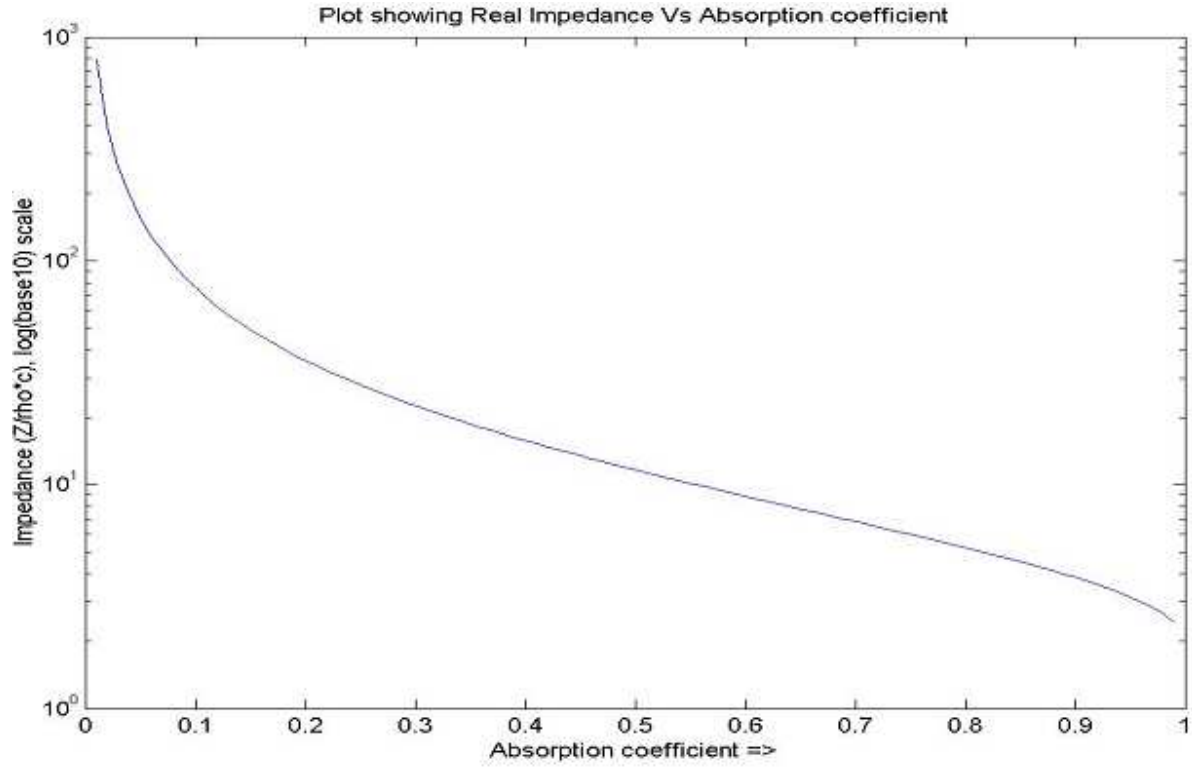

Fig. 3.4a

For the L-shaped room shown (fig.3.3), we calculated the eigenmodes for both rigid and absorptive surfaces (absorption coefficient of all walls α=0.2). The used mesh was discretized with an average element edge length of 25 cm. Fig. 3.4b shows the eigenmodes spectrum for absorption case.
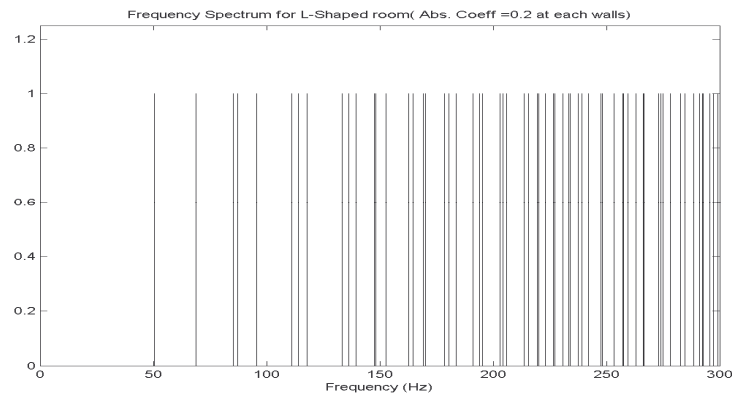

Fig. 3.4b: Eigenmodes Spectrum (Absorption coefficient of all the walls α=0.2).

Rigid Walls, f(Hz)	α = 0.2 of each wall, f(Hz)
50.35	50.33
68.93	68.92
85.36	85.35
87.25	87.24
95.53	95.53
111.20	111.19

Table 3.3 Real part of eigenfrequencies for L-shaped Room.

Next to roughly visualize the number of modes below Schroeder frequency, we calculate it using the relation:

$$f \cong 2000\sqrt{\frac{T60}{V}}$$

where, T_{60} is the reverberation time and V is the volume occupied by the given room.

The Schroeder frequency for the room (fig. 3.3) is 265 Hz. As one can see from the graph above (fig. 3.4), the density of modes below Schroeder frequency is lower than in higher frequency region so a uniform distribution of sound energy cannot be assumed. Hence the proper care of absorption is required to solve the problem of undesired resonances. Moreover, we can also expect feedback problems at the preferred frequencies. Such detailed investigation is not possible with the particle model.

3.2.3. Loudspeaker Placement

Room modes develop as reflected sound interferes with itself. Interference causes additions of up to 6 dB where two equal reflections sum, as well as cancellations of the whole signal where they are of opposite phase. Every modal frequency has an associated three dimensional pressure distribution in the given room. Some mode shapes (in the X-Y plane, Z= 0) for the shoebox model, have been shown in the figures (fig.3.5) plotted using Matlab.
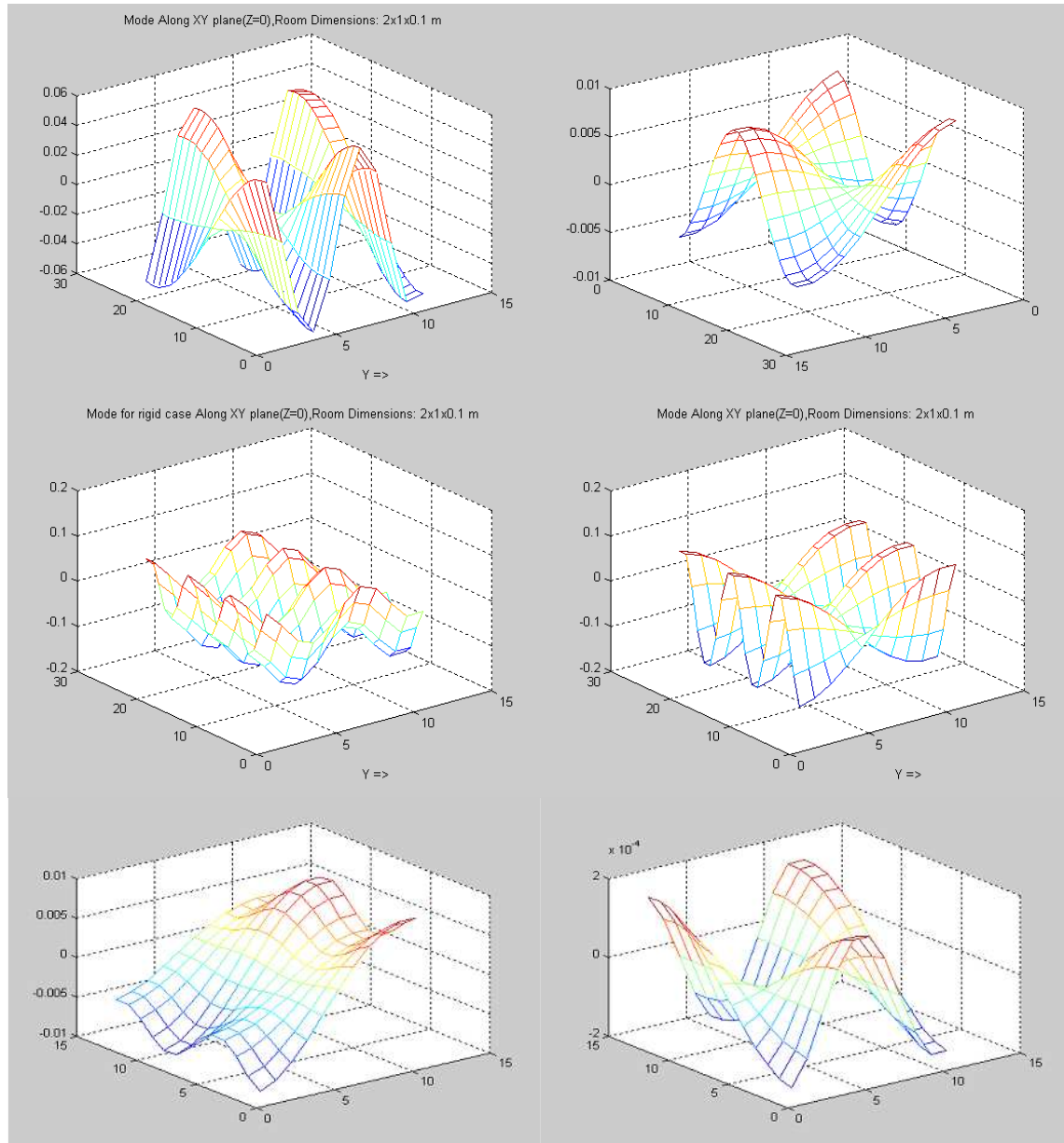
Fig. 3.5: Eigenmodes

In order to have the better listening experience at the listener position, the dimensional ratios of walls should be chosen in such a way such that the modal frequencies are uniformly spaced. However, we must also consider the fact that the listener and source will interact most efficiently when sound sources are placed in the high pressure region of the mode. The loudspeaker placement will accentuate or diminish the coupling with the modal pressure variations at each of the modal frequencies. Similarly, a listener will hear different modal emphasis depending on where he is seated. For example even for the good sound systems, if the source is placed at the

minimum pressure region of the mode, the room may not respond to that frequency. Physically it means that the signal would not be heard at this particular frequency. Hence it is essential to know the location of antinodes (maximum pressure) and nodes (minimum pressure) to approach the problem of subwoofer placement.

Figures (3.5) show mode shapes for some eigenmodes. So one can clearly see the minimum pressure lines from the graph and hence can decide where one should not place a sound source. There is a large amount of literature available for the speaker placement problem [47, 48].

3.3. Transfer Function Calculations

In the previous section, we calculated the stiffness, mass and damping matrices for the general room which are needed for the calculation of eigenmodes. Also, using the same matrices one can perform frequency domain simulations in order to obtain the transfer function and time domain simulations to obtain the impulse response of the system. The transfer function of the room as mentioned previously can be calculated after solving the FEM linear set of equations as explained in chapter 1 (equations 1.8 and 1.12) for the low frequency region and with the desired step size i.e. at the frequencies with some fixed intervals. We are restricted to the low frequency region because of the large computational time required for calculating all frequencies in a high resolution mesh grid model.
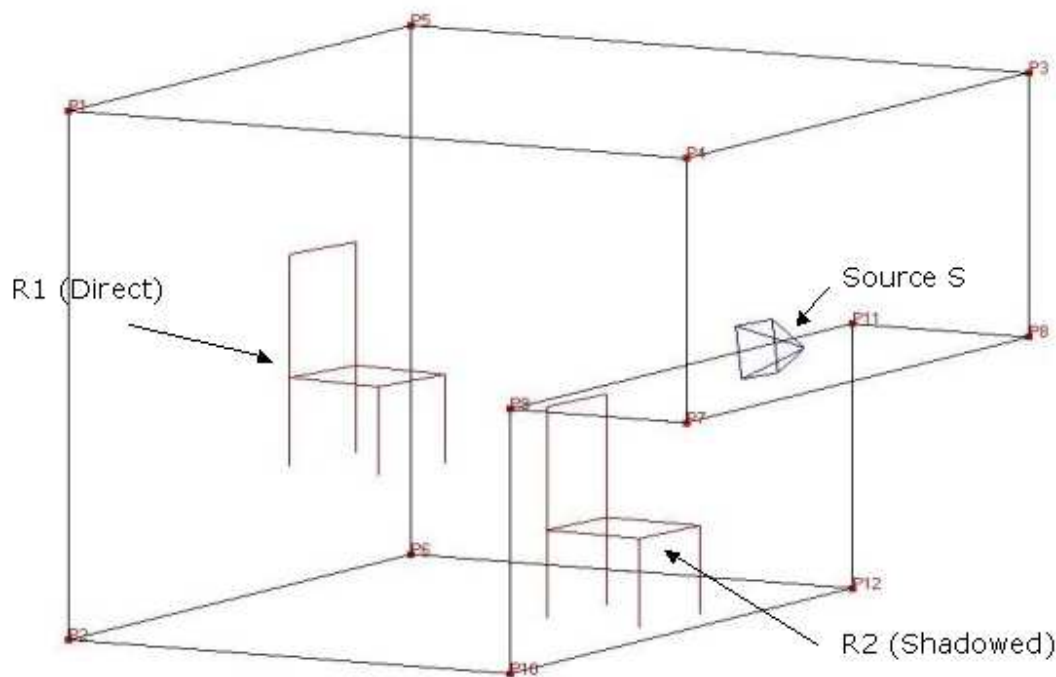

Fig. 3.6

For the same L-Shaped room shown in the previous section (fig.3.3), transfer functions in the low frequency region were calculated using FEM and then using the mirror image method in EASE at two different locations (Fig. 3.6), one in the shadowed area and the other facing directly

71

the speaker. A point source (S) is located at (3.48, 1.25, 0.75), with the assumption that it vibrates with the volume velocity amplitude of 1.0 m³/s.

The reason behind choosing the two different locations and comparing the two approaches, is that in the direct field the sound field is mainly generated due to direct sound and strong early reflections, one can expect to observe the reasonable similar results between particle approaches and FEM. At the second location, the results could differ due to diffraction and late reflections at shadowed region. Hence transfer functions were calculated using mirror image method and FEM at both the locations.

Case 1. Direct Field

Room	L-shaped (fig.3.6)
Methods	Mirror Image and FEM
Field	Direct
Listener position	R1 {1,1.25,1}

A mirror image calculation was performed using the first 25 orders. The reflectogram and frequency response obtained in the low frequency region are shown below(fig. 3.7, fig. 3.8a).
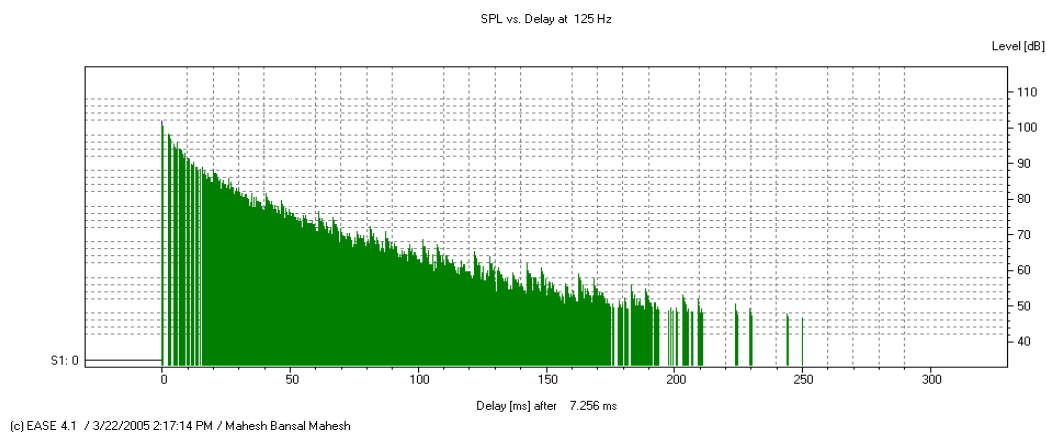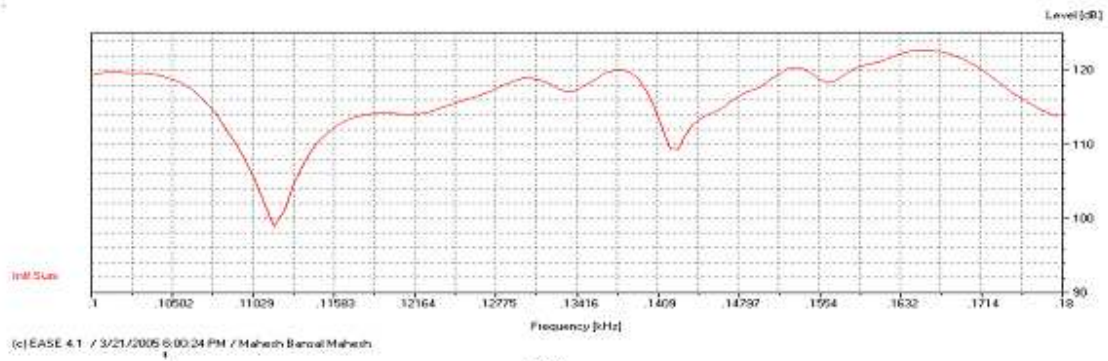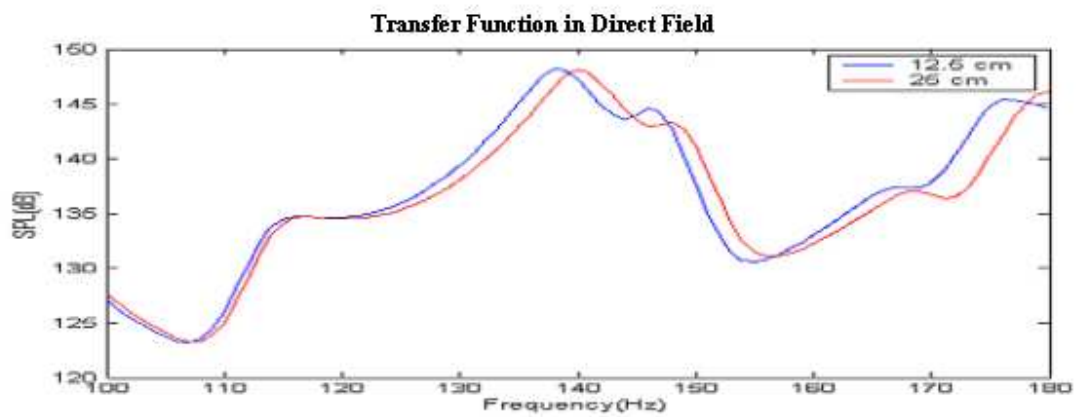

Fig. 3.7

72

(a)

(b)

Fig. 3.8a Frequency Response Using Mirror Image Method; 3.8b: Using FEM.

Then we performed the FEM analysis to calculate the transfer function at the listener position. The used mesh was discretized with an average element edge length of 25 cm and 12.5 cm. The results obtained is shown in figure (fig. 3.8b).

We have shown the comparison between 100-180 Hz. Below 90 Hz, its not possible to simulate the result using image source method in EASE. Although the transfer functions obtained are quite similar, still the transfer function obtained using FEM (fig. 3.8b) is slightly shifted towards higher frequencies because of mesh size and non-exact impedance value assumed. However, the shift is lesser in case of 12.5 cm as compare to 25 cm. This further implies that as frequency increases, better resolution is required.

Case 2. Shadowed

Room	L-shaped (fig.3.6)
Methods	Mirror Image and FEM
Field	Shadowed
Listener position	R2 {2.5,1.25,0.25}

73

Similarly for the same order in mirror image and same mesh size in FEM, we calculated the transfer function at the second location. The graphs obtained are shown below (fig.3.9a, fig.3.9b).
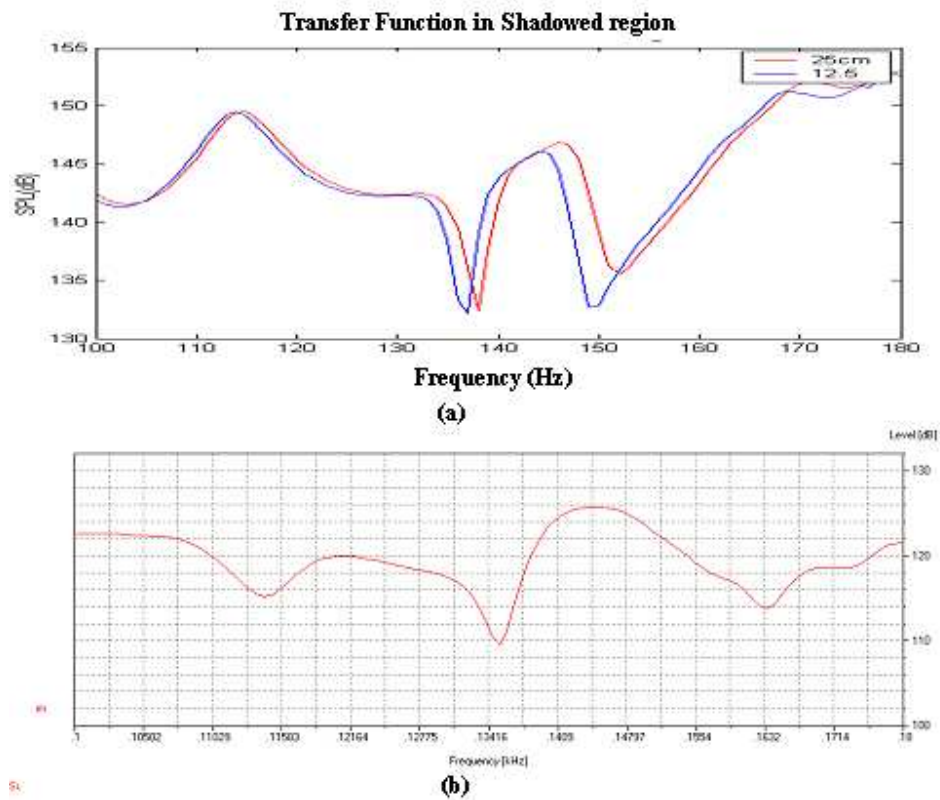

Fig. 3.9a: Frequency Response using FEM; 3.9b: Mirror Image Method.

For a more detailed picture, we plotted the eigenmodes and frequency response for both locations on the same plot (fig. 3.10).

Eigen Modes distribution for L-shaped Room

Frequency Response at R1, direct field
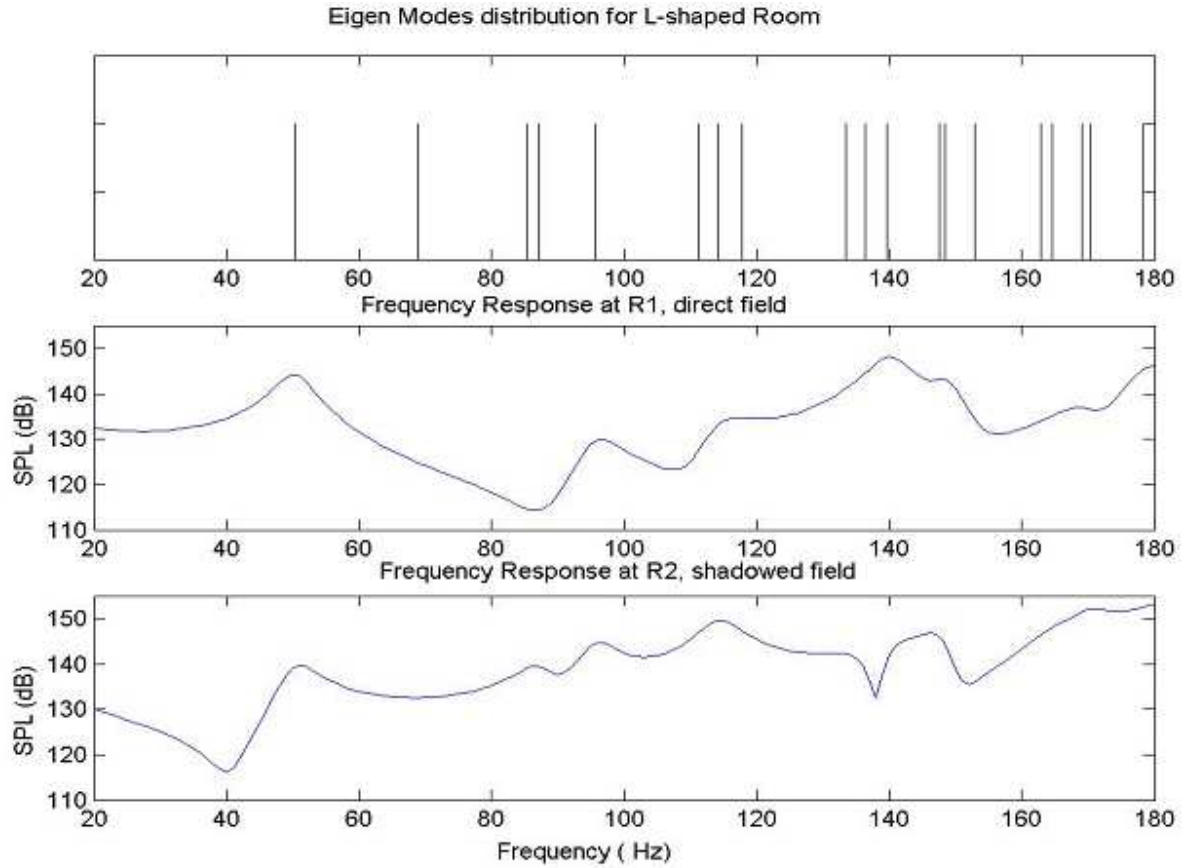
Frequency Response at R2, shadowed field

Fig. 3.10: Frequency responses and modes spectrum (FEM).

One can see in the transfer function obtained from FEM that there are peaks corresponding to eigenmodes (fig. 3.10) calculated in the previous section for the same room and with the same absorption coefficient at walls.

The transfer function obtained from the FEM model was different from the particle model in the shadowed region, but showed great similarity at the second location where the receiver was facing the speaker directly. This can be explained by the fact that in the second case, direct sound and first order reflections dominate the pressure distribution whereas in the shadowed region there is no direct sound. Moreover, in the shadowed region there exists some energy distribution due to diffraction at edges. One can clearly compare the behavior for both cases. However still better resolution and higher order elements [12] are needed to apply the model at higher frequencies.

Although the FEM analysis is time intensive, once it has been completed the results can be examined at any number of observation points. The limitation of FEM is that the acoustical properties of the room must be known precisely. As of now, the data for the complex impedance for walls and the general materials used are only partially available. Once these data become more widely accessible, development in complex shaped room predictions using FEM will play a more important role in room acoustics.

3.4. Comparison with Benchmark Problem

A set of benchmark problems [49] are available where acousticians can compare their results with others. Hence it is like a common platform to compare the results with different approaches. Next to compare our simulation results with measurements, we solved one of the computational benchmark problems. Problem B1-3f (fig. 3.11) was chosen to calculate the sound pressure level at 28 locations.
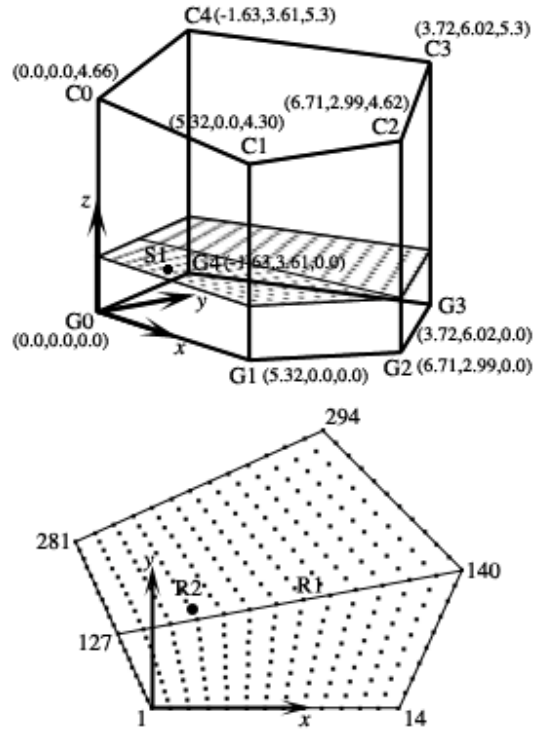

Fig. 3.11

Geometry:

Irregularly shaped reverberation room (about 165 m^3) with a point source.

Boundary Condition:

The absorbing coefficient of all faces is 0.01. A point source (S1) is located at (2.45, 0.0, 1.38), assuming its stationary vibration with volume acceleration amplitude 1.0 m^3/s^2.

First we applied our meshing scheme to divide the whole geometry into small elements (Figure 3.12). Then we evaluated the local integrals for each element using Gaussian quadrature. The mesh contains around 11913 nodes. Hence there arises the question of handling such large matrices. Compressed Storage Format (CSR) has been used to handle the large sparse matrices. For transfer function calculations, the whole set of algebraic equations was solved using quasi minimal residual method [44].
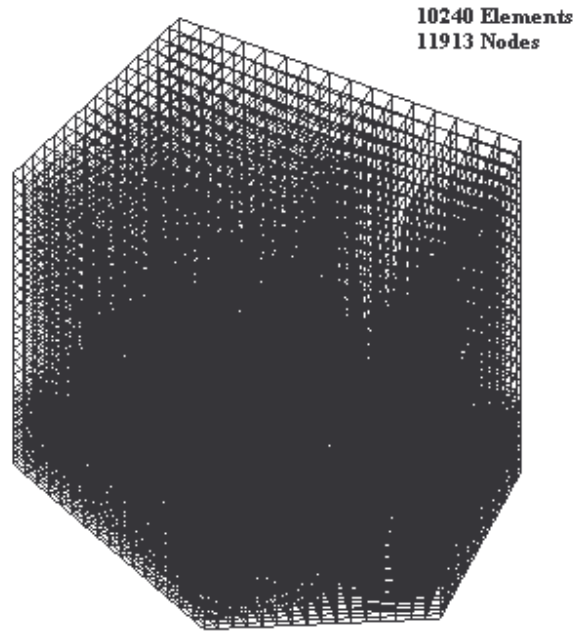
76

Fig. 3.12

Sound pressure levels at initial 28 locations were calculated. The coordinates of 28 points are listed in Appendix C.

The obtained results at 31.5 Hz and 63 Hz were then compared with the measured and others simulation data as shown in the next set of figures (fig 3.13, 3.14). First at 31.5 Hz, a qualitative comparison between both FEM calculations (Imoto, Bansal) shows the peak at 7th and 22nd receiver locations. The measured data shows the dip at 15th receiver location and in FEM plots as well. At 63 Hz, in all the three plots, a dip can be observed around 10th and 25th receiver locations. However, a slight shift in the FEM plot can be observed in Bansal as compare to Imoto. This could be due to errors associated with the impedance values assumed for the walls and slight inexactness of receiver locations (meshing nodes locations). In our case, we assumed all the walls to be rigid as the absorption coefficient is very low.

Hence considering the errors associated one can observe that the results obtained with our meshing scheme are quite in agreement with others measured and simulated data.
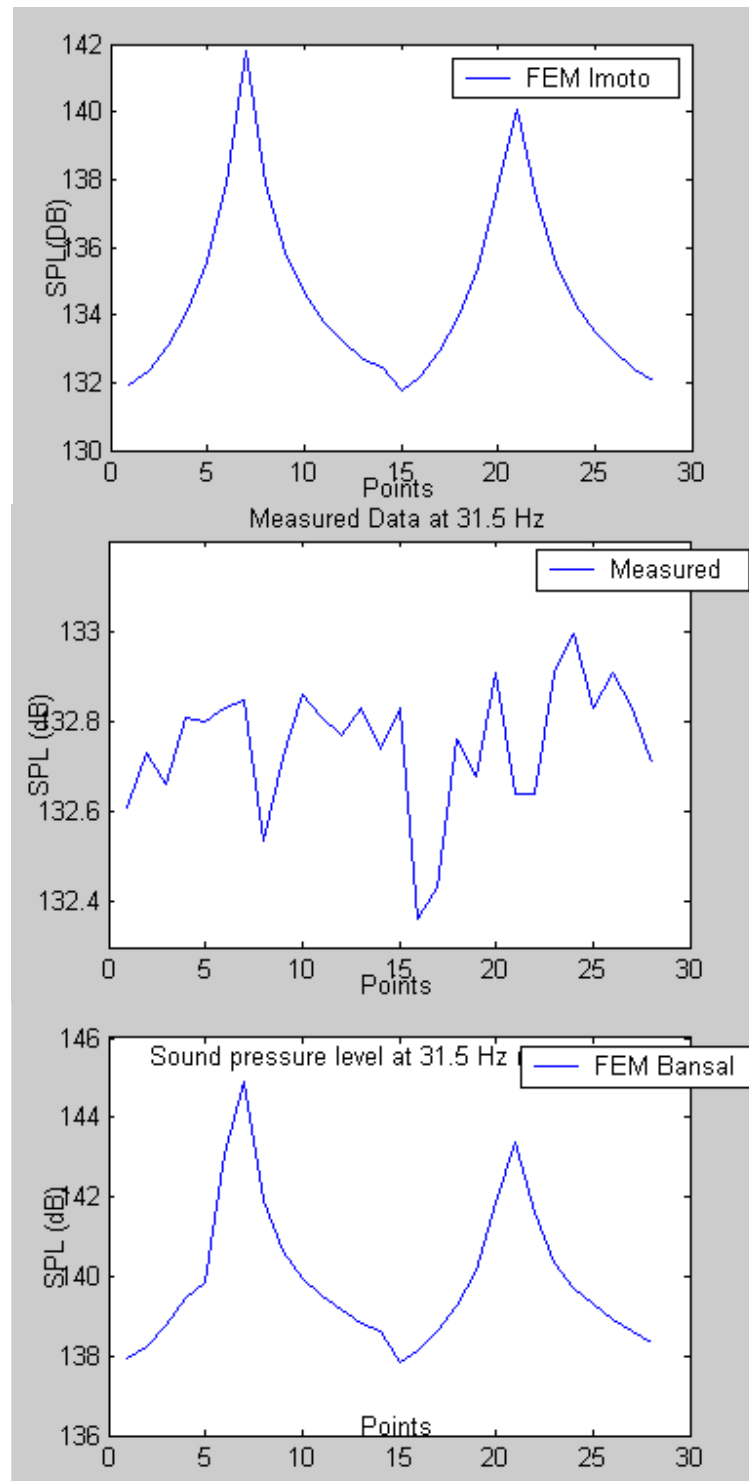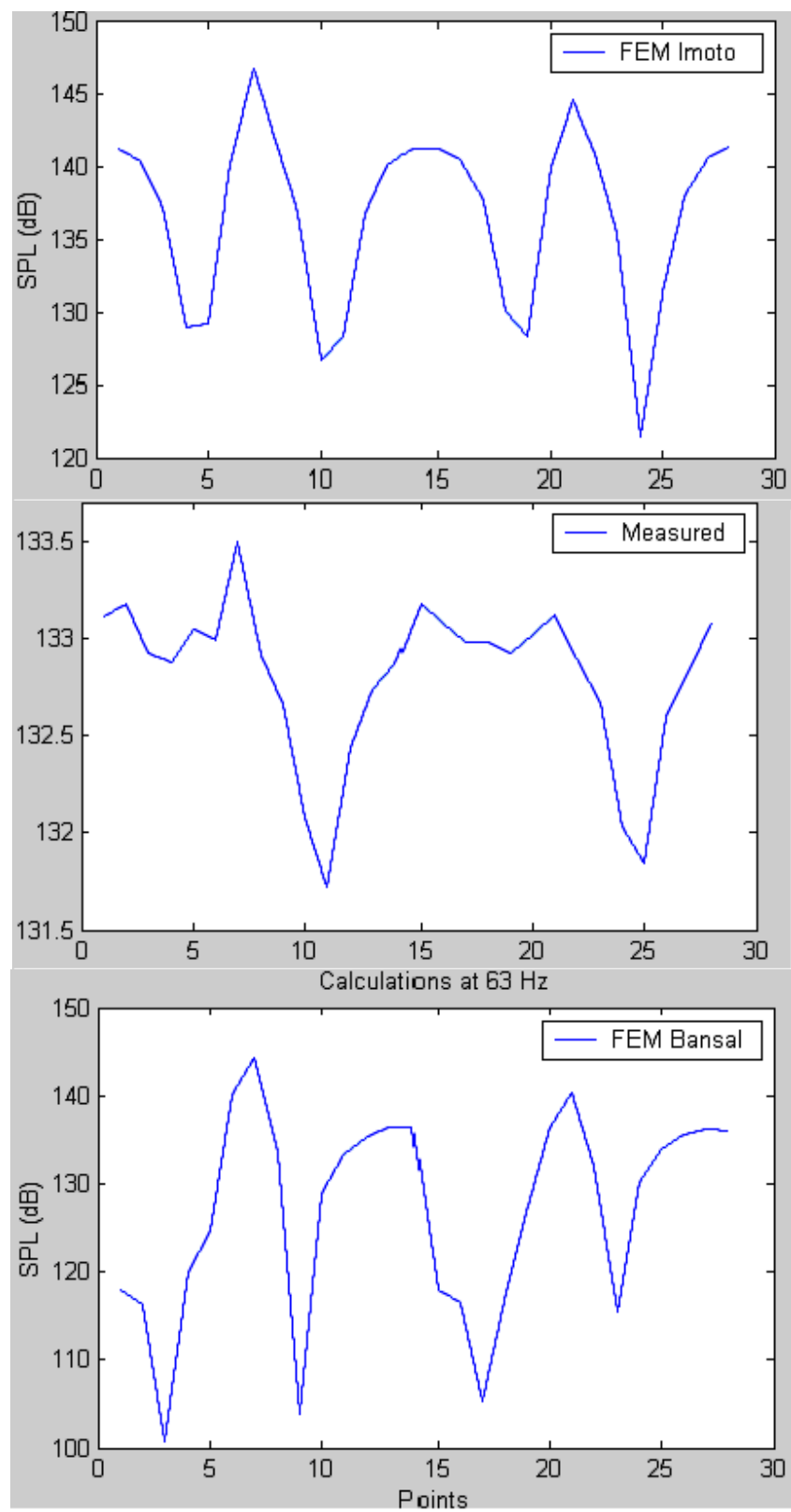
Fig. 3.13

Fig. 3.14

79

3.5.   Concluding Remarks

In this chapter we have investigated the sound behavior using our meshing approach and FEM. First, modal analysis was performed for rigid cases and then we moved to the general quadratic eigenvalue problem. With absorbing surfaces at the walls, a shift in the modal spectrum was seen. Also, the nodal lines (minimum pressure) for the non-rectangular room can be obtained which further helps in determining where to place the loudspeakers optimally.

Then the calculated transfer function obtained by FEM analysis gave a more detailed picture of acoustic behavior. In the shadowed region, it showed the rise in sound energy distribution as compared to particle model due to diffraction. Moreover, peaks corresponding to eigenmodes were obtained. Finally we have performed the FEM analysis on the benchmark problem and we have compared the results. We have shown that with our new meshing scheme, the results are quite in agreement with the measured data. We conclude that this wave based method makes it possible to perform the broad-band acoustic analysis for a given room. However, for the mid-frequency bands the large memory requirements and accuracy expected may afford special care.

4. CHAPTER

Extension of Sound Particle Model using BEM

4.1. INTRODUCTION

As we have seen in the previous chapter, particle-based approaches like ray tracing and image source methods are not fully complete without taking into account the wave nature of the sound. For instance, scattering behavior of incident plane wave on arbitrary surface cannot be explained only by these approaches. Hence, in order to study the behavior of sound field effectively, need of incorporating the scattering behavior into existing particle model arises.

There are many researches concerning scattering behavior and many scattering indices have been proposed [19, 51, 52]. As one of the indices, the scattering coefficient is defined as the ratio of the non-specularly reflected sound energy to the total reflected energy [19]. Due to measurement difficulties, the available literature for scattering coefficient values is very limited [20, 53]. Hence the need of a computational tool in order to predict the scattering coefficient arises.

In this chapter we investigate the use of BEM in order to calculate the Mommertz [19] incident angle dependent scattering coefficient of any arbitrary surface and then we compare it with the available measured data [20]. We also introduce a point source model in order to verify our approach asymptotically. As part of the research a new software tool "EASE Scatterer" was developed and is presented here.

4.2. SCATTERING COEFFICIENT

The scattering coefficient is defined as the ratio of the non-specularly reflected sound energy (fig. 4.1) to the total reflected energy. Specularly reflected rays are those which follow the Snell's law i.e. angle of incident is equal to the angle of reflection.
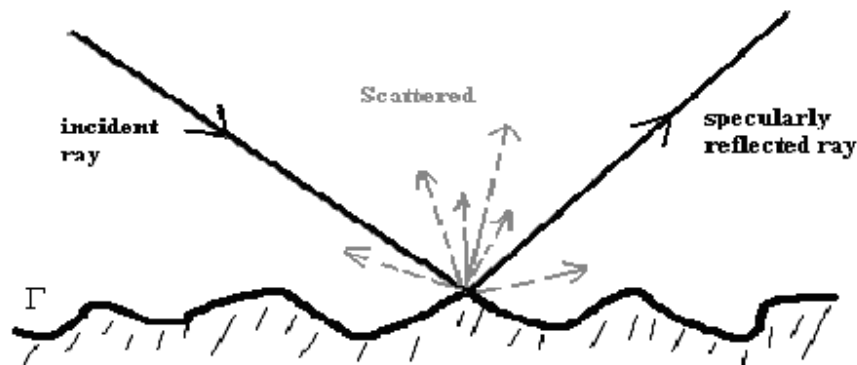

Fig. 4.1a

Mathematically in 2D it can be written as follows:

$$S(\theta) = 1 - \frac{E_{spec}}{E_{total}}$$

where, E_{spec} is speculary reflected and E_{total} is the total scattered energy. The scattering coefficients can be incorporated in the existed particle models to simulate the sound field effectively. Therefore, evaluation of scattering coefficients for arbitrary and periodic surfaces (like staircase, repetitive designs on walls etc) is highly desirable for the ideal sound field simulation.

4.2.1. Boundary Element Method

Mommertz proposed the approach of calculating scattering coefficients utilizing the reflection directivity of surfaces in free field. This approach suits the numerical modeling using BEM as well. Consider an incident plane wave as shown in figure 4.1a on any arbitrary surface. Then the governing equation can be expressed using 1.17:

$$c(r_0)p(r_0) + \int_{\Gamma} \frac{\partial G(r;r_0)}{\partial n} p(r)d\Gamma(r) - \int_{\Gamma} G(r;r_0)\frac{\partial p(r)}{\partial n} d\Gamma(r) + p_{in}(r_0) = 0$$

where

$$c(r_0) = \begin{cases} 1, r_0 \in \Omega \\ 0.5, r_0 \in \Gamma \end{cases}$$

First we discretize the surface into small elements (fig. 4.1b) such that:

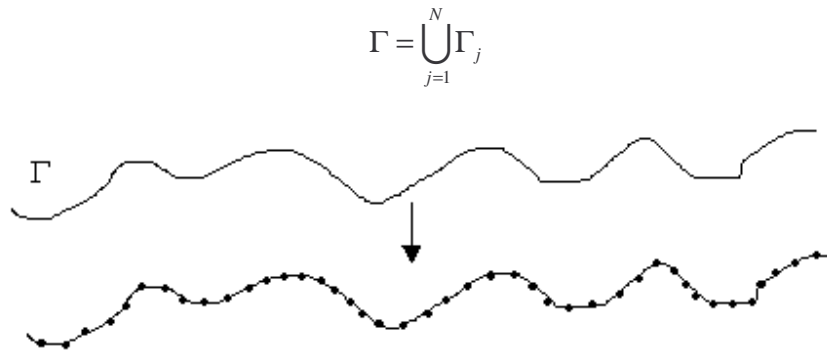$$\Gamma = \bigcup_{j=1}^{N} \Gamma_j$$

Fig. 4.1b

Now, we recall the equation 1.18 for discretized surface from the first chapter:

$$c(r_i)p(r_i) + p_{in}(r_i) + \sum \left\{ \int_{\Gamma_j} \frac{\partial G(r;r_i)}{\partial n} d\Gamma(r) \right\} p(r_j) = \sum \left\{ \int_{\Gamma_j} G(r;r_i) d\Gamma(r) \right\} \frac{\partial p(r_j)}{\partial n}$$

For the rigid case,

$$\frac{\partial p}{\partial n} = 0$$

Therefore the right hand side of equation 1.18 vanishes.

Next, we calculate the incident pressure p_{in} at each node. It is difficult to compute this incident wave pressure at boundary element points, which are shadowed or cannot be seen directly by the incident wave. As an approximation in this model, we have calculated the incident pressure at such points assuming them to be in direct sound field. In other words, one reference line was taken and the incident pressures were calculated on nodes depending upon the distance from the line.

Finally, the algebraic system of equations (eq. 1.18) can be solved to obtain reflected pressure at boundaries using effective solvers. In the next step, pressure at desired receiver locations can be obtained again using the equation. For scattering coefficient calculations, the reflected pressure at some far field distance (depending on the size of surface) can be calculated.

The incidence angle dependent scattering coefficient is calculated from the reflection directivities (R) for the given sample and for the flat reference plate of negligible thickness with the same size. Mathematically it can be represented by:

$$S(\theta) = 1 - \frac{\left| R_{Sample\_Re\,ference} \right|^2}{R_{Sample} R_{Re\,ference}}$$

where,

R_{Sample} is the summation of product of scattered (from sample) sound pressure and its complex conjugate. $R_{Reference}$ is the summation of product of scattered (from reference plate) sound pressure and its complex conjugate. $R_{Sample\_Reference}$ is the summation of product of scattered sound pressures of sample and complex conjugates of reference plate.

4.2.2. Point Source Model

In addition to the BEM model, the complex reflection properties are also calculated utilizing an elementary wave method [55] based on the geometrical parameters of the surface. Radiating point sources are placed along the boundary (fig. 4.2) of the structure utilizing a density sufficient for the considered wavelength. Based on the source locations the complex pressures of the individual elementary waves are summed up in the far field to obtain the polar response.
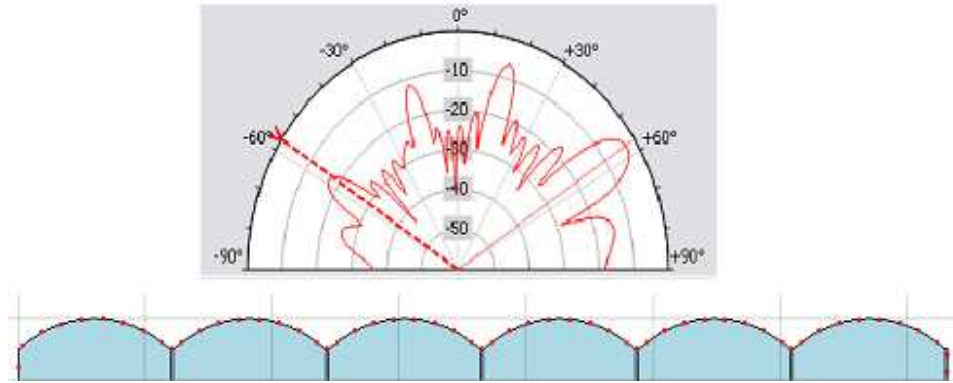
Fig. 4.2: Scat. Behavior for Incident Angle: –56.9°

In short, a fairly simple approach is used to compute the reflected wave front. Naturally, this response depends on the angle of incidence and on the frequency. Fig. 4.2 illustrates the scattering behavior at –56.9° using the point source model at 1 KHz. It is noteworthy that with this model algorithm neither shadowing nor diffraction effects are taken into account explicitly.

4.3.   EXAMPLES AND RESULTS

Next we apply our methodology of both approaches to different surfaces to investigate the scattering behavior of incident plane waves.

4.3.1. Semi Ellipses (10 cm deep)

A model was created in EASE Scatterer as shown in fig. 4.3 and the scattering coefficients for 1/3 octave center frequencies were calculated using BEM and point source model for different incident angles. Throughout the chapter, the surfaces are assumed to be rigid.
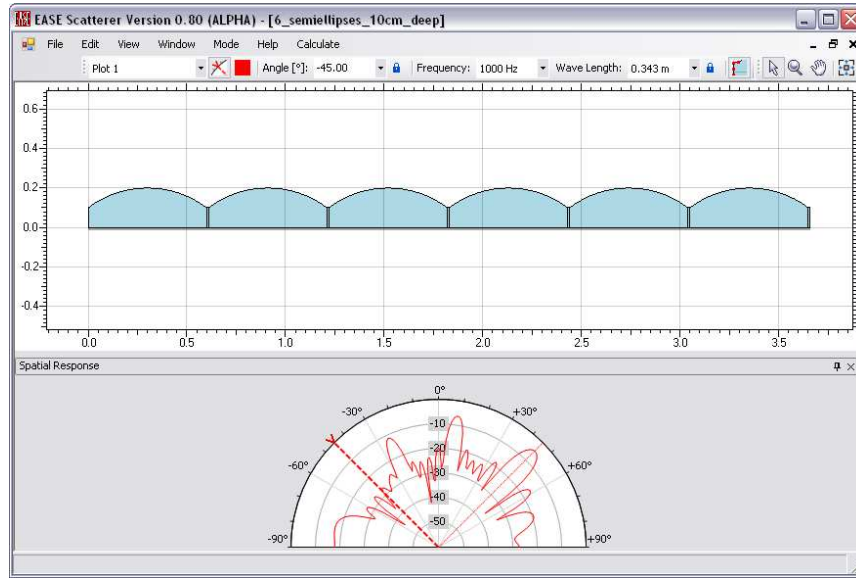
Fig. 4.3: Semi Ellipses Model

4.3.1.1. Qualitative Analysis

Figures 4.4a and 4.4b show the simulated results at 1/3-octave center frequencies. One can observe that for normal angle of incidence (0°), point source model and BEM matches fairly well but for oblique incidence (-56.9°), the BEM gives more accurate results if one compares them with the measured data. This may be due to the fact that in this case, for oblique incidence, the interaction between the neighboring elements is taken care of by the BEM approach more effectively. For instance, there are first and second order reflections taking place within the structure and the point source approach does not take this into account.

Furthermore, the average of the values of scattering coefficients at 1/12 and 1/24 octave band center frequencies in 1/3 octave band were also calculated (fig. 4.4a, 4.4b) to verify and avoid numerical inaccuracies at certain frequencies (if any). They also matches fairly well with the measured data. Therefore, single frequency analysis at 1/3 octave band center frequencies is sufficient and quite practical to roughly estimate the scattering coefficients in this case.
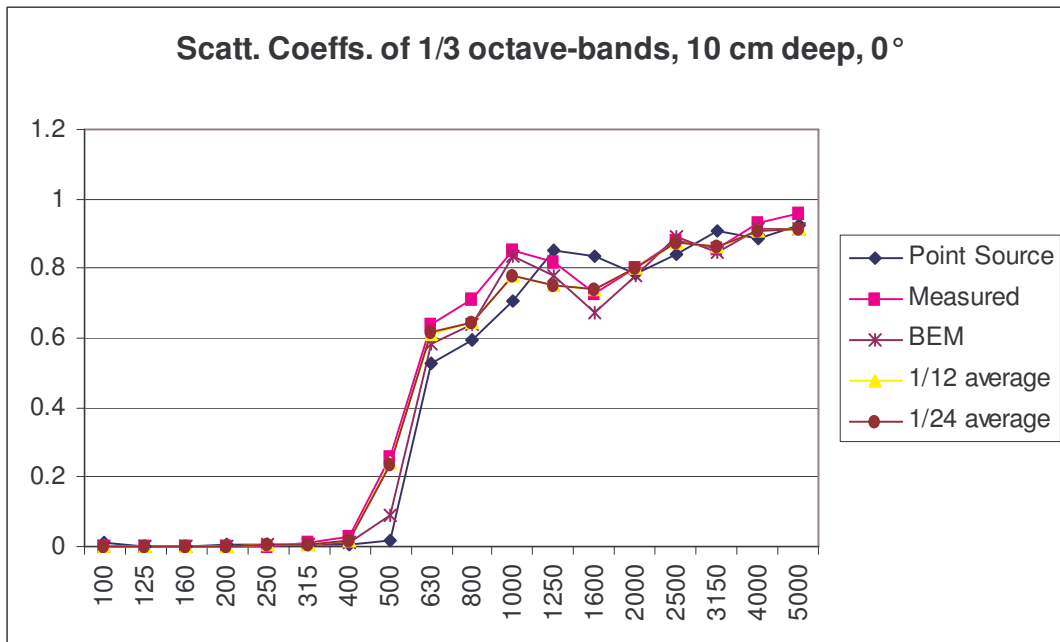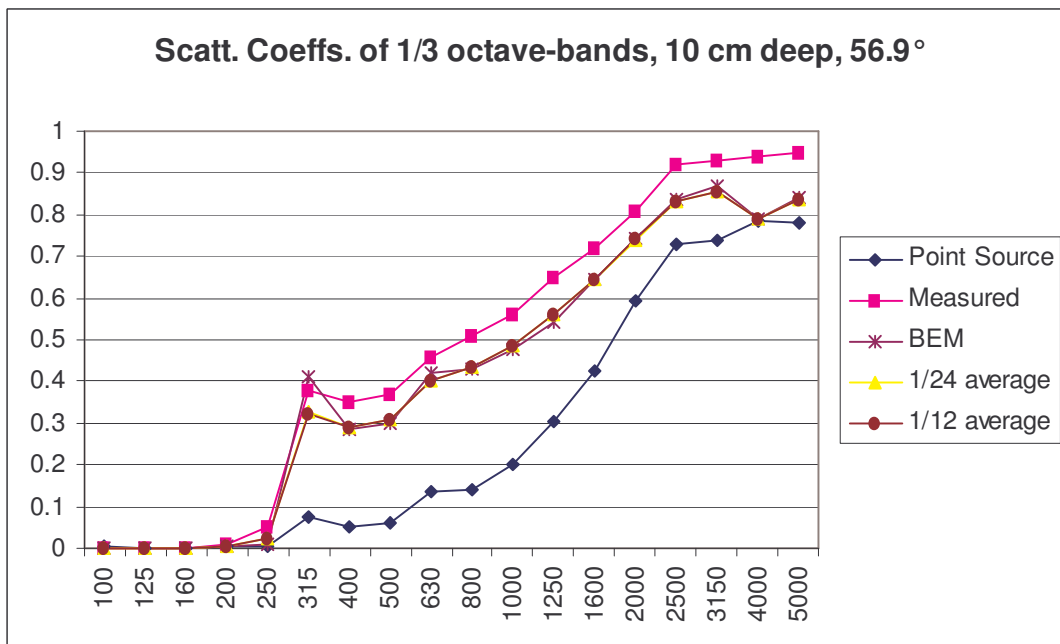
Fig. 4.4a: Incident Angle 0°

Fig. 4.4b: Incident Angle -56.9°

4.3.1.2. Quantitative Analysis

Next we try to observe the quantitative differences between measured and simulated data.

Fig. (4.5a, 4.5b) shows the differences between measured and simulated data over frequencies using BEM and point source approaches.
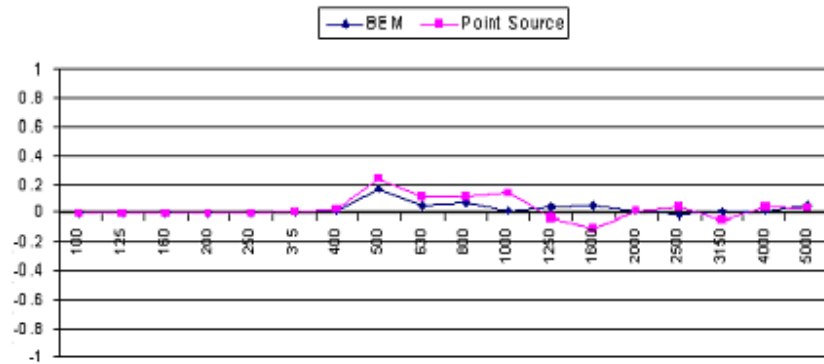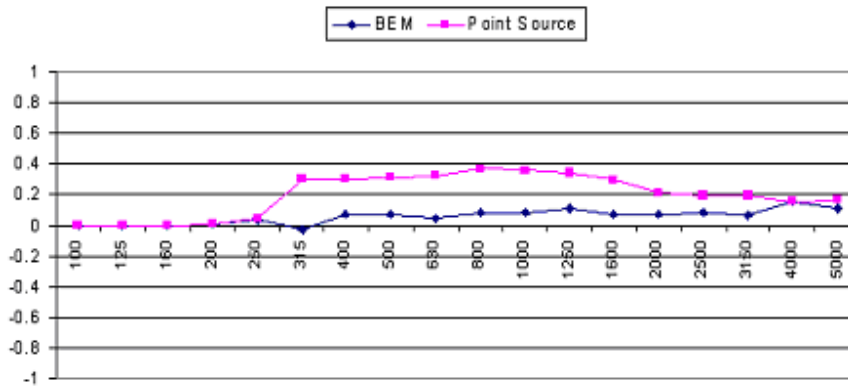

Fig. 4.5a: Incident Angle 0°

Fig. 4.5b: Incident Angle -56.9°

Now to compare the point source model and BEM quantitatively, we calculated the root mean square errors (Table 4.1) for both the cases.

Table 4.1.- Root Mean square errors

Incident Angle	BEM	Point Source
0°	0.0479	0.08366
-56.9°	0.0734	0.2387

From the data (Table 4.1), it is quite clear that the point source model can provide a good estimation of scattering coefficients but BEM is more accurate.

Figures below (4.6a, 4.6b) show some more results for 20 cm deep semi ellipses model. It becomes again clear that the BEM approach is more effective to investigate scattering behavior.
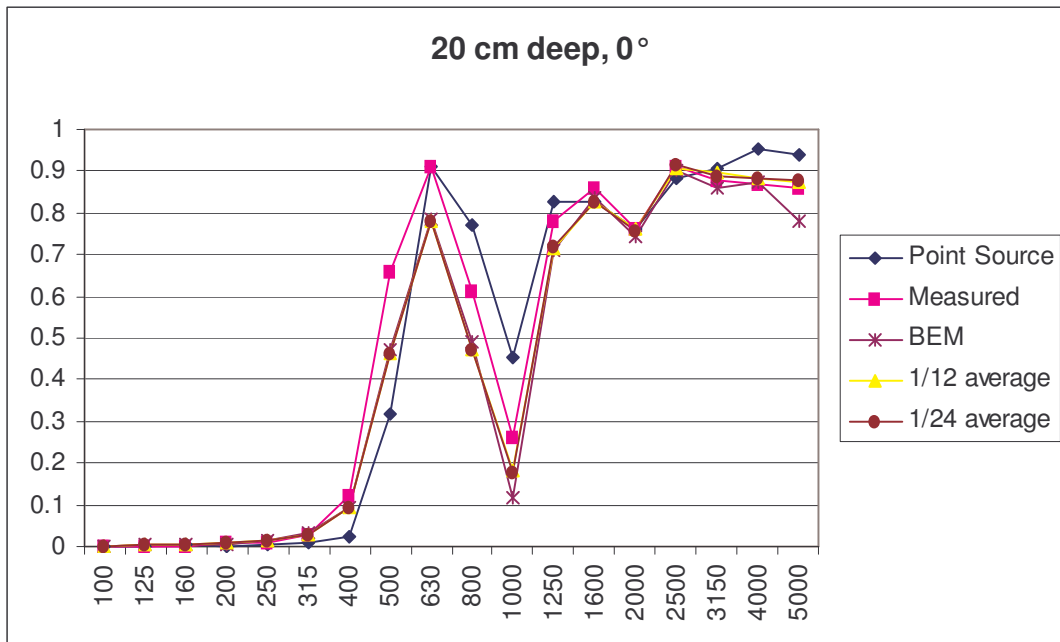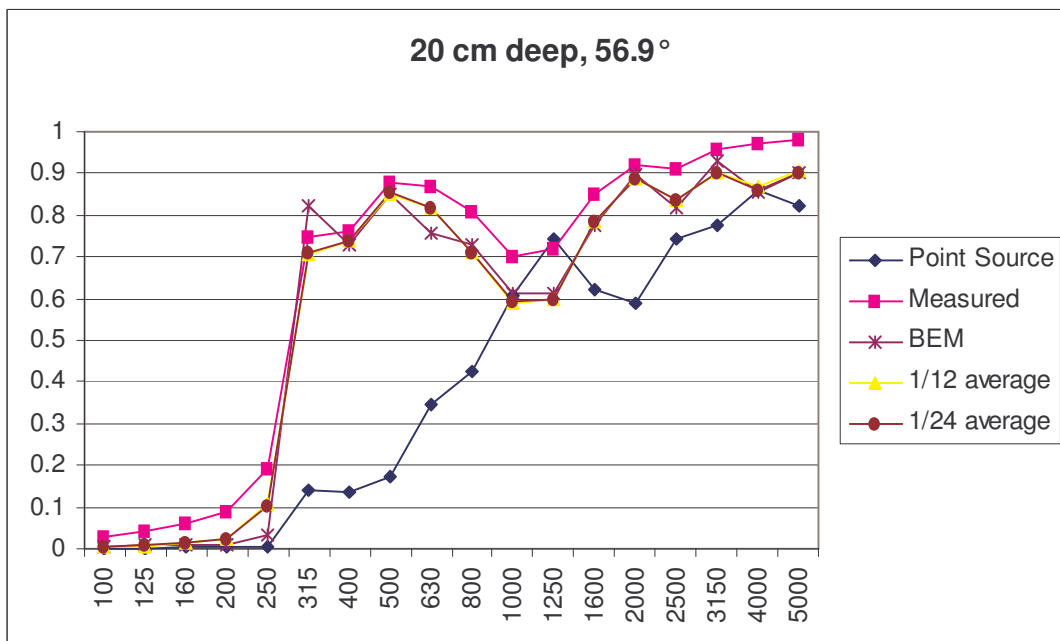
Fig. 4.6a

Fig. 4.6b

4.3.2. Schroeder Diffusers

Now we take a little complicated project to compare our results. A Schroeder diffuser model was created as shown in Figure 4.7:
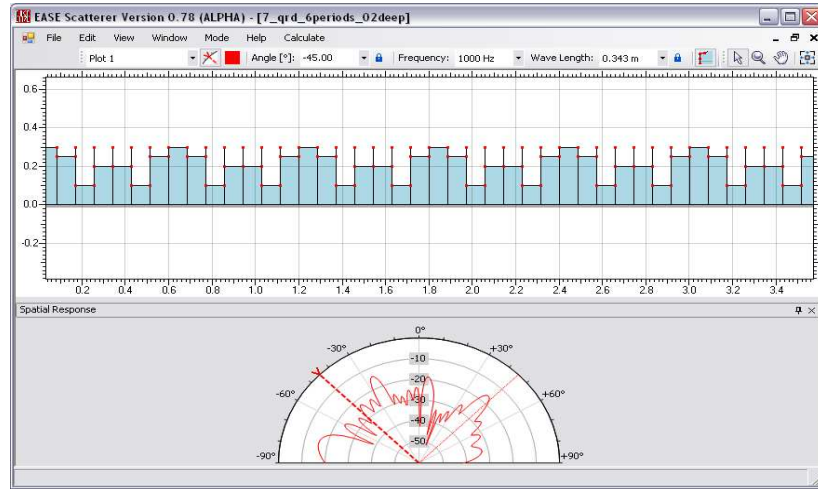
Fig. 4.7: Scattering behavior using BEM

4.3.2.1. Qualitative Analysis

Fig. 4.8a shows the scattering coefficients for the Schroeder diffuser for normal angle of incidence. As there is not much interaction between neighboring elements, point source model and BEM both are effective in predicting the scattering behavior. In fig 4.8a. at 1000 Hz and in fig. 4.8b at 630 Hz there are some mismatches with the measured data. Again, the average of the values of scattering coefficients at 1/12 and 1/24 octave band center frequencies in 1/3 octave band were also calculated. One can notice that after taking average scattering coefficient values the mismatches are removed. Such "fictitious" frequencies could be due to numerical inaccuracies associated with BEM model. However, once again it can be observed from fig. 4.8b that for oblique angles, the point source model is not reliable for complicated surfaces whereas BEM is quite efficient considering the errors associated with the measurements as well.
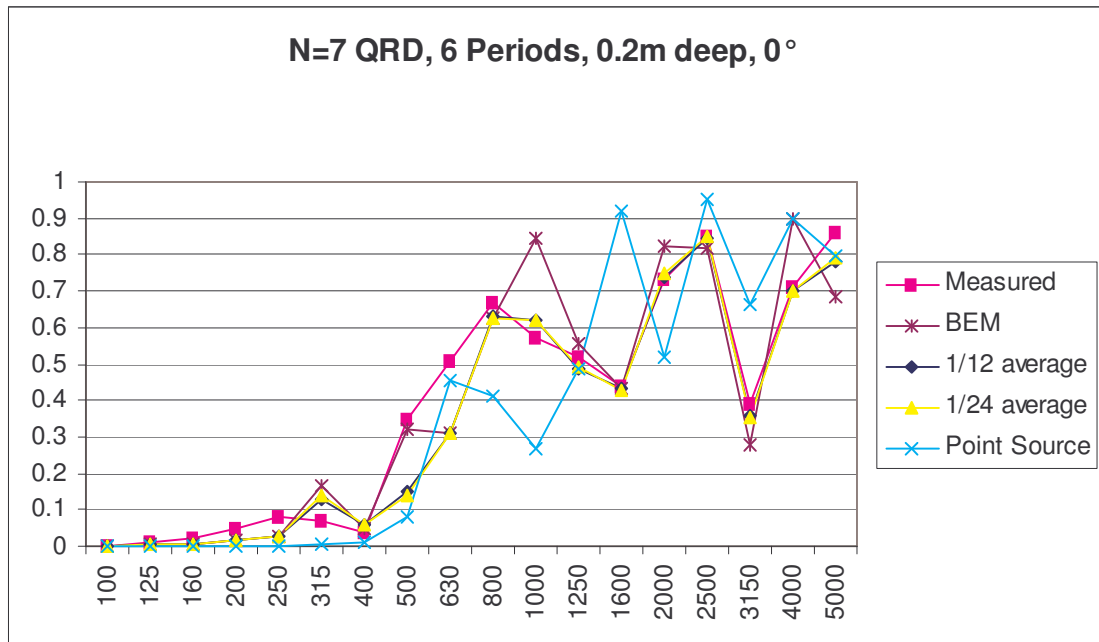
Fig. 4.8a: Incident Angle 0°
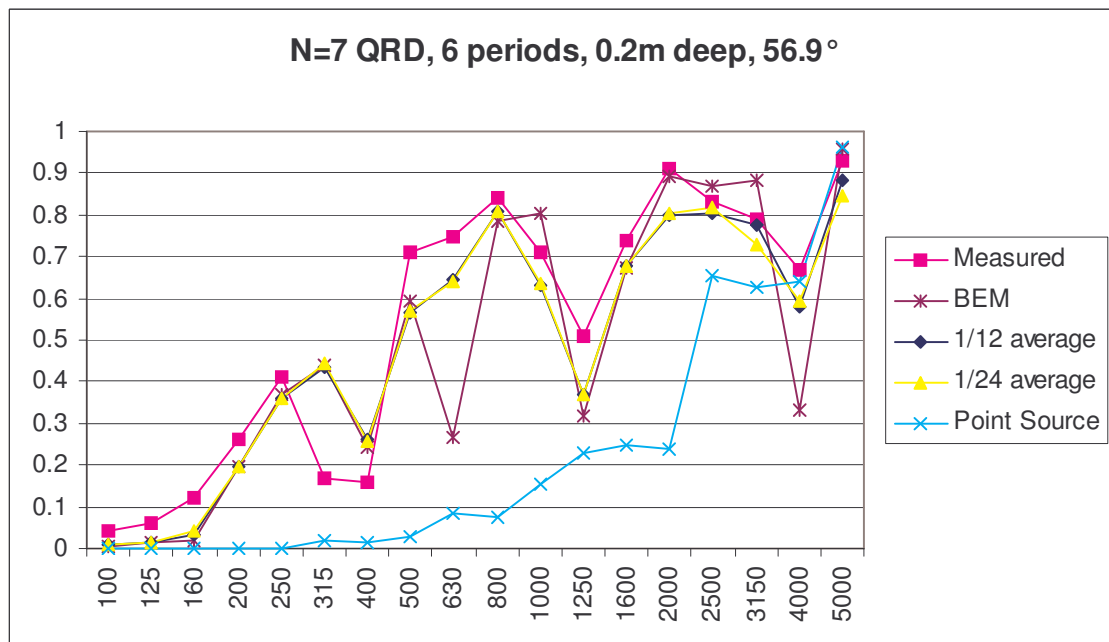
Fig. 4.8b: Incident Angle -56.9°

4.3.2.2. Quantitative Analysis

As before, plots (fig. 4.9a, 4.9b) show deviations from measured data for both cases:

90
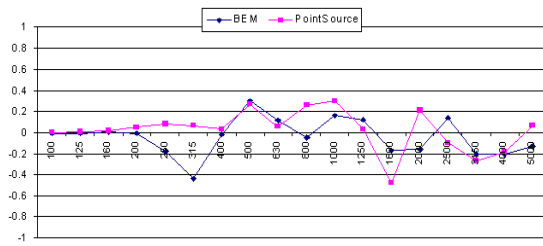
Fig. 4.9a: Incident Angle 0°   Fig. 4.9b: Incident Angle -56.9°
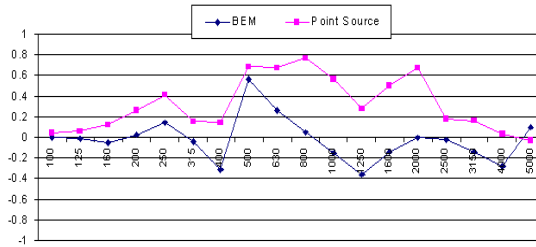
Table 4.2.- Root Mean Square errors

Incident Angle	BEM	Point Source
0°	0.1736	0.19
-56.9°	0.2001	0.4040

Table 4.2 further confirms that errors associated with the point source approach are comparable to the BEM for normal incident angle but almost double in case of oblique angle of incidence.

4.3.3. Semi-Cylinders (12 periods, 7.32 m wide, Incident Angle: -56.9°)

In this example, we just provide a qualitative overview of obtained simulation results.

Fig. 4.10a: Scattering behavior at –56.9°

Fig. 4.10b: Comparison (BEM, Point Source)

Fig. 4.10c : Comparison (BEM, Point Source)

Looking at the figures 4.10b, 4.10c, and from the previous examples, it is quite clear that the advanced BEM approach matches significantly better with the measured data compared to the point source model. For simple geometries point source approach is also acceptable whereas for

complicated geometries like Schroeder diffusers, BEM is needed. This might be as sharp edges cause wave related phenomena like diffraction and more interaction wi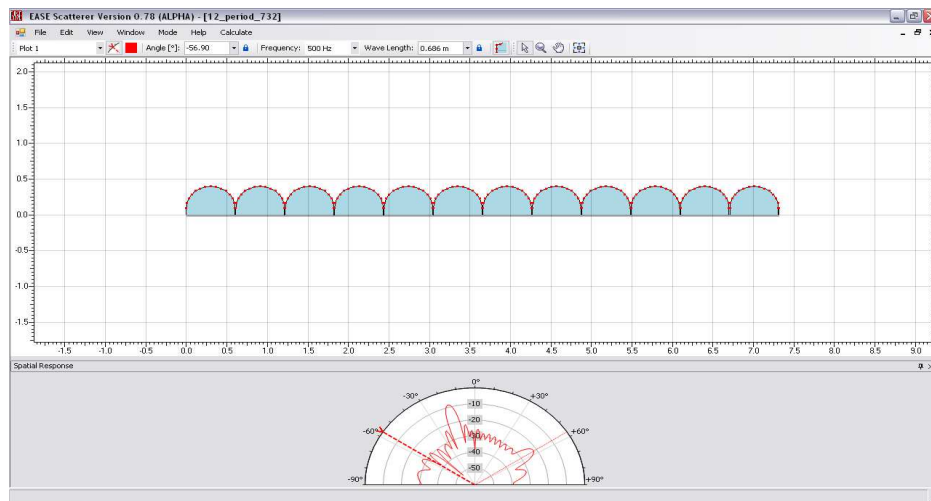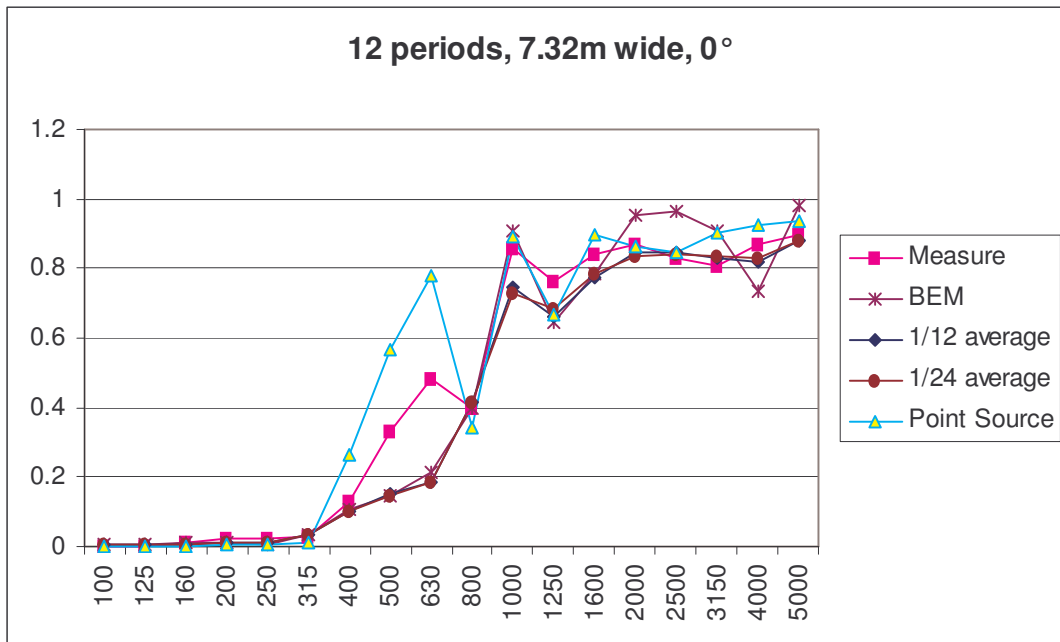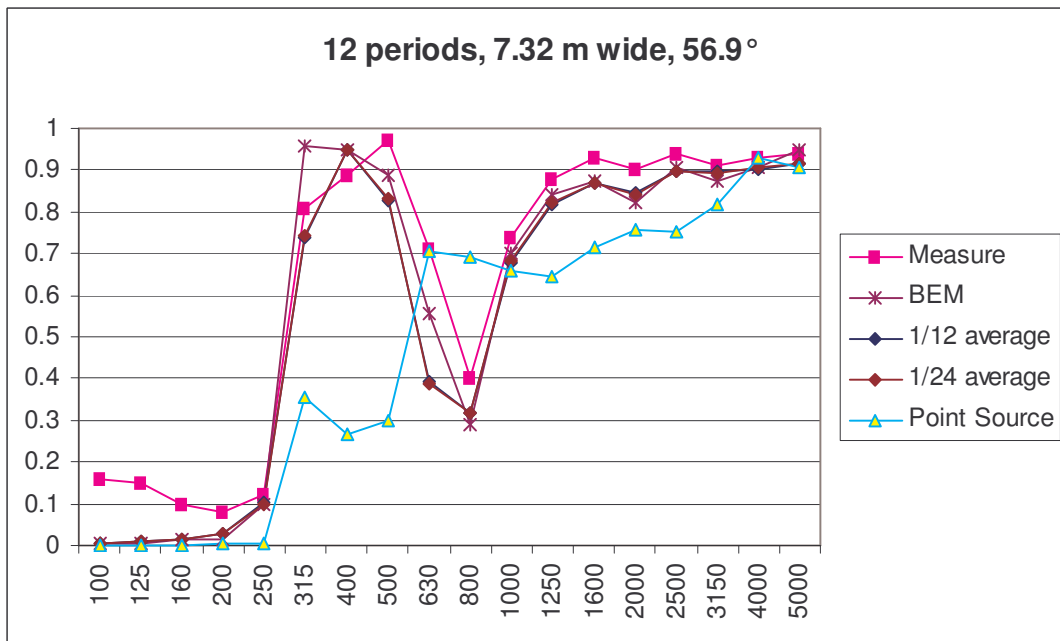thin the structure. BEM takes all these interactions into account. Hence we conclude that BEM can be used effectively in predicting scattering coefficients for various surfaces.

4.4.   RANDOM INCIDENT SCATTERING COEFFICIENT

Next we will discuss whether using a single incident scattering coefficient for all incident angles is valid for room acoustic modeling. We will consider different geometries and examine the scattering coefficients for various incident angles. The objective here is to observe the behavior of scattering coefficients over various incident angles and to further emphasize that using a single scattering coefficient is just an approximation. Normally such single random incident scattering coefficients are calculated using Paris' formula [56].

4.4.1. Triangles (9 periods, 45°)

A model consisting of nine triangles each having 45° angle (fig. 4.11a) was created in EASE Scatterer and scattering coefficients were calculated from 90° to -90° at an interval of 5°.
.
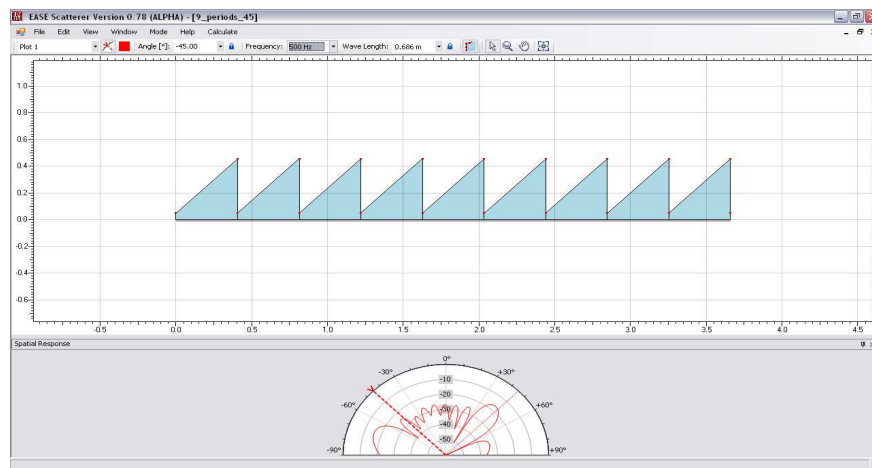
Fig. 4.11: Triangle Model (9 periods)

The next plot (4.11b) shows the angle dependent scattering coefficients at different frequencies for triangles with 9 periods.
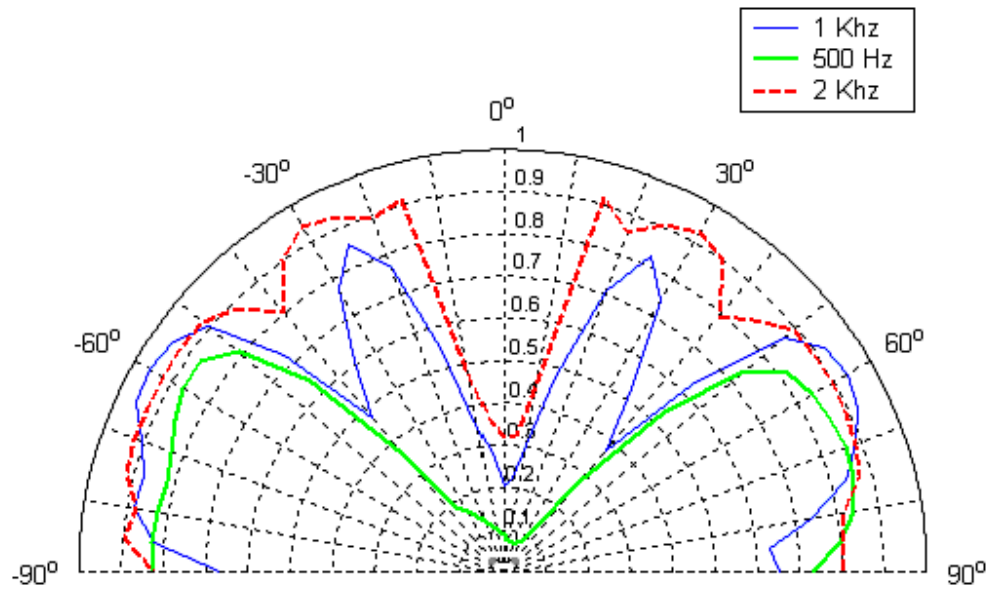
Fig. 4.11b: Scat. Coeff. for different incident angles

4.4.2. Schroeder diffuser (N=7,QRD)

Similarly, for Schroeder diffuser the angle dependent scattering coefficients at 1 KHz were calculated. The results are shown in figure 4.12.
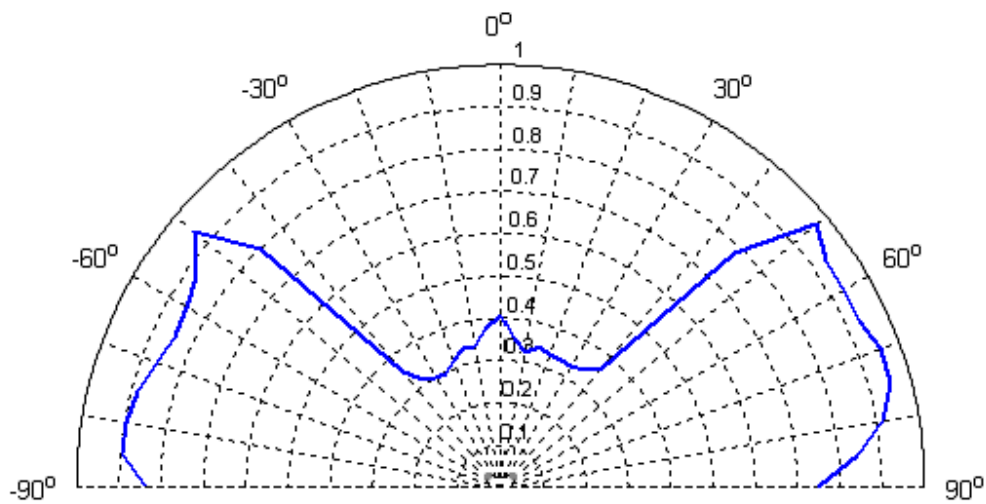
Fig. 4.12: Scat. Coeff., Schroeder

4.4.3. Semi-Ellipse : 10 cm deep

The results for semi-ellipse geometry at 1 KHz are plotted in figure 4.13.
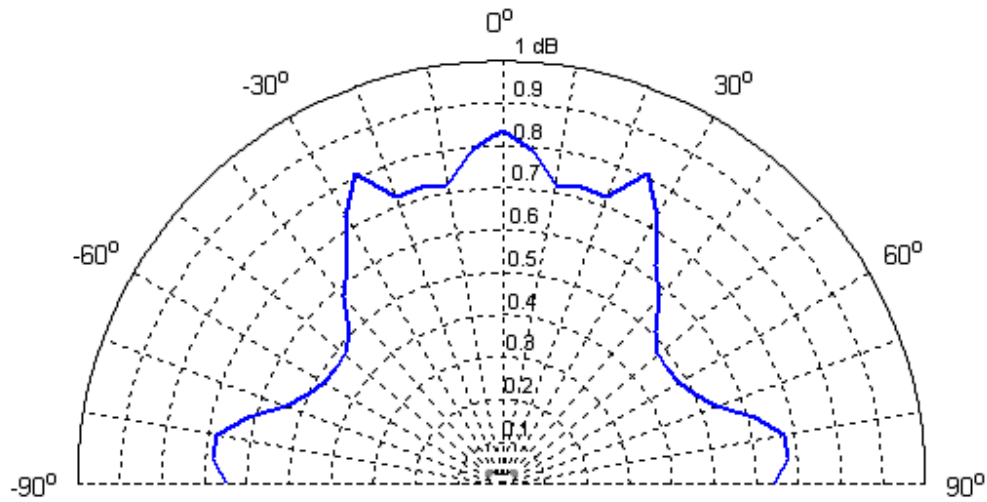
Fig. 4.13: Scat. Coeff., Semi Ellipses

One can observe from the figure 4.11b, that the scattering coefficient values at 1 KHz are ranging from 0.223 to 0.958 and 0.3 to 0.95 in figure 4.12. Therefore, using only a single scattering coefficient for all incident angles and for a single reflection does not seem to be valid. However, roughly speaking if the order of reflections n is high in room acoustic simulations, then one can assume that the incident ray is coming at various angles and therefore in an average sense, a random incident scattering coefficient can be calculated by integrating the directional scattering coefficients in the upper semicircle using the Paris' formula.

If one considers the Semi Ellipses model (fig 4.3) at 1 KHz, the scattering coefficients (fig 4.13) are not varying much over various incident angles. This explains that depending upon the geometry as well; the values of scattering coefficients should be used with care.

4.5.   CONCLUDING REMARKS

The scattering behavior of incident plane waves at arbitrary surfaces using BEM and point source model has been investigated. It has been shown that while the point source model gives reasonable good results, the BEM approach is more effective in terms of quality and quantity. A new computational tool called EASE Scatterer has been developed to calculate the angle dependent scattering coefficients of any arbitrary surface. This will help in simulating the sound field for arbitrary surfaces more accurately. Moreover, the variations of scattering coefficients as the incident angle changes have been shown and the resulting limitations of use of a single scattering coefficient in room-acoustic modeling have been discussed.

5. CHAPTER

Conclusions and Future Work

5.1. SUMMARY

In this thesis, we have investigated the use of powerful numerical methods like FEM and BEM to extend the existing sound particle models. We have shown for low frequencies, how one can incorporate the wave nature of sound to obtain a better impulse response.

Chapter 1 starts with discussing the existing approaches and models for simulation in room acoustics. It explains shortly the methodology behind ray tracing and mirror image methods. It has been shown that these approaches consider sound to behave like a particle. At high frequencies and for larger rooms, these approaches are very effective to obtain impulse response of a system. However, when the dimensions of room become comparable to the wavelength, these approaches fail to model the wave nature of sound like diffraction and interference. Therefore the need of incorporating the wave model arises. Hence the first chapter introduces then the methodology behind wave based approaches (FEM, BEM, FDM). The first step of such approaches includes discretization of the given geometrical domain. This step of subdividing into small elements is also called as mesh generation. Then the basis/shape functions are defined along each node of meshed element. The mathematical theory behind element based approaches has been discussed. It has been shown using examples how to define basis functions for the given meshed element.

Chapter 2, is mainly devoted to mesh generation. This chapter introduces a newly developed meshing approach called cutting plane algorithm. The cutting plane algorithm is based upon applying a sequence of cuts on the given room to obtain convex and trivalent polyhedrons. This simple shaped polyhedrons can then meshed into hexahedral elements using mid-point subdivision scheme. It has been shown that with the proper choice of the cutting scheme, a quality automated hexahedral mesh for many surfaces can be obtained. Special schemes have been suggested and the general idea of cutting procedure especially suited for architectural spaces has been given. The cutting procedure is not very specific or fixed, it can be modified according to the desired outcome. For instance, if only convex polyhedrons are needed, one doesn't have to cut the polyhedron all through and no more multivalent vertex cuts are required. Furthermore, to model curved geometries, a new projection technique has been introduced. It has been shown that for curved polyhedrons it is quite effective. A robust and automatic mesh generator is very hard to realize. This work as a first step has given an approach which is quite effective to generate mesh especially suited to architectural spaces.

In Chapter 3, the wave nature of sound in closed shapes using FEM was investigated. First, modal analysis was performed for rigid cases and then we moved to the general quadratic eigenvalue problem. With absorbing surfaces at the walls, a shift in the modal spectrum was

seen. Also, the nodal lines (minimum pressure) for the non-rectangular room can be obtained which further helps in determining where to place the loudspeakers optimally.

Then the calculated transfer function obtained by FEM analysis gave a more detailed picture of acoustic behavior. In the shadowed region, it showed the rise in sound energy distribution as compared to particle model due to diffraction. Moreover, peaks corresponding to eigenmodes were obtained. Finally we have performed the FEM analysis on the benchmark problem and we have compared the results. We have shown that with our new meshing scheme, the results are quite in agreement with the measured data.

In chapter 4, the scattering behavior of incident plane waves at arbitrary surfaces using BEM and point source model has been investigated. A new computational tool EASE Scatterer has been developed. It has been shown that while the point source model gives reasonable good results, the BEM approach is more effective in terms of quality and quantity. Some mismatches were observed at certain fictitious frequencies for complicated surfaces like Schroeder diffusers. These mismatches were then removed after taking the average scattering coefficient value. Afterwards, the variations of scattering coefficients as the incident angle changes have been analyzed and the resulting limitations for use in room-acoustic modeling have been discussed.

5.2. FUTURE WORK

The contributions made in this thesis may be viewed in terms of future work, as follows. The new meshing scheme can possibly be useful for other application field as well. As it is already mentioned that geometries with roughly less than 40-50 notches can be meshed automatically using our cutting plane algorithm just by the click of the button, there is still a need of having more predetermined cutting schemes to obtain quality shaped convex polyhedrons. Moreover, due to lack of measurement data we were unable to simulate the results of real life acoustic model. Hence as a next step, a real life studio measurement and simulation comparison using our meshing approach is to be performed. In the fourth chapter, we have developed a computational tool EASE Scatterer to investigate scattering from arbitrary 2D surfaces. Therefore to simulate more realistic geometries, need of incorporating 3D geometries as well in the computational tool.

References

[1] M. Kleiner, B.-I. Dalenbäck and P. Svensson."Auralization - an overview". J. Audio Eng. Soc.,41(11):861-875,1993 Nov.

[2] Rindel, J.H., Naylor, G., "Computer modeling of Sound Fields in Rooms-The State of the Art and Outlook to the future-", ICA 14, F2-1, 1992.

[3] R. Lyon and R. DeJong. "Theory and application of statistical energy analysis". Butterworth-Heinermann, Newton, MA, 2nd edition, 1995 .

[4] T. Koizumi; N. Tsujiuchi; I. Kubomoto; E. Ishida, "Estimation of the Noise and Vibration Response in a Tractor Cabin Using Statistical Energy Analysis", SAE Paper 1999-01-2821, (1999).

[5] A. Kulowski, "Algorithmic representation of the ray tracing technique". Applied Acoustics 18 (6):449-469,1985.

[6] A. Krokstad, S. Strom, and S. Sordal. "Calculating the acoustical room response by the use of a ray tracing technique". J. Sound vib., 8(1):118-125, 1968.

[7] J.B. Allen and D.A. Berkley. "Image Method for efficiently simulating small-room acoustics". J. Acoust. Soc. Am.,65(4):943-950, 1979.

[8] M. Vorländer. "Simulation of the transient and steady-state sound propagation in rooms using a new combined ray-tracing/image-source algorithm". *J. Acoust. Soc. Am.*, 86(1):172-178, 1989.

[9] G. M. Naylor. ODEON - another hybrid room acoustical model. *Applied Acoustics*, 38(2-4, Special Issue on Computer Modelling and Auralisation of Sound Fields in Rooms):131-143, 1993.

[10] Mahesh Bansal, Stefan Feistel, Wolfgang Ahnert, "First Approach to combine Particle Model Algorithm with Modal Analysis using FEM", AES 118 convention, 28-31 May, 2005, Barcelona.

[11] A Craggs, Acoustic Modeling, "Finite Element Method, Encyclopedia of Acoustics, Chapter 14, John Wiley & Sons, New York, 1997.

[12] Otsuru, T., Tomiku, R.,"Basic Characteristics and Accuracy of Acoustic Finite Element Using Spline Function in the Applications onto Finite Element Sound Field Analysis ,"J. Acoust. Soc. Jpn(E),pp.87-96, 2000.

[13] Seybert, A.F. and Wu,T.W.(1997) Acoustic modeling: Boundary Element Methods. Encyclopedia of Acoustics, Chapter 15, Malcolm J. Crocker, ed. John Wiley and sons, Inc., New York, 173-184.

[14] D.W. Herrin, T. W. Wu and A.F. Seybert, "Practical issues regarding the use of Finite and Boundary Element Methods for Acoustics", Building Acoustics, 10(4),257-279, 2003.

[15] D. Botteldooren. Finite-difference time-domain simulation of low-frequency room acoustic problems. J. Acoust. Soc. Am., 98(6):3302-3308, 1995.

[16] L. Savioja, J. Backman, A. Järvinen, and T. Takala. Waveguide mesh method for low-frequency simulation of room acoustics. In Proc. 15th Int. Congr. Acoust. (ICA'95), volume 2, pages 637-640, Trondheim, Norway, June 1995.

[17] Ailred and Newhouse, "Applications of the Monte Carlo Method to Architectural Acoustics," Journal Acoustic Society America, Vol. 30, No. I0, Oct 1958, pages 903-90.

[18] Haviland, J. K. and B. D. Thanedar. "Monte Carlo Applications to Acoustical Field Solutions," Journal Acoustic Society America, Vol. 54, No. 54, 1973.

[19] E. Mommertz: Determination of scattering coefficients from the reflection directivity of architectural surfaces. Applied Acoustics 60 (2000) 201-203.

[20] Trevor J. Cox and Peter D'Antonio: Acoustic Absorbers and diffusers, Theory and Application.

[21] Hughes, T. J. R. Finite Element Method - Linear Static and Dynamic Finite Element Analysis

[22] P. K. Bannerjee and R. Butterfield, Boundary Element Methods in Engineering Science, McGraw-Hill, London, 1981.

[23] C. A. Brebbia and S. Walker, Boundary Element Techniques in Engineering, Newnes-Butterworths, London, 1980.

[24] Bernard Chazelle, "Convex Partitions Of Polyhedra", SIAM Journal on Computing, volume 13, 488-507, August 1984.

[25] B. Joe. Tetrahedral mesh generation in polyhedral regions based on convex polyhedron decompositions, International Journal for Numerical Methods in Engineering, 37, 693-713, 1994.

[26] P. J. Frey. H. Borouchaki and P.L. George. "Delaunay tetrahedralization using an advancing front approach". In Proc 5th International Meshing Roundtable. pages 31-46 Sandia National Laboratories.

[27] M. A. Price, C. G. Armstrong and M. A. Sabin, Hexahedral mesh generation by medial surface subdivision: I. Solids with convex edges, Int. Journal. numer. methods eng., 38, 3335-3359 (1995).

[28] M. A. Price, C. G. Armstrong and M. A. Sabin, Hexahedral mesh generation by medial surface subdivision. Part II. Solids with flat and concave edges, Int. Journ. of num meth. In engg. Vol. 40, 111-136 (1997).

[29] Weidong Min, (1997) "Generating Hexahedron-Dominant Mesh Based on Shrinking-Mapping Method", Proceedings, 6th International Meshing Roundtable, pp.171-182.

[30] Lori Freitag, Mark Jones, and Paul Plassmann, (1995) "An Efficient Parallel Algorithm for Mesh Smoothing", Proceedings, 4th International Meshing Roundtable, pp.47-58.

[31] Freitag, Lori A. and Carl Ollivier-Gooch, (1997) "Tetrahedral Mesh Improvement Using Swapping and Smoothing", International Journal for Numerical Methods in Engineering, vol. 40, pp.3979-4002.

[32] Staten, Matthew L. and Scott A. Canann, (1997) "Post Refinement Element Shape Improvement for Quadrilateral Meshes", AMD-Vol. *220* Trends in Unstructured Mesh Generation, pp.9-16

[33] R. Schneiders, (1996) "Refining Quadrilateral and Hexahedral Element Meshes", 5th International Conference on Numerical Grid Generation in Computational Field Simulations, Mississippi State University, pp.679-688

[34] J. Ruppert and R. Seidel. On the difficulty of tetrahedralizing 3-dimensional non-convex polyhedra. In Proc. 5th Annu. ACM Sympos. Comput. Geom.. pp 380-392,1989.

[35] M. A. Yerry and M. S. Shepherd, Automatic three dimensional mesh generation by the modified-octree technique. Int. journal. numer. methods eng., 20, 1965,1990 (1984).

[36] T. D. Blacker and M. B. Stephenson, "Paving: a new approach to automated quadrilateral mesh generation", Int. j. numer. methods eng., 32, 811-847 (1991).

[37] E.K. Buratynski." A fully automatic three dimensional mesh generator for complex geometries". Int. J. Numeric Met. Eng 30: 931-952 (1990).

[38] M. B. Stephenson, S. A. Cannan and T. D. Blacker, Plastering: a new approach to automated 3D hexahedral mesh generation, Progress Report 1, Sandia National Laboratories, *Report SAND*89-2192, 1992.

[39] T. S Li, R. M. McKeag and C. G. Armstrong, "Hexahedral meshing using midpoint subdivision and integer programming ", Comput. Methods Appl. Mech. Eng., 124, 171-193 (1995).

[40] Mahesh Bansal, Stefan Feistel, Wolfgang Ahnert, Large Scale FEM analysis of a Studio Room, Presented at 120 AES convention, Paris.

[41] M. A. Sabin, "Criteria for comparison of automatic mesh generation methods", Adv. Eng. Software, 13, 220-225 (1991).

[42] Timothy J. Tautges, Ted Blacker and Scott Mitchell, (1996) "The Whisker-Weaving Algorithm: A Connectivity Based Method for Constructing All-Hexahedral Finite Element Meshes," International Journal for Numerical Methods in Engineering, Vol.39,pp.3327-3349

[43] Y. Saad, Numerical Methods for Large Eigenvalue Problems, Algorithms and Architectures for Advanced Scientific Computing, Manchester University Press, Manchester, UK, 1992.

[44] R.W Freund and N.M. Nachtigal. AMR: A quasi-minimal residual method for non-hermitian linear systems. Numeri. Math,60: 315-339-1991.

[45] B.M. Irons "Quadrature rules for brick based finite elements", Int. Journal for numerical methods in engineering, 3 ,293-294 , 1971.

[46] J.H. Rindel, Modelling the Angle-Dependent Pressure Reflection Factor, Applied Acoustics 38(1993) 223-234.

[47] S.E. Olive, P. Schuck, S. Sally, M. Bonneville,"The Effects of Loudspeaker Placement on Listener Preference Ratings", J. Audio Eng. Soc., 42, pp. 651-669 (September 1994)

[48] P. D'Antonio, C. Bilello and D. Davis,"Optimizing Home Listening Rooms", 85th AES Los Angeles Convention, Preprint 2735 (November1988).

[49] Benchmark problems: http://gacoust.hwe.oita-u.ac.jp/AIJ-BPCA/index.html

[50] J. H. Wilkinson & C. Reinsch, Linear Algebra Springer-Verlag 1971.

[51] M. Vorländer and E Mommertz: Definition and measurement of random-incidence scattering coefficients, Applied Acoustics 60 (2000) 187-199.

[52] K. Fujiwara and K. Masuda: On the random reflection characteristics of a wall with periodical unevenness, Proc. Spring Meet. Acoust. Soc. Jpn (1989) 581-582.

[53] ISO 17497-1:2004: Sound-scattering properties of surfaces, Part 1: Measurement of the random-incidence scattering coefficient in a reverberation room.

[54] L.C. Wrobel: The Boundary Element Method.

[55] W. Ahnert, S. Feistel and S. Bock: Prediction of scattering coefficients for use in room-acoustic simulation, Reproduced Sound 22, Oxford, 3rd-4th November 2006 (also: 4th Joint meeting, ASA and Acous. Soc. of Jpn., Honolulu, Hawaii).

[56] H. Kuttruff: Room Acoustics, 4th ed. (Spon Press, London, 2000), Chap. 2, 31-58.

[57] Borish, J. "Extension of the Image Model to Arbitrary Polyhedra," Journal Acoustic Society America, Vol. 75, No.6, June 1984, pages 1827-1836.

[58] Schroeder, M. R. "Digital Simulation of Sound Transmission in Reverberant Spaces (Part 1)," Journal Acoustic Society America, Vol. 47, No. 2, 1970, pages 424 -431.

[59] L. Savioja, J. Backman, A. Järvinen, and T. Takala. Waveguide mesh method for low-frequency simulation of room acoustics. In *Proc. 15th Int. Congr. Acoust. (ICA'95)*, volume 2, pages 637-640, Trondheim, Norway, June 1995.

[60] Sadiku, M. N. O., Numerical Techniques in Electromagnetics, Boca Raton: CRC Press, Inc., 1992.

[61] P.J. Davis, P. Rabinowitz, "Methods of numerical integration" , Acad. Press (1984) (Edition: Second)

[62] W. Gautschi, "Gauss–Kronrod quadrature — a survey" G.V. Milovanović (ed.) , Numer. Meth. and Approx. Th. , III , Nis (1988) pp. 39–66.

[63] T. Shuku and K. Ishihara, 'The analysis of the acoustic field in irregularly shaped room by the finite element method', J. Sound Vib. , 29, 67-76 (1973).

Appendix A

Legendre - Gauss Quadrature

Weighting Factors	Function Arguments
N = 2	
$W_1 = 1.000000000$	$x_1 = -0.577350269$
$W_2 = 1.000000000$	$x_2 = 0.577350269$
N = 3	
$W_1 = 0.555555556$	$x_1 = -0.774596669$
$W_2 = 0.888888889$	$x_2 = 0.000000000$
$W_3 = 0.555555556$	$x_3 = 0.774596669$
N = 4	
$W_1 = 0.347854845$	$x_1 = -0.861136312$
$W_2 = 0.652145155$	$x_2 = -0.339981044$
$W_3 = 0.652145155$	$x_3 = 0.339981044$
$W_4 = 0.347854845$	$x_4 = 0.861136312$
N = 5	
$W_1 = 0.236926885$	$x_1 = -0.906179846$
$W_2 = 0.478628670$	$x_2 = -0.538469310$
$W_3 = 0.568888889$	$x_3 = 0.000000000$
$W_4 = 0.478628670$	$x_4 = 0.538469310$
$W_5 = 0.236926885$	$x_5 = 0.906179846$
N = 6	
$W_1 = 0.171324492$	$x_1 = -0.932469514$
$W_2 = 0.360761573$	$x_2 = -0.661209386$
$W_3 = 0.467913935$	$x_3 = -0.238619186$
$W_4 = 0.467913935$	$x_4 = 0.238619186$
$W_5 = 0.360761573$	$x_5 = 0.661209386$
$W_6 = 0.171324492$	$x_6 = 0.932469514$

Appendix B

Notch Detect Algorithm

A notch is defined to be an edge whose adjacent faces create internal dihedral angle greater than 180°. To identify such edges we have used the following algorithm:

Algorithm:

For the edge under consideration **g** connected by vertices v1 and v2, we find its two adjacent faces i.e. F1 and F2. Then first, we calculate the face normal of F1 say N1. Afterwards, we find an edge on F2 having one vertex from **g** say v2 to v3 or from v1 to v3.
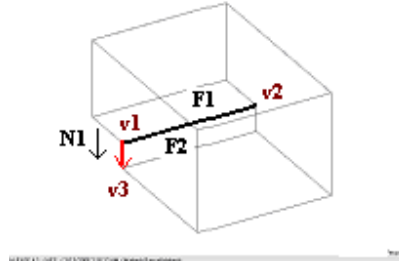

Fig. A1

If the angle between this edge vector and N1 is less than 90°, then the edge is a notch. In the above example (fig A1), the edge (marked by thick black bold line) is a notch as both the vectors N1 and (v1-v3) are creating an angle 0° (< 90°).

Intersection Algorithms

Here we explain some standard intersection algorithms used in our meshing scheme.

Plane-Line intersection:

A plane having normal (A, B, C) can be represented by the equation

$$A x + B y + C z + D = 0 \qquad (1)$$

where all points (x, y, z) lie on the plane. Equation of the line through points P1 (x1, y1, z1) and P2 (x2, y2, z2) is given by:

$$P = P1 + u\ (P2 - P1) \tag{2}$$

Substituting (1) into (2) gives:

A (x1 + u (x2 - x1)) + B (y1 + u (y2 - y1)) + C (z1 + u (z2 - z1)) + D = 0

Finally solving for u results:

$$u = \frac{A\ x1 + B\ y1 + C\ z1 + D}{A\ (x1 - x2) + B\ (y1 - y2) + C\ (z1 - z2)}$$

- o   the denominator is 0 then the normal to the plane is perpendicular to the line. Thus the line is either parallel to the plane and there are no solutions or the line is on the plane in which case are infinite solutions.
- o   if it is necessary to determine the intersection of the line segment between P1 and P2 then just check that u is between 0 and 1.

Appendix C

Receiver location	Coordinates (x y z)
1	0.000 0.000 1.200
2	0.409 0.000 1.200
3	0.818 0.000 1.200
4	1.227 0.000 1.200
5	1.636 0.000 1.200
6	2.046 0.000 1.200
7	2.455 0.000 1.200
8	2.864 0.000 1.200
9	3.273 0.000 1.200
10	3.683 0.000 1.200
11	4.092 0.000 1.200
12	4.501 0.000 1.200
13	4.910 0.000 1.200
14	5.320 0.000 1.200
15	-0.081 0.180 1.200
16	0.345 0.192 1.200
17	0.773 0.204 1.200
18	1.200 0.215 1.200
19	1.628 0.227 1.200

20	2.055 0.238 1.200
21	2.482 0.250 1.200
22	2.910 0.262 1.200
23	3.337 0.273 1.200
24	3.764 0.285 1.200
25	4.190 0.297 1.200
26	4.619 0.308 1.200
27	5.047 0.320 1.200
28	5.474 0.332 1.200